Single-molecule fluorescence microscopy studies of DNA-surface interactions on chemically graded organosilane surfaces

By

Zi Li

B.S., Ocean University of China, 2013

AN ABSTRACT OF A DISSERTATION

Submitted in partial fulfillment of the requirements for the degree

DOCTOR OF PHILOSOPHY

Department of Chemistry
College of Arts and Sciences

KANSAS STATE UNIVERSITY
Manhattan, Kansas

2018

Abstract

This dissertation describes the application of wide-field single-molecule fluorescence microscopy techniques to investigations of DNA-surface interactions on chemically graded organosilane surfaces. The adsorption and desorption behaviors of double-stranded (ds) plasmid DNA along the amino-trimethoxysilane and octyl-trichlorosilane gradients were explored as a function of solution pH, solution ionic strength and surface properties. The results provide an improved fundamental understanding of DNA interactions with different surfaces and are certain to aid in the development and advancement of DNA-based biological and biomedical devices. Three distinct experiments were performed in completion of the work for this dissertation.

In the first study, total internal reflection fluorescence (TIRF) microscopy was employed to study DNA interactions with aminosilane gradient surfaces under relatively acidic and basic environments. Electrical potentials were applied to assist DNA adsorption and desorption. The single-molecule data clearly showed that DNA capture and release was achieved on the monolayer and submonolayer coated regions of the aminosilane gradient surface under relatively basic pH conditions, with the help of an electrical potential. Meanwhile, DNA adsorption was found to be quasi-reversible on the multilayers at the high aminosilane end of the gradient in the relatively acidic solution. The results of these studies demonstrate the importance of manipulating the electrostatic interactions of DNA with charged surfaces in order to achieve DNA capture and release. The fundamental knowledge of the DNA-surface interactions gained in these studies will be helpful in diverse fields ranging from the layer-by-layer assembly of polyelectrolyte-based thin films to the selective electronic sensing of charged biomolecules.

In the second study, the local dielectric properties of the least polar environments in dsDNA were assessed by using the solvatochromic dye, nile red, as a polarity-sensitive probe. TIRF spectroscopic imaging methods were employed in these studies. Although the dielectric constant within the least polar regions of dsDNA was previously predicted by theoretical and computational methods, no experimental measurements of its value had been reported to date. The results provide important knowledge of the factors governing the polarity of DNA microenvironments to which intercalators bind, and provide vital experimental support for the values determined in computational studies.

In the third study, TIRF microscopy and single molecule tracking methods were employed to study DNA interactions with an opposed two-component C8-silane and aminosilane gradient surface as a function of solution pH. The mobility of surface-adsorbed DNA molecules was explored and quantified in these studies. The preliminary results further demonstrated the importance of electrostatic interactions over hydrophobic interactions in governing the adsorption of DNA to surfaces. The mobility of surface-adsorbed DNA was found to be largely independent of position along the two-component gradient. These studies were originally undertaken as a route to observation of cooperative effects that are believed to govern DNA-surface binding. Unfortunately, no clear evidence of cooperative effects was observed at the mixed regions of the two-component gradient surface.

Single-molecule fluorescence microscopy studies of DNA-surface interactions on chemically graded organosilane surfaces

By

Zi Li

B.S., Ocean University of China, 2013

A DISSERTATION

Submitted in partial fulfillment of the requirements for the degree

DOCTOR OF PHILOSOPHY

Department of Chemistry
College of Arts and Sciences

KANSAS STATE UNIVERSITY
Manhattan, Kansas

2018

Approved by:

Major Professor
Dr. Daniel A. Higgins

Abstract

This dissertation describes the application of wide-field single-molecule fluorescence microscopy techniques to investigations of DNA-surface interactions on chemically graded organosilane surfaces. The adsorption and desorption behaviors of double-stranded (ds) plasmid DNA along the amino-trimethoxysilane and octyl-trichlorosilane gradients were explored as a function of solution pH, solution ionic strength and surface properties. The results provide an improved fundamental understanding of DNA interactions with different surfaces and are certain to aid in the development and advancement of DNA-based biological and biomedical devices. Three distinct experiments were performed in completion of the work for this dissertation.

In the first study, total internal reflection fluorescence (TIRF) microscopy was employed to study DNA interactions with aminosilane gradient surfaces under relatively acidic and basic environments. Electrical potentials were applied to assist DNA adsorption and desorption. The single-molecule data clearly showed that DNA capture and release was achieved on the monolayer and submonolayer coated regions of the aminosilane gradient surface under relatively basic pH conditions, with the help of an electrical potential. Meanwhile, DNA adsorption was found to be quasi-reversible on the multilayers at the high aminosilane end of the gradient in the relatively acidic solution. The results of these studies demonstrate the importance of manipulating the electrostatic interactions of DNA with charged surfaces in order to achieve DNA capture and release. The fundamental knowledge of the DNA-surface interactions gained in these studies will be helpful in diverse fields ranging from the layer-by-layer assembly of polyelectrolyte-based thin films to the selective electronic sensing of charged biomolecules.

In the second study, the local dielectric properties of the least polar environments in dsDNA were assessed by using the solvatochromic dye, nile red, as a polarity-sensitive probe. TIRF

spectroscopic imaging methods were employed in these studies. Although the dielectric constant within the least polar regions of dsDNA was previously predicted by theoretical and computational methods, no experimental measurements of its value had been reported to date. The results provide important knowledge of the factors governing the polarity of DNA microenvironments to which intercalators bind, and provide vital experimental support for the values determined in computational studies.

In the third study, TIRF microscopy and single molecule tracking methods were employed to study DNA interactions with an opposed two-component C8-silane and aminosilane gradient surface as a function of solution pH. The mobility of surface-adsorbed DNA molecules was explored and quantified in these studies. The preliminary results further demonstrated the importance of electrostatic interactions over hydrophobic interactions in governing the adsorption of DNA to surfaces. The mobility of surface-adsorbed DNA was found to be largely independent of position along the two-component gradient. These studies were originally undertaken as a route to observation of cooperative effects that are believed to govern DNA-surface binding. Unfortunately, no clear evidence of cooperative effects was observed at the mixed regions of the two-component gradient surface.

Table of Contents

List of Figures

List of Acronyms and Definitions

2D	Two-dimensional
A	Adenine
AFM	Atomic force microscopy
APTMOS	3-aminopropyltrimethoxysilane
APTES	3-aminopropyltriethoxysilane
C	Cytosine
C8-silane	Trichloro(octyl)silane
CCD	Charge-coupled device
CE	Counter electrode
CM	Clausius-Mossotti
DCLP	Dichroic long pass filter
DI	Deionized
DNA	Deoxyribonucleic acid
dsDNA	Double-stranded deoxyribonucleic acid
FTIR	Frontier Transform Infrared
G	Guanine
HIC	Hydrophobic interaction chromatography
ITO	Indium tin oxide
LbL	Layer-by-layer
MSE	Mean-square error
NA	Numerical aperture
NR	Nile red

PBS	Phosphate-buffered saline
PCR	Polymerase chain reaction
PDMS	Poly(dimethylsiloxane)
PEO	Polyethylene oxide
PO	Paraffin oil
QCM	Quartz crystal microbalance
RE	Reference electrode
RH	Relative humidity
ssDNA	Single-stranded deoxyribonucleic acid
SE	Spectroscopic ellipsometry
S/N	Signal to noise ratio
SPR	Surface plasma resonance
T	Thymine
TIRF	Total internal reflection fluorescence
TMOS	Tetramethylorthosilicate
VPD	Vapor phase deposition
WCA	Water contact angle
WE	Working electrode
XPS	X-ray photoelectron spectroscopy
ΔH	Change in enthalpy

Acknowledgement

First but most importantly, I would like to express my sincere gratitude and deep appreciation to my major advisor, Dr. Daniel Higgins. During the five years of my PhD studies, Dr. Higgins has been providing me his constant academic guidance, continuous support and encouragement. I am highly thankful for his valuable advice in my research work, his time for revising my writings and his patience with me. He is an excellent advisor that a PhD graduate student could ask for. I feel very fortunate to have had such a wise and kind professor as my mentor.

I am also grateful to my co-advisor, Dr. Maryanne Collinson (Virginia Commonwealth University, VCU) for her scientific advice and suggestions on my research work. During the collaboration work with Dr. Collinson's group, I was lucky to be able to meet with Dr. Collinson at VCU. I could not be more thankful for her time and kindness when I was doing experiments at VCU. I would also like to thank Dr. Jun Li, for his guidance and constant help during my PhD studies. Dr. Emily McLaurin and Dr. Keith Hohn are thanked for their time and contributions as being my supervisory committee. I would like to thank Dr. Jianfa Bai for willing to be the chairperson for my final Ph.D. examination.

I would like to acknowledge the staff in Chemistry department at K-state, Ron Jackson, Tobe Eggers and Jim Hodgson. They have been very helpful in the instrumental troubleshooting and in designing experimental necessities for my research. I also acknowledge the funding support from national science foundation to our research projects.

I am very thankful to have my amazing previous and current lab mates and collaborators. Dr. Kayesh Ashraf is thanked for helping me make XPS measurements for my first gradient project, as well as his help with zeta potential measurements. Kallol Roy from Dr. Collinson's group is also thanked for his time helping me with my experiments at VCU. Dr. Luxi Swisher and

Kaushalya Perera are thanked for their help in my early PhD research. My previous lab mates, Dr. Seok Chan Park, Dr. Dipak Giri and Dr. Hao Xu are acknowledged for their time on helping me troubleshooting wide-field microscope, for their valuable research discussions with me and for their good influences on my PhD studies. I would also like to thank my current lab mates: Ruwandi Kumarasinghe and Judith Bautista. They have been very good friends to me and we support each other during our PhD studies.

Finally, my sincere gratitude falls in my family and friends. My father, Changjun Li and my mother, Ruifang Wu, have always been supporting me, providing me their unconditional love. I love them from the bottom of my heart. I am also thankful for all my friends in the U.S. and China, especially Man Zhang, Jing Yu, Bo Hao, Bo Wang, Mengjiao Wu and Anying Wang. I am so blessed to have them in my life when I first came to the U.S. I will never forget their companionship during my PhD studies. I would also like to thank my boyfriend Francisco Gonzalez and his mother for their love in the past two years and many more years coming.

Dedication

This work is dedicated to my proud and loving parents, Ruifang & Changjun.

Chapter 1 General Introduction

1.1 DNA-surface interactions

Deoxyribonucleic acid (DNA) is one of the major types of macromolecules that are essential for all life on earth. The information that a chain of DNA carries is enormous and mostly still mysterious. In order to lift the veil of mystery behind DNA, scientists have never stopped studying this incredible biomolecule since the groundbreaking discovery of the double helix, twisted-ladder structure of DNA by James Watson and Francis Crick.[1] With regard to the research on DNA, DNA interactions with surfaces are vital to immobilize DNA onto substrates for applications such as DNA barcoding,[2] gene mapping,[3, 4] drug delivery,[5] DNA biosensors[6-12] and DNA microarrays.[7, 12-15] In addition to the importance of DNA-surface interactions in advanced technologies, the fundamental knowledge of DNA interactions with charged surfaces is advantageous for studying DNA interactions with proteins.[16] Because many proteins interact with DNA via positively charged amino acids on their surfaces. Therefore, investigations of DNA interactions with the charged surfaces (i.e., aminosilane modified surfaces under acidic and neutral pH environments) can serve as models for studying DNA-protein interactions.[17] Owning to the composition and structure of DNA, DNA-surface interactions include electrostatic interactions, hydrophobic interactions, hydrogen-bonding, base-stacking (π-π) interactions and van der Waals interactions.

Over the last several decades, there has been extensive interests in the development of advanced techniques and devices for detection, analysis, and delivery of biomolecules. For example, one popular area of research has been in the development of DNA biosensors and DNA microarrays. Much effort has been devoted to these two applications for the purposes of DNA hybridization detection and performing fast diagnosis.[11, 12, 18-20] To enhance the efficiency and sensitivity of DNA biosensors and microarrays, the amount of DNA immobilized onto the

supporting substrates needs to be well controlled. Taking the DNA hybridization sensors for example, too large amount of immobilized single-stranded DNA (ssDNA) on the sensor surface will cause the steric crowding effect and consequently make it difficult for the target DNA to hybridize with the probe DNA. In the result, the efficiency of the hybridization sensors will be dramatically decreased. On the contrary, if the amount of immobilized probe DNA are not sufficient, the sensitivity of the hybridization sensor will be low. In order to achieve a higher efficiency and sensitivity for DNA hybridization sensors, in addition to optimizing surface probe coverage, another possible approach that has been used previously is to apply electrical potentials to assist DNA hybridization.[19] By applying positive electric potentials to the sensor surface, more target DNA molecules can be attracted to the surface to hybridize with the probe DNA.[19]

Many other factors such as surface properties and DNA-surface interactions can also affect the performance of DNA hybridization sensors. For instance, Elder et al.[21] have studied the effect of hydrophobic and hydrophilic surfaces on the stability of double-stranded DNA (dsDNA). The results showed that the hybridized short dsDNA can be stabilized by the hydrophobic surfaces and destabilized by hydrophilic surfaces, whereas the hybridized long dsDNA can be destabilized by the hydrophobic surfaces and stabilized by hydrophilic surfaces. This effect of surface properties on the stability of dsDNA is attributed to the more terminal bases in the short dsDNA and the large amount of central bases in the long dsDNA. Hydrophobic surfaces prefer to interact with the more hydrophobic base-stacking region of DNA, while hydrophilic surfaces might disturb the terminal hydrogen bonds between DNA base pairs.

Another example to illustrate the significance of DNA-surface interactions lies in the field of biomolecule separation and purification. Traditional techniques for DNA separation and purification require the utilization of organic solvents and chaotropic salts,[22-24] which are both

polymerase chain reaction (PCR) inhibitors. The innovation of solid phase purification devices incorporating with charged surfaces and/or applying pH-dependent DNA capture and release avoids the use of PCR inhibitory organics and chaotropes.[24-26] Moreover, these solid phase purification devices can be developed into a microchip, which is likely to shorten analysis times, reduce reagent usage and sample consumption. Obviously, the optimization of this solid phase purification device needs a full knowledge of DNA-surface interactions.

Depending upon the objectives of research on DNA interactions with surfaces, DNA-surface interactions have been studied by different types of techniques including atomic force microscopy (AFM),[27-29] fluorescence microscopy,[30-33] surface plasma resonance (SPR),[10, 12] quartz crystal microbalance (QCM),[11, 34] X-ray photoelectron spectroscopy (XPS),[35] ellipsometry,[36] etc. QCM can obtain the kinetics of DNA adsorption/desorption by analyzing the changes in quartz resonance frequency, but it cannot provide the information about where DNA molecules adsorb to, nor the behavior of adsorbed DNA on the surface.[11, 34] The same issues also occur in SPR because SPR measures the changes in reflectivity from the supporting substrates during the time when the DNA molecules interact with the surfaces and when the target DNA molecules hybridize with the immobilized probe DNA.[12] Important information related to where and how DNA molecules interact with surfaces cannot be revealed by SPR either. For AFM, although it does allow for individual molecules adsorbed to a surface to be observed, it is challenging to obtain in situ dynamic information of DNA interactions with surfaces. Single molecules fluorescence detection and tracking methods afford a means to easily obtain the dynamics and kinetics of DNA-surface interactions at different conditions.[31, 32, 37-39] In this case, the behaviors of DNA adsorption/desorption to different regions of the surface can be demonstrated by analyzing the data obtained by single molecule fluorescence and tracking methods. Therefore, in this dissertation,

AFM is employed to access the conformations of DNA adsorbed to the surfaces, and importantly, wide-field fluorescence microscopy is employed to observe and study DNA-surface interactions (DNA adsorption/desorption) in real-time under different conditions.

1.2 Surface Chemical Gradients

To study DNA-surface interactions for the applications in biological and biomedical devices, amine-terminated charged surfaces[40-43] and nonpolar hydrophobic surfaces[21, 44-47] are the most frequently used. Interactions of DNA molecules with surfaces are most commonly investigated using surfaces of uniform composition. For example, a surface with a uniform density of amine groups, carboxylic acid groups or hydrophobic hydrocarbons might be prepared and implemented in these studies. In some cases, mixed monolayers of two or more such components might be used. In depth studies of DNA-surface interactions usually proceed by preparing individual surfaces and studying DNA behaviors on them one at a time. In fact, some of the methods mentioned above (QCM) require that the surface be uniform, because they offer no spatial resolution. Moreover, preparation of a large number of samples with uniform chemical surfaces is tedious, time-consuming and less cost-effective.

One method to dramatically speed experimental throughput is to use surface combinatorial libraries with methods that afford some spatial resolution. These surfaces incorporate small regions modified by different functional groups or by mixtures of different functional groups. These are usually prepared by depositing a series of the fractions of the surface modifiers or a series of the percentages of the mixtures of the surface modifiers across sample substrates. However, such combinatorial libraries still exhibit only discrete compositional and property variations. A better option would be to use surfaces with continuous variations in composition and properties. In order to incorporating the continuity of changes in chemical compositions and surface properties, surface

chemical gradients are introduced and start to gain enormous attractions for various research studies such as the studies of DNA-surface interactions.

Surface chemical gradients are surface-bound thin films with continuously changing chemical and/or physical properties along the direction of the gradient deposition.[48-50] A number of methods have been employed to generate chemical gradients on substrates. Generally, those methods can be categorized into two typical material fabrication strategies: top-down and bottom-up approaches. In the top-down approaches, different lithography methods are often employed to generate the patterns or the shape of the gradients on the substrates, following with developing and etching procedures to obtain the final surface modifications. In the bottom-up approaches, chemical gradients are generated by gradually depositing the chemicals (e.g. oligomers, polymers) as molecular precursors through natural diffusion, or exerting external forces (e.g. controlled-rate infusion of chemicals, dipping/dragging sample substrates in/from starting chemical ingredients). The simplest and most common way to prepare surface chemical gradients was initially invented by Chaudhary et al.[51] In this method, chemical precursors (e.g. organosilanes) are vaporized and deposited on appropriate substrates from the vapor phase. The vaporized chemical precursors diffused naturally and were deposited along the length of the substrates under a certain time period. During this fixed amount of time period, the regions that are closer to the precursor reservoir have higher surface coverages of the chemical precursors and less chemical precursors are deposited at the far end of the substrate. Due to the simplicity of this method, and its applicability for the deposition of organosilane, vapor phase deposition is applied to prepare the chemical gradients in this dissertation. The details of the method will be introduced in **Chapter 3**.

The methods described above can be used to prepare surfaces suspected to incorporate chemical gradients. However, use of these surfaces as gradients requires first verifying that a

gradient has been successfully formed. Also, an in-depth understanding of the experimental results obtained along the gradient also requires detailed knowledge of the gradient properties such as wettability, hydrophobicity, charge density, etc.

To accomplish the goals mentioned above, a number of technical measurement tools have been employed to verify that gradients have been obtained and to characterize and access surface compositions, functionalities, and chemical or physical properties at positions along the surface chemical gradients. At the most fundamental level, the gradients exhibit variations in their elemental compositions. X-ray photoelectron spectroscopy (XPS) provides a route to obtaining information on the elemental composition along a gradient by probing the binding energies of the core electrons in certain atoms. This technique will be introduced in detail in **Chapter 3**. In order to obtain the thickness and roughness characteristics along a certain surface chemical gradient, spectroscopic ellipsometry (SE), as a non-destructive characterizing method, can be used to measure the changes in the polarizations of the incident light interacting with surface thin films. Because the polarization signals depend on the thickness, as well as the properties of surface materials, SE is universally employed for the analysis of thin films. Water contact angle measurements are the most common method for the confirmation of a chemical gradient that has been obtained and for the characterization of the wettability properties along a chemical gradient.

The aforementioned methods give information on the macroscopic properties of chemical gradients, but there are also many interesting questions about the microscopic variations in gradient properties. Atomic force microscopy (AFM) and singe molecule fluorescence detection represent such tools that can be used to probe the microscopic properties of surface chemical gradients. AFM measures the deflection of the laser beam reflected from the piezoelectric cantilever while it oscillates above or on the top of the operating surfaces. It can reveal the

morphological and topographical characteristics of surface chemical gradients with a high resolution in the nanometer range. Although AFM methods are helpful for obtaining the structures and topographies of surface chemical gradients, some of other surface properties such as polarity, cannot be examined by AFM. Fortunately, single molecule fluorescence detection methods employed different dye molecules with various properties can reveal the intrinsic properties of surface chemical gradients while the dye molecules are interacting with surfaces along the chemical gradients. By analyzing the data obtained from the interactions of a certain dye molecule with surfaces along the gradient, the changes in certain surface properties can be verified and characterized.

Because of the gradual changing in the surface properties on chemical gradients, surface chemical gradients have been applied in a large variety of disciplines such as material science, biology and biomedical science. First of all, in material science, chemical gradients can be used as a library of combinatorial materials allowing for the development of new materials and the optimization of the properties of materials. To this end, instead of preparing and testing a number of samples with various properties of interest, preparation of one single chemical gradient can provide the continuously changing chemical or physical properties that allow for most efficient experimentation on materials of different compositions/properties. For example, van Dover and coworkers[52] have applied a composition-spread approach to the Zr-Sn-Ti-O system, in which a single film with different compositions of those elements is fabricated in order to efficiently evaluate a wide range of compositions for the development of new capacitor materials. The application of chemical gradients as combinatorial material libraries in searching for and evaluating new materials dramatically enhances the efficiency of this originally labor-intensive process. Additionally, in biomedical science, surface chemical gradients can be employed to

investigate macromolecule (e.g. proteins and DNA) adsorption and cell adhesion on surfaces having variable wettability, hydrophobicity and polarity, for example. As representative work in this area, Jin Ho Lee and coworkers[53] have applied polyethylene oxide (PEO) chemical gradients to the investigation of the interactions of plasma proteins and platelets with PEO materials of different chain lengths and as a function of the surface density of these polymeric materials.

A common and intriguing application of wettability gradients has come from the original demonstration by the Whitesides group that they can be used to drive the motions of liquid droplets.[51] For this purpose, Giri et al.[47] have employed hydrophobic organosilane chemical gradients to drive aqueous droplets of lambda DNA solutions along a surface, leaving adsorbed, elongated and aligned DNA in their wake. The results showed that the self-propelled liquid droplets containing DNA molecules can stretch DNA efficiently, allowing for the applications in DNA barcoding and studies of protein-DNA interactions. Importantly, unlike many alternative methods for accomplishing the same elongation and alignment of DNA, this method has advantage that no external force needs to be exerted to drive the aqueous droplets. The DNA-containing water droplets placed on the wettability gradients move spontaneously along the gradient surface from hydrophobic to hydrophilic end. The use of wettability gradients to manipulate DNA or other biomolecules without external stimuli allow for the development of fully automated and inexpensive devices for the use of gene analysis and for the studies of DNA-protein interactions.

1.3 Objectives and Motivations of the Present Research

In the present research, total internal reflection fluorescence microscopy, spectroscopic imaging and single molecule tracking methods were employed to study the interactions of plasmid DNA with organosilane gradient surfaces and the dielectric properties of the interior regions of DNA. Two types of organosilane gradient precursors were employed to form thin-film gradients:

3-aminopropyltrimethoxysilane (APTMOS) and trichloro(octyl)silane (C8-silane). These precursors allowed for the investigation of electrostatic interactions and hydrophobic interactions of DNA with surfaces, one of the primary objectives of this research project. Understanding the electrostatic and hydrophobic interactions of DNA with surfaces is important to the full realization of their potential applications in designing DNA biosensors, DNA microarrays and advancing techniques of DNA purification and separations.

Another primary objective of the research performed in this dissertation is to use surface chemical gradients as a means to efficiently and comprehensively explore the interactions between DNA and surfaces of various chemical coverages along the length of the gradients. With continuous changes in chemical surface coverage, the properties of the organosilane thin-film gradients also change, altering DNA-surface interactions. In addition to organosilane surface coverage, solution pH also affects the properties of the thin-film chemical gradients, leading to the variation of DNA-surface interactions. For example, due to the protonation of amine groups on the surface under acidic and neutral pH conditions, the charge densities of aminosilane surfaces increase with the decrease in solution pH. The increase in the density of protonated amine groups on the surface might introduce stronger electrostatic interactions between the DNA molecules and the charged surfaces. By employing chemical gradients, various parameters of interest such as solution pH, ionic strength, and application of electrical potentials can be investigated efficiently.

The local dielectric properties of DNA molecules were studied as well. These studies were performed in solution and along the chemical gradients as DNA adsorbed to the gradient surfaces. A unique method was employed to determine the dielectric properties of the DNA. This involved spectroscopic imaging method of nile red doped DNA, at the single molecule level. This method involves the partitioning of nile red (a solvatochromic dye) into the interior of the DNA to detect

and quantitatively determine the dielectric constants of the DNA molecules, emphasizing the properties of the least polar environments in the DNA. Knowledge of the local dielectric properties of DNA under different conditions is vital for the design of intercalating small-molecule drugs, their applications in drug delivery systems, and for a more complete understanding of protein-DNA interactions.

1.4 Outline of this dissertation

This dissertation comprises eight chapters in total. **Chapter 2** introduces the fundamental properties of DNA, the different types of DNA-surface interactions and their importance, and the common techniques that have been employed to characterize DNA molecules adsorbed on surfaces. **Chapter 3** covers experimental details such as the fluorescent dyes employed to label DNA molecules in the present research and the preparation of thin-film organosilane gradients using the vapor phase deposition method. The methods used for characterization of the surface chemical gradients are subsequently illustrated, including water contact angle measurements, ellipsometric film thickness measurements, and X-ray photoelectron spectroscopy. The last section of **Chapter 3** describes the instrumental details of AFM and wide-field fluorescence microscopy, as they pertain to studies of DNA interactions with surfaces. In **Chapter 4**, the interactions between YOYO-1 labeled plasmid DNA molecules and aminosilane gradients prepared on silica-coated ITO substrates are investigated as a function of solution pH, applied potential, and aminosilane surface coverage. In **Chapter 5**, quantitative information on the local dielectric properties of plasmid DNA is obtained in buffer solutions with various ionic strengths and on the aminosilane gradients, using a solvatochromic dye and a unique spectroscopic imaging method. **Chapter 6** explores plasmid DNA interactions with a hydrophobic and charged two-component opposed gradient. The mobility of surface-adsorbed DNA molecules is obtained using single molecule

tracking methods under various pH environments. General conclusions and future directions of the present research are then given in **Chapter 7**. All references cited are listed at the end of this dissertation. An appendix followed after the list of references is also given, providing additional information related to the studies in this dissertation.

Chapter 2 DNA Interactions with Chemically Modified Surfaces

2.1 Properties of DNA

DNA is composed of a series of nucleotides. Each nucleotide includes a sugar moiety (deoxyribose), a nitrogenous base and a negatively charged phosphate group as the linkage between nucleotides. Four nitrogenous bases are usually found in DNA, which are, namely, adenine (A), thymine (T), guanine (G), cytosine (C). The chemical structures of these four nitrogenous bases are shown in **Figure 2.1**. Single-stranded DNA (ssDNA) binds to its complimentary strand via the formation of hydrogen bonds between pairs of the nitrogenous bases to form double-stranded DNA (dsDNA). Due to the specific shapes and hydrogen bonding properties of DNA nitrogenous bases, A and T only bond with each other, while C and G exclusively bond to each other.[54, 55] The formation of hydrogen bonds between two bases (A/T and G/C) are also shown in **Figure 2.1** with three hydrogen bonds formed in G/C base pairs and two hydrogen bonds formed in A/T base pairs. The diameter of the duplex DNA is ~ 2 nm[55, 56] and the length of each nucleotide is ~ 0.34 nm.[55] The structure of dsDNA is a double-helix incorporating shallow, wide major grooves, and deep, narrow minor grooves. The rigidity of dsDNA is higher than ssDNA due to its helical structure.[57] The rigidity or flexibility of DNA is an important property because it determines its ability to condense into small granules.[57] Much research has been devoted to developing means to control the condensation of DNA for the purpose of gene therapy.[58-61]

Double-stranded DNA can be dissociated into two ssDNA by breaking the hydrogen bonds formed between the DNA bases under conditions such as extreme pH (e.g. pH > 10 or pH < 3),[62, 63] high temperature,[55, 64] and the presence of organic solvents.[65] This dissociation of dsDNA is called DNA denaturation or DNA melting. Usually, dsDNA molecules rich in A/T base pairs are

easier to denature than those rich in G/C base pairs.[66] The reason is that A/T base pairs possess lower stacking energy than G/C base pairs.[66] To avoid DNA denaturation in dsDNA experiments, proper solution pH values and temperatures must be selected.

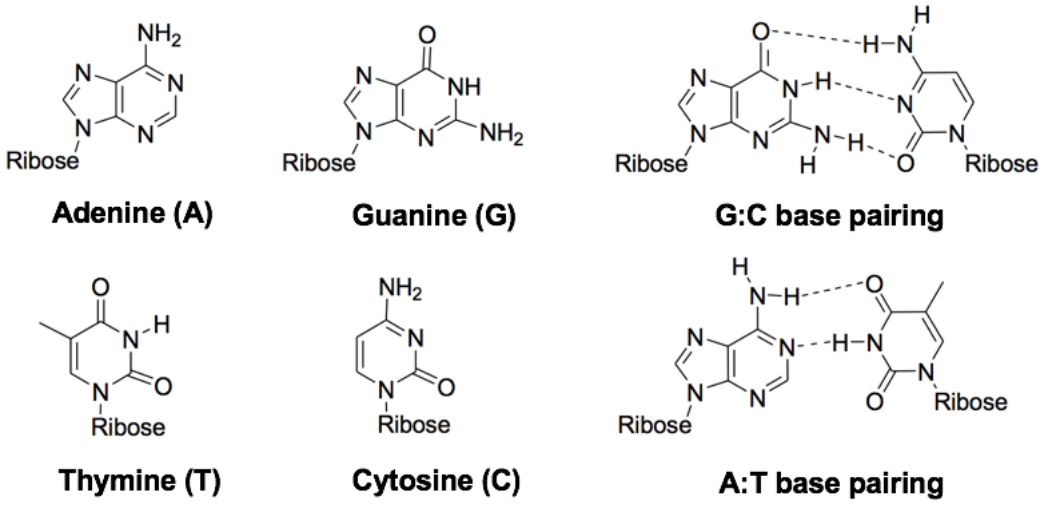

Figure 2.1 The chemical structures of four nitrogenous bases in DNA: Adenine (A), Guanine (G), Thymine (T) and Cytosine (C) and DNA base pairing of G:C and A:T via the formation of hydrogen bonds.

2.2 Types of DNA Interactions with Chemically Modified Surfaces

Due to the composition of DNA and the double helix structure of duplex DNA, various types of interactions can occur between DNA and a surface. It is necessary to study these interactions in detail for a better understanding of the applications of the interactions with surfaces. For instance, the knowledge of the interfacial behaviors of DNA with surfaces will aid in the design of DNA hybridization sensors.[21, 45, 67]

Non-covalent interactions[68] of DNA with chemically modified surfaces include base-stacking (π-π) interactions, van der Waals interactions, electrostatic interactions, hydrophobic effects and hydrogen bonding. These are interactions for which no covalent bond is present between DNA and

available binding sites on the surface. They also commonly exist in interactions of macro-biomolecules like protein-protein interactions and protein-DNA interactions.[16, 69, 70] Herein, the focus is on the three most typical interactions of DNA with surfaces. These include electrostatic interactions, hydrophobic interactions, and hydrogen bonding.

2.2.1 Electrostatic Interactions

Electrostatic interactions occur between charged molecules and charged surfaces. They can be either attractive or repulsive, depending on the signs of the charges. The simple rule is that like charges repel and opposite charges attract. As the pK_a of the phosphate groups on the DNA backbone is ~ 2,[66] DNA molecules are usually negatively charged. The negative charges on the DNA phosphate groups cause repulsive interactions between each nucleotide in DNA. Electrostatic repulsion induces the rigidity of DNA molecules.[57, 71, 72] Double-stranded DNA exhibits greater rigidity than ssDNA because of its greater charge.[57]

Negatively charged DNA can be easily adsorbed to the positively charged surfaces via electrostatic interactions. As a highly negative-charged polyelectrolyte, DNA attracts cations to neutralize the negative charges on its phosphate backbone. The charge neutralization of DNA by cations in solution screens the negative charges on DNA. This process also induces the changes in DNA structures and conformations.[27, 73] Tamar Schlick et al.[73] reported that DNA adopts highly compact and bent interwound configurations at high salt concentrations, while DNA supercoils are much more open and loosely interwound at low salt concentrations. The strength of electrostatic interactions between DNA and positively charged surfaces can be altered by the addition of salt,[74] by changing the pH,[26, 75, 76] and by manipulating the surface charge.[29, 76, 77]

Amine-terminated surfaces are the most popular surfaces for the introduction and application of the electrostatic DNA-surface interactions. For instance, Carrie et al.[76] studied DNA retention

(a fraction of the amount of DNA retained by the substrate after washing) on aminosilane modified surfaces at various solution pH. At the acidic pH (pH < 7), DNA molecules were found retained on the amine-terminated surfaces owning to the electrostatic interactions between DNA and the surface-bound protonated aminosilane. Using the electrostatic interactions between DNA and amine-terminated surfaces, Kim et al.[78] have proposed to align and immobilize DNA molecules by employing the amine-functionalized polymer films for the purpose of the nano-device fabrication. Pasquardini et al.[26] have used aminosilane coated substrates to purify genomic DNA from the human whole blood. The release of surface-bound purified DNA was achieved by washing the substrates with alkaline solutions.

2.2.2 Hydrophobic Interactions

Hydrophobic interactions happen when nonpolar molecules desire to aggregate to avoid exposing their nonpolar surfaces to polar aqueous solutions. Hydrophobic interactions are prevalent in DNA and can also participate in governing its interactions with chemically modified surfaces.[79] The nitrogenous bases are the most hydrophobic elements of DNA. The hydrophobicity exhibited by DNA has been widely studied as a means to compact DNA using condensing agents.[80-82] Compared to dsDNA, ssDNA exhibits higher hydrophobicity due to the exposure of the nitrogenous bases.[44, 83] In the dsDNA double helix, the bases are wrapped inside the helical structure. While such hydrophobic effects help in the assembly of dsDNA, positioning of the bases inside the double helix suppresses their interactions with nonpolar surfaces.[44, 46]

The fact that ssDNA shows greater hydrophobicity than dsDNA has been extensively studied as a means to purify plasmid DNA using hydrophobic interaction chromatography (HIC).[44, 46, 84] HIC has been widely employed to purify therapeutic proteins,[85] but not for plasmid DNA. In 1999, Diogo et al.[46] first proposed to use HIC as the final operation in a simple purification process to

purify plasmid DNA vector for applications in gene therapy and DNA vaccination. The nucleic acid impurities such as RNA and denatured genomic DNA exhibiting greater hydrophobic characteristics are retained in the HIC column and separated from double-stranded plasmid DNA. Nevertheless, double-stranded DNA also shows certain hydrophobic characteristics due to the hydrophobic base stacking.[86] Several research studies have explored the hydrophobic interactions between dsDNA and hydrophobic surfaces. Lei et al.[87] investigated dsDNA interactions with hydrophobic graphene oxide (GO). They demonstrated that the adsorption of DNA to GO, in the presence of divalent cations, can prevent dsDNA from being digested by enzymes. Later, Kim et al.[86] reported the effect of pH and salt on dsDNA adsorption on the hydrophobic GO. The results showed that dsDNA adsorbed progressively as the solution pH decreased from 6.0 to 4.0 because of the decrease in electrostatic repulsion between DNA and carboxylate groups on the GO. They also stated that the addition of salt, especially the divalent cations, enhances the hydrophobic interaction between DNA and graphene oxide. This enhancement in hydrophobic interactions is also attributed to the decrease in the repulsive interactions between negatively charged DNA and GO surfaces by salt electrostatic neutralization.

2.2.3 Hydrogen-bonding

The formation of a hydrogen bond requires a hydrogen that is covalently bonded to an electronegative atom (C, N, O, F) and another electronegative atom that is in a close proximity with the hydrogen. The nitrogenous bases of DNA form base pairs with each other via the formation of hydrogen-bonds. G/C base pairs form three hydrogen bonds, whereas A/T base pairs simply form two hydrogen bonds. The large number of hydrogen bonds between complementary base pairs, along with the base stacking interactions in DNA provide greater structural stability. However, rather than hydrogen-bond base pairing, base stacking interactions (π-π interactions)

are actually the major contributors to duplex stability.[88-90] This conclusion is supported by the observation that double helix formation is not driven by entropy but rather by enthalpy.[91] To explain this phenomenon in detail, first, the nitrogenous bases of ssDNA form hydrogen bonds with the surrounding water molecules in solution. To form the duplex structure of dsDNA and the hydrogen bonds between bases, the hydrogen bonds between the bases of ssDNA and water molecules must be broken. Thus, upon duplex formation, the net change in enthalpy is due to ΔH (hydrogen bonds formed) $-\Delta H$ (hydrogen bonds broken). This process is exothermic for DNA duplexes of any length at ambient temperature.[92] However, the formation of dsDNA through hydrogen bonding of two ssDNA is unfavorable in the entropy point of view. The hydrophobic base stacking interactions stabilize and protect the hydrogen bonds between the bases. Without the base-stacking interior, those hydrogen bonds would be easily destroyed. Therefore, the stability of the duplex structure of DNA is mainly because of the base stacking interactions. Besides the hydrogen bonds between the base pairs, the functional groups on their outer edges are exposed to the surrounding aqueous solutions. Those functional groups are accessible in the major and minor grooves of DNA. This is also the reason that dsDNA molecules can bind to other molecules like proteins or small drugs though major or minor groove binding.

2.3 Characterization of DNA Conformations and Behaviors on surfaces

2.3.1 AFM Imaging of Static Surface-Adsorbed DNA

Information on the morphological and structural characteristics of surface-adsorbed DNA is often acquired by AFM imaging.[27-29, 93-95] Mica substrates are commonly used for AFM imaging of DNA because their surfaces can be atomically smooth, allowing for the features of DNA supported on these surfaces to be directly visualized. Since DNA and mica are both negatively charged in solutions, electrostatic repulsions between them prevent DNA molecules from

adsorbing to mica surfaces. The attachment of DNA to mica surfaces can be accomplished by two approaches. In one case, modification of the bare mica substrate with aminosilane such as 3-aminopropyltrimethoxysilane is necessary to fix the DNA molecules to the mica surface.[27, 28, 96] Under acidic or neutral pH solutions, the protonated, surface-bound amine groups lead to DNA adsorption via electrostatic interactions. In another case, DNA can be adsorbed onto clean mica surfaces by addition of divalent cations to the DNA solution. The most commonly used divalent cation is Mg^{2+}. The divalent cations function as a bridge between the negatively charged DNA and mica surfaces, inducing DNA adsorption to the surface.

A number of studies have employed AFM to study the effects of solution ionic strength on DNA adsorption and conformation. For example, by using AFM, Pastre et al.[97] found that surface-adsorbed DNA molecules can be progressively released by increasing salt concentrations. In the AFM images, they found that the loosely bound DNA molecules appeared as bright dots, while the strongly bound DNA molecules clearly showed their conformations. In addition, DNA compaction (or condensation) by multivalent cations has also been investigated by using AFM. Tongu et al.[98] employed AFM and observed that DNA was compacted in the presence of spermidine (3+) and Mg (2+) multivalent cations. Moreover, DNA stretching behaviors on the silanized mica surfaces have also been studied by AFM.[28, 99] Recently, Liu et al.[100] studied DNA self-assembly on the mica surfaces by AFM imaging. Short DNA duplexes as nano-motifs can self-assemble into different 2D arrays on the mica surface by manipulating DNA-surface interactions. The self-assembled 2D arrays of DNA were clearly observed under AFM. These self-assembled DNA arrays on surfaces provide potential applications in structural DNA nanotechnology[101] and high-resolution molecular lithography.[102, 103]

2.3.2 Fluorescence Microscopy

Fluorescence microscopy has been widely applied to study the dynamics of DNA in solution and on surfaces.[31, 37, 104, 105] Specifically, total internal reflection fluorescence (TRIF) microscopy is often employed to examine the dynamics of conformational changes and adsorption/desorption behaviors of DNA at liquid/solid interfaces.[30, 31, 106] By staining DNA molecules with appropriate dyes, direct visualization of DNA conformational changes as a function of pH, buffer concentration, various surface modifications, can be easily achieved. Observation of DNA by fluorescence microscopy in real time enables the study of DNA-surface interactions at the single molecule level. Single molecule studies take each interaction event into consideration rather than averaging the results. Numerous studies of DNA interactions with various surfaces demonstrating the utility of single molecule experiments have been published recently. For example, Edward Yeung's group has employed TRIF microscopy to monitor the motion and adsorption/desorption behaviors of DNA at the fused-silica/water interface and the C18/water interfaces as a function of pH and buffer composition.[31] They also studied the driving force of DNA adsorption by the addition of methanol for modulating hydrophobic interactions in aqueous solution.[31] Their results provided data necessary to help better understand chromatographic separations of DNA.

2.4 Applications

A full understanding of DNA-surface interactions under various circumstances can aid in the development of advanced DNA-related devices such as DNA biosensors, DNA microarrays, DNA purification and extraction chips. Depending on the application of interest and surface modification of different devices, a comprehensive understanding of DNA adsorption and desorption behaviors is of importance for the innovation and optimization of new devices. Several examples of what has been reported in the literature are given below.

Takahito Nakagawa et al.[25] have fabricated an aminosilane coated microchip device for DNA extraction. This device employed the electrostatic interactions between DNA and protonated amine groups on the microchip surfaces at pH ~ 7.5 to capture the DNA. In these studies, DNA capture was optimized by changing the surface amine density. The captured DNA molecules were then collected by eluting with an alkaline buffer of higher pH. The buffer released the DNA by deprotonation of the protonated amine groups. The ability to control the surface charges on amine-terminated surfaces by changing the solution pH affords the means to control DNA adsorption and thus can be used in the development of devices for DNA capture and release. In later work from the same research group, Tsuyoshi Tanaka et al.[40] employed aminosilane-modified magnetic nanoparticles to investigate the role of phosphate ions in controlling DNA adsorption/desorption behaviors for applications in DNA purification. As a result, they found that the addition of phosphate ions suppresses DNA adsorption to aminosilane-modified magnetic nanoparticles but facilitates DNA desorption behaviors. This phenomenon can be used to efficiently recover the adsorbed DNA molecules from the aminosilane-modified magnetic nanoparticles during DNA purification.

Juewen Liu's group[7] has summarized the recent developments in studies of DNA adsorption and desorption onto gold nanoparticles and graphene oxide as a function of salt concentration, solution pH, temperature, and DNA secondary structure. While DNA adsorption occurs on gold nanoparticles via the electrostatic interactions with the presence of salts, adsorption on graphene oxide happens via aromatic stacking and hydrophobic interactions. Better knowledge of these phenomena will contribute to the development and optimization of DNA biosensors and microarrays.

Biwu Liu and Juewen Liu have studied ssDNA adsorption by ITO nanoparticles.[107] Due to the high conductivity and optical transparency of ITO, it has become a popular material for biosensor development. In their study, ssDNA adsorption by ITO nanoparticles was investigated as a function of surface charge, solution ionic strength, DNA length and sequence. They found that ssDNA adsorption onto ITO was driven by electrostatic interactions between the phosphate groups and the ITO surfaces at acidic pH. The positively charged ITO surfaces under the acidic conditions were verified by zeta potential measurements. However, the origin of the positive charges on ITO surfaces was not mentioned in the paper. The addition of salt can screen the electrostatic repulsions between DNA and ITO at slightly alkaline pH. DNA desorption can be achieved by adding phosphate ions because phosphate ions can displace the adsorbed DNA at the ITO nanoparticle surfaces. This fundamental and systematical study of DNA adsorption by ITO nanoparticles provides significant insights into DNA interactions with ITO surfaces. The knowledge obtained will aid in the development of DNA biosensors.

2.5 Summary

In summary, three important DNA-surface interactions – electrostatic interactions, hydrophobic interactions, and hydrogen bonding – were discussed in this chapter. Examples of each interaction were given in order to understand them in detail. The methods that were employed for characterizing DNA-surfaces interactions (i.e., atomic force microscopy and fluorescence microscopy) were also introduced. Previous research studies that used these two characterization techniques were also selectively provided. Finally, specific examples of applications in DNA-surface interactions were described for the purpose of understanding the importance of studying DNA-surface interactions.

Chapter 3 Experimental Consideration

3.1 DNA Staining

In order to detect and visualize DNA using fluorescence microscopy, it is essential to label the DNA molecules with fluorescent dyes. The identification of appropriate fluorescent dyes for DNA staining is also of vital importance for future studies at the single molecule level. Fluorescent dyes can be attached to DNA either through covalent or noncovalent binding. Covalent binding of fluorescent dyes to DNA molecules often involves modifications of DNA with specific functional groups at its 3' or 5' ends. These functional groups form the desired covalent bonds to corresponding functional groups added to the fluorescent dyes. Covalent attachment of the dye to DNA forms a robust linkage. However, this process can be costly and time-consuming. In contrast, noncovalent attachment of the dye can be much simpler and more general, if less robust. **Figure 3.1** shows the three different noncovalent binding modes by which fluorescent dyes most commonly interact with DNA during staining. These are intercalation, groove binding, and external binding. Groove and external binding of the dyes to DNA often involves electrostatic interactions between the dyes and DNA molecules. The dye may also interact with the exposed bases within the DNA grooves. Intercalation involves insertion of the dyes between the DNA base pairs and is usually driven by π - π stacking or hydrophobic interactions. Intercalating dyes are exclusively employed in the work described in this dissertation. The staining ratio, or more specifically, the DNA base-pair-to-dye ratio, is an important parameter that needs to be controlled carefully to effectively label the DNA molecules, while avoiding distortion of the DNA structure. If loading of the DNA by fluorescent dyes is too significant, distortions of the DNA structure may occur and these can lead to a change in the persistence length of the DNA, and its full contour length.[108] These changes are often associated with an unwinding of the DNA double helix.[109]

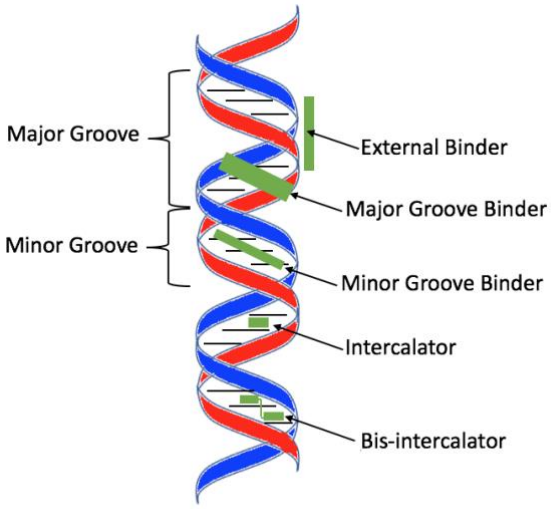

Figure 3.1 Schematic diagram of different binding modes of dyes to DNA.

3.1.1 YOYO-1 as a Fluorescent Stain of DNA

1,1'-(4,4,8,8-tetramethyl-4,8-diazaundecamethylene)bis[4-[(3-methylbenzo-1,3-oxazol-2-yl)methylidene]-l,4-dihydroquinolinium] tetraiodide, known as YOYO-1, is the most widely used cyanine dye for DNA staining. It is an intercalator that inserts between DNA base pairs. The difference between YOYO-1 dye and other common intercalators is that it contains two monomers (**Figure 3.2a**) that can simultaneously intercalate between two sets of DNA base pairs. This binding mode has therefore been appropriately named the bis-intercalating mode (**Figure 3.1**).

While YOYO-1 binds strongly to the DNA through bis-intercalation, it also affords other advantages that help make it a nearly ideal stain for DNA imaging. YOYO-1 has very low intrinsic fluorescence in the absence of DNA but exhibits a large enhancement of fluorescence upon binding to DNA. The low fluorescence of free YOYO-1 in aqueous solution is attributed to the rapid non-radiative decay of the excited YOYO-1 dye via torsional motions of the methane bridge located between the two aromatic rings at the ends of the YOYO-1 molecule (**Figure 3.2a**). However, the intercalation of YOYO-1 dyes between the DNA base pairs restricts their conformational mobility,

allowing for the enhancement of their fluorescence up to 1000 folds.[110] The peak absorption and fluorescence emission wavelengths of DNA-bound YOYO-1 are 489 nm and 509 nm, respectively. These wavelengths are easily accessible using modern laser light sources and common optical detectors such as photomultiplier tubes and CCD cameras.

The high affinity of YOYO-1 for DNA makes it a very attractive dye for staining of DNA in optical imaging experiments. However, as mentioned earlier, staining ratio of dyes can cause distortion of the DNA structure. The following result is the alteration of mechanical properties of DNA. These changes caused by YOYO-1 intercalation have been widely studied.[111, 112] Several research groups have shown that the contour length of DNA increases by 35 ~ 38 % at a staining ratio of one YOYO-1 dye per four base pairs.[111] Therefore, careful consideration of such factors is required when employing YOYO-1 as a DNA staining dye.

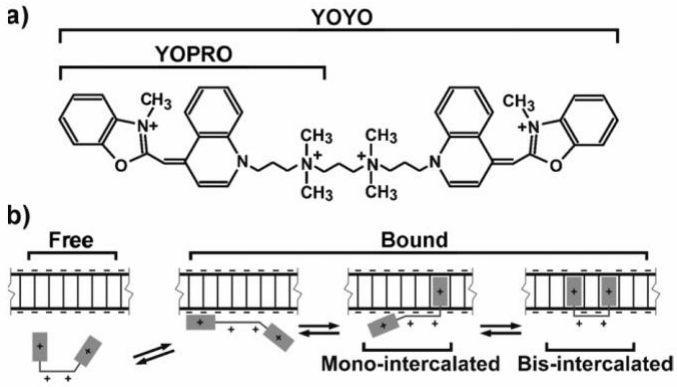

Figure 3.2 a) Structure of YOYO-1 dye b) Schematic diagram of YOYO-1 binding with DNA.[113] Reproduced with permission from Ref (113). Copyright Angewandte Chemie International Edition 2012, 51, 1811-1815.

3.1.2 Nile Red (NR) as a Fluorescent Stain of DNA

Nile Red, as a highly fluorescent, solvatochromic dye, has been extensively employed to examine the dielectric properties of different materials such as liquids,[114] organic polymers,[115, 116]

zeolites,[117] nanotubes[118] and mesoporous silica.[119] The structure of NR is shown in **Figure 3.3**. Computation models suggest that NR could bind to DNA either through intercalation or minor groove binding.[120] However, experimental work presented later in this dissertation (**Chapter 5**) clearly demonstrates, for the first time, that NR behaves as an intercalator, likely binding to DNA through interactions of its aromatic rings with those of the DNA bases. As with YOYO-1, NR is also non-fluorescent in aqueous solution but becomes highly fluorescent in nonpolar environments like those experienced upon intercalation into DNA. The increase in fluorescence yield of NR upon binding to DNA comes from restriction of certain molecular motions that otherwise provide a pathway for fast non-radiative decay of the NR in its excited state.[121] Namely, intercalation into hydrophobic environments within DNA limits its ability to form a twisted intramolecular charge transfer state upon excitation.[121]

The details of the solvatochromic shift in NR emission upon binding to DNA provide strong evidence that binding occurs through intercalation. Solvatochromism in NR is manifested as a red shift in its adsorption and emission spectra of NR with an increase in the micropolarity of its surroundings.[122] This behavior of NR also allows it to be used as a means to determine the dielectric constant of the least polar regions within the DNA molecule. In work described later in this dissertation (**Chapter 5**), NR is also used for the first time to experimentally confirm that the base pair stacks found in dsDNA have a very small dielectric constant, and to provide quantitative measurements of its value.

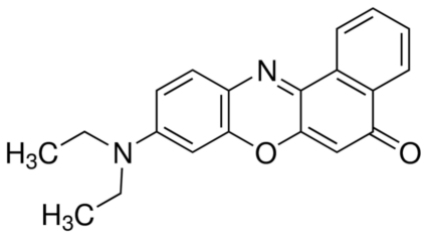

Figure 3.3 Structure of the Nile Red (NR) dye.

3.2 Preparation of Chemical Gradients

Various methods for preparing chemical gradients have been proposed and applied in different studies. Among all the gradient preparation approaches reported to date, vapor phase deposition (VPD) is the simplest way to form a chemical gradient on flat surfaces. Therefore, the chemical gradients employed in **Chapters 4, 5, 6** were all prepared by VPD. The details of the VPD method, as implemented in this dissertation, are described below.

3.2.1 Silica Base Layer

Our group has shown that the chemical gradients of organosilane precursors are most efficiently formed on a silica base-layer-coated substrate.[123, 124] The silica base layer is necessary to provide sufficient hydroxyl groups on the substrate surface to facilitate further modification by organosilane precursors. Thus, chemical gradients employed in this dissertation were all prepared using silica base-layer-coated substrates of indium-doped tin oxide (ITO), glass coverslips and silicon wafers.

Silica base layers were formed on the aforementioned substrates by spin coating (5000 rpm, 30 s) a silica sol prepared by mixing tetramethylorthosilicate (TMOS, 98%), 200 proof ethanol, and 0.1 M hydrochloride acid in a volume ratio of 1:99.6:5.4. The mixture was stirred for 1 h and then stored in a desiccator for 23 h prior to use. The base layer adhered best to the surface of recently cleaned substrates. Therefore, the ITO slides, glass coverslips and silicon substrates employed were plasma cleaned for 5 min before spin coating of the base layer. The silica base-layer-coated substrates were stored in a desiccator for at least overnight prior to use.

3.2.2 Vapor Phase Deposition of Organosilanes

Vapor phase deposition was employed in the preparation of organosilane chemical gradients. As noted above, all such gradients were prepared on silica base-layer-coated substrates. The VPD method was originally reported by Chaudhury and coworkers.[51] In this method, a clean substrate is exposed to organosilane vapor from a reservoir containing the organosilane precursor dissolved in a suitable solvent such as toluene or paraffin oil. The organosilane precursor vaporizes from the reservoir and diffuses to deposit onto the clean base-layer-coated substrate. A surface chemical gradient is formed by the concentration gradient that appears above the substrate due to the diffusion profile of the precursor vapor in the gas phase.

The chemical gradients employed in **Chapter 4, 5** and **6** were prepared by VPD on TMOS base-layer-coated substrates. **Figure 3.4** shows the apparatus used to deposit the aminosilane gradients in **Chapters 4, 5** and **6**. It includes a platform to support the substrate and the aminosilane reservoir. These elements were housed inside a Plexiglas chamber that allowed for control over the ambient relative humidity (RH). It is well known that silanes require a small amount of water present on the substrate to allow for hydrolysis of the silane and its condensation with the surface.[125, 126] The chamber was also critically important in helping to eliminate air currents that otherwise would destroy the diffusion profile of precursor vapor.

While gradients can be obtained from the vapor diffusion profile alone[127] in work performed for this dissertation, it was found that better reproducibility in the position and steepness of the gradient could be achieved when a barrier was added to restrict diffusion of the silane precursor vapor. To this end, two PDMS spacers (14 mm × 3 mm × 1 mm) were attached to the long edges of the substrate at a distance of 8 mm or 12 mm from the short edge of the 22 × 26 mm ITO slides (**Chapter 4** and **Chapter 6**) or the 25 × 25 mm glass coverslips (**Chapter 5**). A cover slip was

placed over the spacers to form a 1 mm (**Chapter 4 and 5**) and 2 mm (**Chapter 6**) deep gap between the cover slip and the base-layer-coated substrate. The cover slip afforded better control over the organosilane deposition so that monolayer-to-submonolayer films of the prepared gradients were produced at the same location in replicate depositions.

Additional details pertaining to gradient deposition included that the substrate was positioned 4 mm from the precursor reservoir. Gradient formation was found to be strongly dependent upon distance between the substrate and reservoir, so significant effort was devoted to finding this optimum distance. Gradient deposition was initiated by filling the reservoir with a mixture of 0.2 g of paraffin oil and 25 µL or 50 µL of organosilane precursor through a small inlet on the top of the Plexiglas chamber. The RH inside the chamber was maintained at 45% ~ 55% for organosilane depositions.

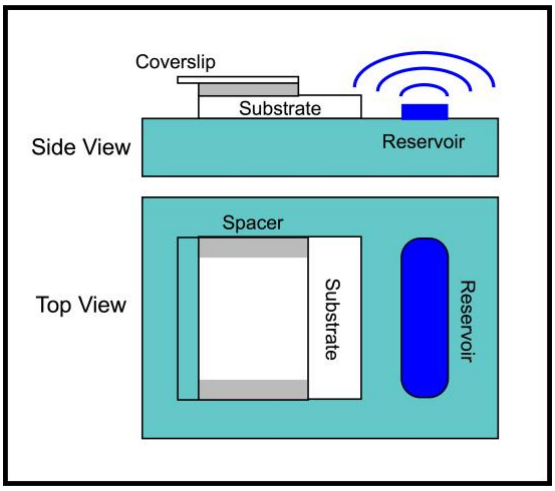

Figure 3.4 Apparatus used for APTMOS deposition in the vapor phase. The base-layer-coated substrate was placed on a platform (light blue) next to a reservoir filled with an APTMOS/paraffin oil mixture (dark blue). The substrate was partially covered with a

coverslip to define the location of the gradient. The coverslip was separated from the substrate by a PDMS gasket (gray).

The organosilanes employed to prepare chemical gradients in this dissertation were 3-aminopropyltrimethoxysilane (APTMOS, **Chapters 4, 5,** and **6**) and trichloro(octyl)silane (C8-silane, **Chapter 6**). They were chosen specifically to allow for studies of the electrostatic interactions and hydrophobic interactions of DNA with surfaces, as well as the dielectric properties of DNA adsorbed to such surfaces.

3.3 Characterization of Chemical Gradients

Different techniques including classical measurements of water contact angles, spectroscopic ellipsometry and X-ray photoelectron spectroscopy, have been employed to characterize the surface chemical gradients prepared for use in this dissertation.

3.3.1 Water Contact Angle (WCA) Measurements

Water contact angle measurements are the most common measurements used for characterizing the macroscopic wettability properties of materials in general and are the most relevant to this dissertation. Herein, sessile drop WCA measurements were used to determine the wettability of the surface chemical gradients that were prepared for the different experiments. The apparatus employed was built in house and is shown in **Figure 3.5**. All the components of this apparatus were fixed on an optical table. In making WCA measurement, the chemical gradient sample was placed on the sample stage. Droplets comprising 1 μL volumes of highly purified water (18 MΩ ·cm resistivity) were then dispensed along the gradients using a microliter syringe. Light from a tungsten lamp, delivered through an optical fiber placed next to the sample, was used to illuminate the droplets for imaging purposes. Images of water droplets on the surfaces were

obtained using a CCD camera attached to a Navitar zoom lens. The droplet images were analyzed using a drop analysis plugin installed in the freely-available ImageJ software package.[128] By this method, the WCAs at different positions along the surface chemical gradients were obtained. Water contact angles were typically measured at 3 mm intervals along each gradient, with three replicate measurements obtained at 3 mm spacings across each gradient.

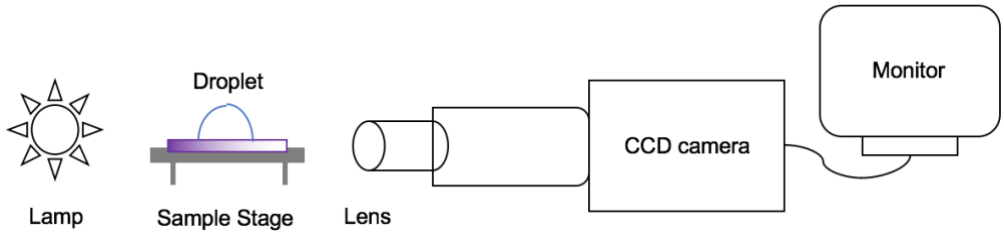

Figure 3.5 Homebuilt apparatus for WCA measurement.

3.3.2 Spectroscopic Ellipsometry (SE) Measurements

Spectroscopic ellipsometry is a nondestructive and noncontact optical technique that has been used to characterize the physical properties of thin films including the film thickness, roughness, refractive index, etc. In this dissertation, SE was employed to measure the thickness of the silica base layer and of the chemical gradient overlayer. The SE instrument (α-SE, J.A. Woollam) employed in this dissertation is composed of a light source, a polarization generator, a polarization analyzer and a detector as shown in **Figure 3.6**. In SE, a change in the polarization state of light reflecting from the surface is measured by the polarization analyzer and detector. The change in polarization is represented by two parameters: the amplitude ratio (ψ), and the phase difference (Δ). These two parameters are related to the ratio of the reflectivity of p- and s-polarizations. Thus, the complex reflectance ratio (ρ) is determined from the measurements of the amplitude ratio and

the phase difference of s- and p-polarized light reflecting from the surface, as defined in **Equation 3.1**.

$$\rho = \frac{r_p}{r_s} = \tan(\psi)\ e^{i\Delta} \qquad \textbf{(Equation 3.1)}$$

As SE measures the ratio of the two reflectance values, it is very accurate and reproducible. However, SE is an indirect method since the film properties cannot be directly acquired in the measurement. Instead, a model must be generated and used to interpret the data. Here, the SE raw data were fitted to the "Si with Transparent Film" model provided in the CompleteEASE software. Due to the similarity in refractive index of the silica base layer and organosilane (n = 1.45) gradients, a single layer model was employed for the analysis.

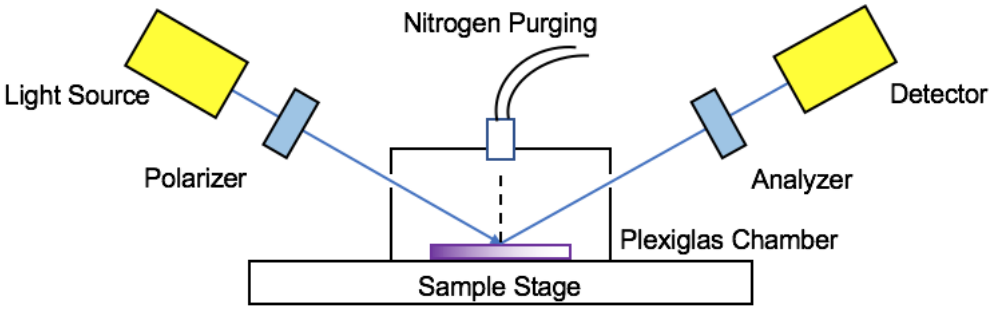

Figure 3.6 Diagram of spectroscopic ellipsometry instrument used for film thickness measurements.

The samples used for thickness measurements were all prepared on silicon substrates. The silicon wafers were cut into a rectangle of 22 × 26 mm dimensions (**Chapter 4** and **6**) or a square 25 × 25 mm in size (**Chapter 5**). The reflectivity of visible light from silica slides is simply too weak to achieve sufficient sensitivity to the deposited gradient films. Use of the silicon wafers yielded the greatly enhanced reflectivity and hence the enhanced sensitivity required to

characterize nanometer and sub-nanometer thick films. Prior to gradient deposition, the thickness of the silica base layer was first measured at a series of positions at 1 mm intervals along the substrate and at three positions across the substrate at 3 mm intervals. After gradient deposition, the full film thickness (silica base layer plus chemical gradient) was measured in the same manner again. The thickness of the chemical gradient was determined by subtracting the base-layer thickness from the full film thickness. To avoid water adsorption during the measurements, all SE measurements were conducted under a dry ($15 \pm 1\%$ RH) atmosphere by purging nitrogen into a Plexiglas chamber placed over the sample. Two holes were drilled into the sides of the chamber to allow the light to pass though the chamber for SE analysis.

3.3.3 X-ray Photoelectron Spectroscopy (XPS)

X-ray photoelectron spectroscopy is a powerful and widely-used technique for characterizing the surface elemental composition of a material. In XPS experiments, a sample surface is irradiated by a beam of X-rays, causing photoelectrons to be emitted from the sample. The kinetic energy of the emitted electrons is then measured to determine their binding energy. The binding energy depends upon several factors such as the element being detected, the orbitals from which the electrons are emitted, and the chemical environment. XPS spectral data show the intensity of the emitted electrons as a function of binding energy. The binding energies of the peaks in the XPS spectra can reveal the elements composition of the film surface that exist on the sample surface.

Herein, XPS was employed to characterize the aminosilane gradient prepared in **Chapter 4**. All XPS measurements were performed on a Thermo Fisher ESCAlab 250 imaging spectrometer. This instrument uses an Al Kα source (1486.68 eV). XPS spectra were obtained at regular intervals along the gradient, starting at 1 mm from the high amine end. A 200 μm spot size, 50 eV pass energy, and a 0.1 eV step size were used. Effects due to charging of the sample surface were

eliminated by measuring all peaks relative to the C(1s) peak at 284.6 eV. The peak of interest is that of the N(1s) orbital. It appears as two separate bands centered at 399.2 eV and 401.6 eV. The former is attributed to free amine, while the latter is assigned to protonated or hydrogen bonded amine sites. The area under the N(1s) peak was obtained by fitting the peaks and subtracting the neighboring background, followed by integration of the signal.

3.4 Instrumentation

3.4.1 Atomic Force Microscopy (AFM)

Atomic force microscopy has been widely used to obtain the surface morphological and structural characteristics of various materials including nanoparticles,[129] carbon nanotubes,[130, 131] polymers,[132, 133] as well as biomolecules like nucleic acids.[27, 28, 94] In this dissertation, AFM was employed to image the supercoiled and relaxed plasmid DNA used in **Chapter 5** and to image the surface-adsorbed supercoiled DNA in **Chapter 6**. In this case, a Digital Instruments Multimode AFM with Nanoscope IIIa electronics was employed. To avoid damaging or otherwise altering the structures of surface-adsorbed DNA molecules, taping mode AFM was employed for imaging. All AFM imaging was performed in air. The scan rate was 0.5 Hz. In order to obtain detectable features due to the surface-adsorbed plasmid DNA, all DNA imaging experiments were performed on aminosilane gradient modified mica surfaces (**Chapter 5**) or on C8-silane and aminosilane two-component opposed gradient modified mica surfaces (**Chapter 6**). DNA solutions were prepared by diluting $1\mu L$ of the stock DNA (1000 μg/mL) with 899 μL of 1 mM Tris-HCl buffer (pH ~ 7.1) and 100 μL of 10 mM $MgCl_2$. A final DNA concentration of 1 μg/mL and 1 mM of $MgCl_2$ was employed to image intact single DNA molecules adsorbed on the surface. The addition of Mg^{2+} allows for stronger adsorption of DNA to the surface. DNA deposition was achieved by incubating

its solution on the organosilane-modified surfaces for 10 min. The sample was then rinsed with highly purified water (18 MΩ ·cm resistivity) and blown dry with nitrogen.

3.4.2 Wide-Field Fluorescence Microscopy

Wide-field fluorescence microscopy has been extensively applied to visualize the features of biological cells[134, 135] or to examine the dynamics of biomolecules,[32, 37, 105] polymers[119, 136, 137] and small organic dye molecules.[118, 127, 138] The light passing into a wide-field microscope illuminates the entire field of view of the sample so that large numbers of fluorescent molecules can be observed and detected simultaneously. For example, the illumination area of the sample is 32 μm × 32 μm in **Chapter 4**. The most important component in the wide-field microscope system is the objective lens. Two parameters are used to describe the properties of the objective: its magnification and numerical aperture (NA). While the magnification determines how large the image is magnified, the NA defines the brightness and the resolution of the recorded fluoresce images or videos. As NA = $n\sin\theta$, the value of NA for a certain objective lens depends upon the reflective index of the imaging medium (n) and the half-angle (θ) defining the cone of light collected. With higher n (e.g. n = 1.52 for the medium of oil) and larger θ, larger NA can be achieved. Since NA is inversely proportional to the resolution (the smallest distance that can be resolved between two objects), better resolution can be obtained by using an objective lens with larger NA. An oil immersion objective lens (n = 1.52 for the oil media, 100 X and NA = 1.49) was employed in the optical experiments performed in this dissertation to efficiently capture light from the sample and to achieve the highest possible spatial resolution. Wide-field fluorescence microscopy has been employed to investigate DNA interactions with chemical gradient surfaces (**Chapter 4** and **6**) and to quantitatively analyze the dielectric properties of plasmid DNA

(**Chapter 5**). The following sections introduce two specific techniques that are based upon wide-field fluorescence microscopy and are employed in this dissertation.

3.4.2.1 Total Internal Reflection Fluorescence (TIRF) Microscopy

Total internal reflection fluorescence microscopy is an extension of conventional epi-fluorescence microscopy. Instead of exciting every fluorophore present in the sample as epi-fluorescence does, TIRF mode microscopy focuses on exciting fluorescent molecules at the interface between the sample and its neighboring medium. The background fluorescence signals in the bulk solution can be efficiently eliminated by employing TIRF microscopy. Hence, the signal to noise (S/N) ratio is improved and much clearer fluorescent images can be obtained using TIRF microscopy. The mechanisms and differences between epi-fluorescence and TIRF microscopy are shown in **Figure 3.7**, and will be described in the following text.

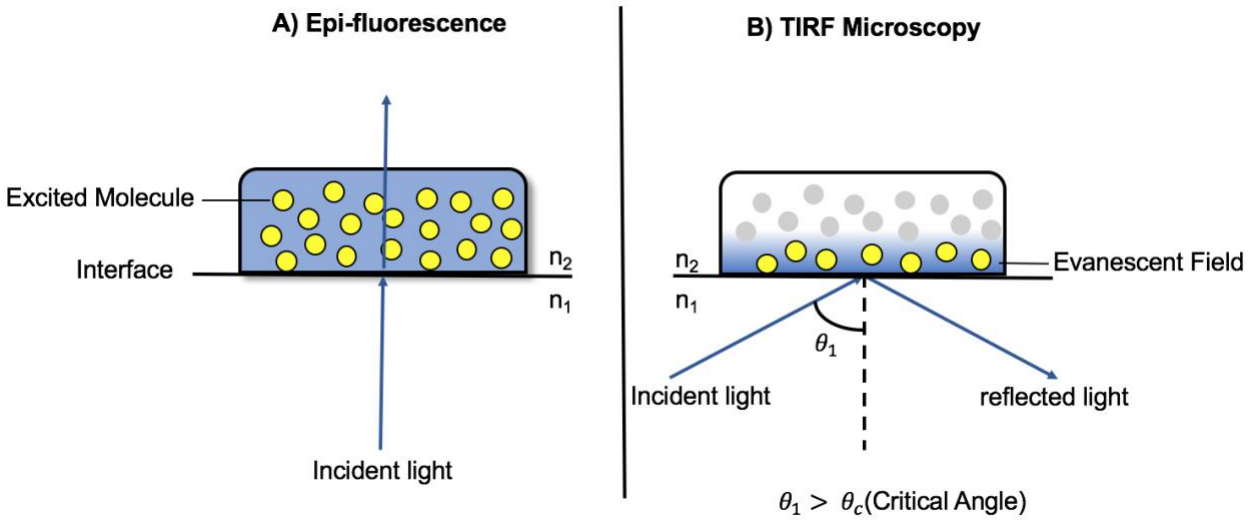

Figure 3.7 Schematic diagram of A) epi-fluorescence and B) TIRF microscopy.

The basic process of TIRF mode microscopy makes use of the fact that the total internal reflection occurs when the excitation light passes from one medium to another at a certain angle. For total internal reflection to occur, the first medium that the light passes through must have

higher refractive index (n_1) than that of the second medium (n_2). Refraction of light from the interface follows Snell's Law, as given in **Equation 3.2**:

$$n_1 Sin(\theta_1) = n_2 Sin(\theta_2) \qquad \textbf{(Equation 3.2)}$$

where θ_1 represents the incident angle in the first medium, with respect to the normal of the interface, while θ_2 represents the refracted angle in the lower-refractive-index medium. As the incident angle θ_1 reaches a certain value called the critical angle, the refracted angle θ_2 becomes 90˚. When the incident angle is larger than the critical angle, the light is totally internally reflected from the interface. Even though the excitation light cannot travel into the second medium, a small portion of the light penetrates a short distance into the second medium, generating an evanescent field or wave. The distance (d) that the evanescent field penetrates into the second medium is governed by the following equation (**Equation 3.3**):

$$d = \frac{\lambda_0}{4\pi}[n_1^2 Sin^2\theta_1 - n_2^2]^{-1/2} \qquad \textbf{(Equation 3.3)}$$

where λ_0 is the wavelength of excitation light in a vacuum, n_1, n_2 and θ_1 are the same as described above. The value of d is in the range of 100 nm to 300 nm depending on the parameters shown in **Equation 3.3**. The intensity of the evanescent field (I) decays exponentially with distance (z) in the z direction perpendicular from the interface following **Equation 3.4**:

$$I(z) = I_0 e^{-z/d} \qquad \textbf{(Equation 3.4)}$$

Here, I_0 represents the intensity of incident light at the interface, where the distance from the interface (z) is zero. As z increases, $I(z)$ decreases exponentially. Owing to this phenomenon, only those molecules within the evanescent field are excited, while those outside the field are not. Therefore, fluorescence background from molecules far from the interface is largely eliminated in TRIF microscopy.

In this dissertation, all the optical experiments were conducted using TIRF microscopy to better visualize DNA molecules at the chemical gradient surfaces. In the experiments, a high magnification oil immersion objective (100 X) with large numerical aperture (NA = 1.49) was employed to efficiently capture light emitted by the dye molecules and to enhance the resolution of fluorescence images and videos collected. TIRF mode was accomplished by using a prism. In this case, a prism attached to a clean glass coverslip was placed on top of the oil immersed objective. The prism allows one to observe the incident light and then to adjust the angle of the incident light to be greater than its critical angle, consequently generating the total internal reflection. This method for achieving the TIRF mode is simple and robust.

The wide-field microscope setup used in **Chapter 4** and **Chapter 6** is shown in **Figure 3.8**. In this case, a 488 nm laser was employed to excite YOYO-1 dye-labeled plasmid DNA. The excitation light was first passed through various optical components (e.g. filters, polarizers, reflecting mirrors), as well as a spinning optical diffuser, and was then reflected by the dichroic mirror (Chroma HQ535/50). The light was focused into the back aperture of the oil immersion objective. The laser light illuminated the YOYO-1 dye-stained DNA at the sample surface. The emission light subsequently obtained from the YOYO-1 dye molecules was collected by the same objective, passed back through the dichroic mirror, and was detected by an electron-multiplying (EM) CCD camera (Andor iXon DU-897). The CCD camera was configured to operate in the conventional gain mode. The laser power was maintained at 0.125 mW to avoid photobleaching to the largest possible extent. Videos 550 frames (0.55 s/frame) in length were recorded at different positions along the gradients for the analysis of DNA adsorption and desorption behaviors.

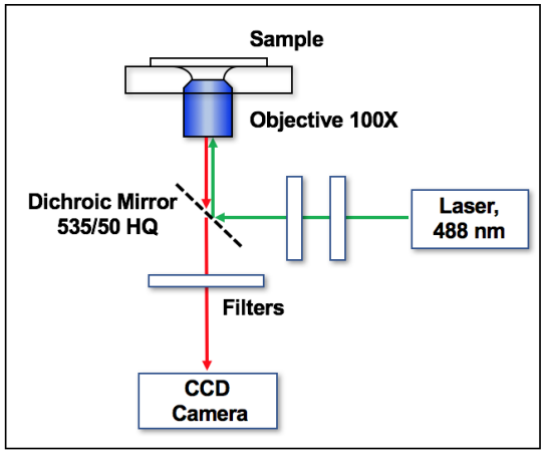

Figure 3.8 Wide-field microscope setup for TIRF mode fluorescence measurements.

3.4.2.2 Two-Channel Spectroscopic Imaging

To investigate the dielectric properties of DNA, a solvatochromic dye (NR) and a two-channel spectroscopic imaging method were employed in **Chapter 5**. **Figure 3.9** depicts a schematic diagram showing how the two-channel spectroscopic imaging experiments were performed. In this case, 514 nm laser light was first passed through a spinning optical diffuser, reflected by a dichroic mirror (Chroma 555 DCLP), and then focused into the back aperture of the oil immersion objective. The emission from the NR dye was collected using the same objective. It passed back through the same dichroic mirror and a 570 nm colored glass long-pass filter (Schott Glass). The fluorescence was then directed into an image splitter (Cairn Research OptoSplit II) incorporating a second dichroic mirror (Chroma 605 DCLP) and two bandpass filters (580/40 nm and 625/40 nm). The image splitter divided the emission fluorescence into two image channels centered at ~ 580 and ~ 625 nm, respectively, each having a ~ 40 nm passband. The CCD camera described above was again used to simultaneously detect the NR fluorescence in these two channels. Fluorescence videos 100-500 frames in length were recorded. These depict DNA motion in solution and DNA molecules adsorbed to the gradient surfaces. Conventional gain mode was again employed for

detecting DNA adsorbed to the surfaces, while electron multiplying gain was employed for detecting DNA in solution.

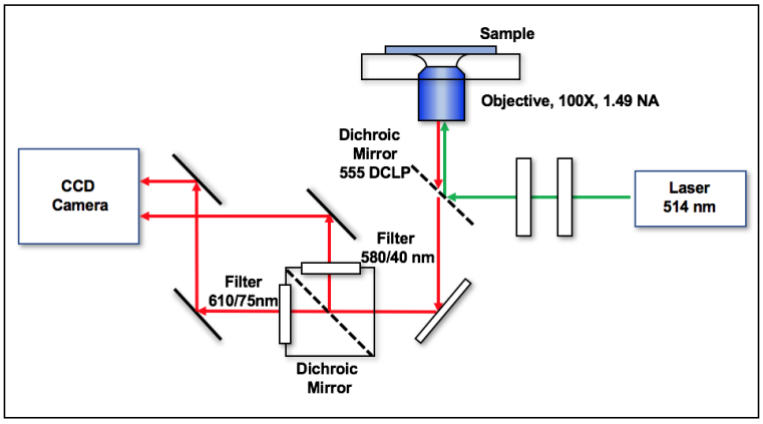

Figure 3.9 Wide-field microscopy setup for two-channel spectroscopic imaging.

Chapter 4 Single Molecule Catch and Release: Potential-Dependent Plasmid DNA Adsorption Along Chemically Graded Electrode Surfaces

Originally published as Zi Li, Kayesh M. Ashraf, Maryanne M. Collinson and Daniel A. Higgins "Single Molecule Catch and Release: Potential-Dependent Plasmid DNA Adsorption along Chemically Graded Electrode Surfaces", *Langmuir*, **2017**, *33*, 8651-8662. This work is reprinted here with permission.

4.1 Introduction

The binding of polyelectrolytes to chemically modified surfaces is of importance to a number of disciplines. For example, in material science, thin polymeric films of controlled thickness and chemical composition can be prepared using layer-by-layer (LbL) deposition methods in which polyelectrolytes of opposite charge are sequentially adsorbed onto a substrate surface.[139-143] The rate of film growth in LbL methods is defined in part by the surface charge density, among other factors.[141] Polyelectrolyte adsorption and desorption in LbL synthesis have also been controlled by application of an electrical potential to the substrate surface.[144] Beyond the creation of synthetic nanostructures, polyelectrolyte binding to charged surfaces is also of importance in the adsorption and desorption of biomacromolecules for separations, sensing and controlled release applications.[143, 145, 146] For example, in the purification of plasmid DNA, the biomolecules are first captured by an ion exchange resin and are later released in pure form by flushing with an appropriate eluent.[147] These same methods may also find utility in selective biosensors that incorporate separation steps. In this case, the analyte of interest would first be captured electrostatically, washed to remove unbound interferents, and finally released and detected.[25, 148] Capture and release devices of this

sort rely upon the ability to reversibly modulate the electrostatic interactions between the analyte and surface. Indeed, applied potentials are now being used to capture and release charged biomolecules (e.g., DNA) for sensing[149, 150] and gene transfer.[151, 152]

Development of optimal materials for use in the aforementioned applications requires detailed knowledge of the relevant interactions between polyelectrolytes and chemically modified surfaces. Exploration and optimization of these interactions could involve preparing a large combinatorial library of materials having different surface functional groups of varying densities, and then testing these materials one at a time. An alternative to such tedious and time-consuming experimentation is to instead prepare surfaces incorporating a chemical gradient in which the composition and/or concentration of surface functional groups varies with position along a single sample.[48, 49, 153] A continuous range of materials compositions and properties can then be accessed by acquiring data as a function of positon along the sample. Applications of chemical gradients to combinatorial materials science have been reviewed by Beers. et al.[154] In this chapter, gradients in aminosilane surface coverage are employed to investigate the dependence of biopolymer adsorption on functional group density, solution pH and applied potential. Double-stranded deoxyribonucleic acid (plasmid DNA) is used as a prototypical charged macromolecule.

The density of DNA adsorbed on surfaces has been explored by a number of optical methods. Ensemble-based methods include UV-visible adsorption,[155] fluorescence[152](including bulk depletion methods),[156] and vibrational spectroscopies.[157] These provide simple routes to determining equilibrium surface concentrations and for monitoring time dependent changes in surface coverage following a perturbation (i.e., a potential step). Unfortunately, they are of limited utility when the samples being explored are inherently heterogeneous. They also provide little or no information on the dynamics of analyte exchange between the surface and solution under

equilibrium conditions. Microscopic methods are better suited to studies of heterogeneous samples, and hence, atomic force microscopy (AFM) has been widely employed to image surface bound DNA, and to determine its local concentration and conformation.[74] While fast-scan AFM instruments exist and are now being employed to follow biomolecule dynamics at surfaces, sub-second phenomena remain difficult to follow over all but small scan regions (i.e. sub-micron areas) in the presence of small topographic features (~ 10 nm heights).[158] Single molecule fluorescence detection and tracking methods afford a means to probe the adsorption and desorption of dye-labeled DNA on heterogeneous surfaces under a broad range of experimental conditions. Indeed, single molecule methods have already been used to explore DNA adsorption and on model chromatographic surfaces,[31] patterned self-assembled monolayers,[30] and on native ITO electrodes.[105, 159] The hybridization kinetics of complimentary DNA strands have also been investigated at the single molecule level,[37] as have the interactions of elongated DNA with thermotropic[160] and lyotropic crystals.[161-163]

In this chapter, the adsorption and desorption of individual dye-labeled plasmid DNA molecules are followed at amine-coated chemically graded ITO electrode surfaces by wide-field fluorescence video microscopy. The dependence of DNA adsorption on surface amine coverage, solution pH and applied potential are explored along the gradient by detecting individual DNA adsorption and desorption events under each set of conditions. The results reveal a strong dependence of DNA adsorption on all three parameters.

4.2 Experimental Considerations

4.2.1 Chemical and Materials

Plasmid DNA (5386 base pairs) was purchased from New England Biolabs and was delivered as a 1000 µg/mL solution in 10 mM Tris-HCl with 1 mM EDTA (pH 8.0 at 25°C). The YOYO-1

dye used to label the DNA was supplied by Molecular Probes, as a 1 mM solution in DMSO. Phosphate buffered saline (PBS) powder was purchased from Sigma-Aldrich. Sodium borate and sodium hydroxide were obtained from Fisher Scientific. The ITO coated cover slips (22 × 26 mm, 0.13-0.17 mm thick, 8-12 Ω/cm^2) used as electrodes were obtained from SPI Supplies. Tetramethylorthosilicate (TMOS, 98%) and (3-Aminopropyl)trimethoxysilane (APTMOS, 97%) were purchased from Sigma-Aldrich. All chemicals were used as received. All buffers and solutions were prepared using pure water with 18 MΩ·cm resistivity.

DNA solutions. DNA buffer solutions were prepared by diluting appropriate amounts of 1× PBS stock and 1 mM borate buffer stock to obtain 0.01 mM PBS (pH ~ 6) and 0.10 mM borate (pH ~ 8) solutions, respectively. These two buffers had similar ionic strengths of 0.17 mM and 0.23 mM, respectively. The stock DNA solution was 1 nM in concentration and was prepared by diluting 3.5 µL of 1000 µg/mL plasmid DNA with 1× PBS to 1 mL. The original DMSO solution of YOYO-1 dye was diluted to 1 µM using DI water. The 40 pM DNA used here was prepared by mixing 80 µL of 1 nM plasmid DNA and 29 µL of 1 µM YOYO-1 dye solution with 2 mL of either 0.01 mM PBS or 0.10 mM borate solution. The YOYO-1 labeled DNA solutions were stored in a refrigerator overnight prior to use, to allow the YOYO-1 dye to fully intercalate into the DNA. The final ratio of DNA base pairs to dye was 15 to 1.

TMOS sol. As demonstrated in recent literature,[123, 124] silane based gradients are best deposited on silica-base-layer-coated substrates. TMOS sols were used to form these base layers and were prepared by mixing TMOS, ethanol (200 proof), and 0.1 M hydrochloric acid in a 1:99.6:5.4 volume ratio. The mixture was stirred for 1 h and subsequently stored in a desiccator for 23 h prior to use.

ITO substrate pretreatment. ITO substrates were thoroughly cleaned by washing with isopropyl alcohol, acetone and DI water. They were then blown dry with nitrogen. The ITO substrates were further exposed to an air plasma for 5 min before deposition of the silica base layer. The TMOS-derived base layer was deposited by spin coating (5000 rpm, 30 s) a 150 µL aliquot of the above TMOS sol onto each plasma cleaned substrate. The base-layer-coated substrates were stored in a desiccator overnight. This method is expected to produce a dense, nonporous silica film,[164] but one that may still incorporate defects and pinholes (see below). For electrical connection, a copper wire was attached to one corner of the ITO using silver epoxy.

Amine gradient deposition. The aminosilane gradient was formed by vapor phase deposition.[51, 127] The apparatus employed is described in **Figure 3.4**. It includes the base-layer-coated substrate and an aminosilane reservoir supported on a platform. These elements were housed inside a Plexiglas chamber that allowed for control over the ambient relative humidity (RH) and also helped eliminate air currents. Just prior to gradient deposition, the silica base layer was activated by treatment in an air plasma for 2 min. This procedure ensured a significant density of reactive hydroxyl groups on the base layer surface. Each substrate was exposed to APTMOS vapor for 8 min. The aminosilane-modified ITO substrate was then used to form the bottom of an electrochemical cell and was subsequently immersed in buffer solution. Fluorescence imaging of DNA adsorption was accomplished by imaging through the ITO substrate (see below).

4.2.2 Gradient Characterization

Water contact angle. Sessile drop water contact angle measurements were made using a home-built apparatus shown in **Figure 3.5**. Images of the water droplets were acquired using a CCD camera with an attached zoom lens (Navitar). Droplet images were analyzed using a plugin available for the ImageJ software package.[128] For these measurements, 1 mM borate buffer (pH =

10) droplets of 1.0 μL volume were deposited on the gradient surface using a microliter syringe. Three replicate measurements were made at each position, with droplets deposited at ~ 3 – 6 mm intervals along and ~ 3 mm spacings across each gradient. All experiments were performed under ambient laboratory conditions.

Film thickness. The thickness of the TMOS-derived base layer and amine gradients were obtained by spectroscopic ellipsometry, using a commercial instrument (α-SE, J. A. Woollam). All thickness measurements were obtained from films deposited on silicon substrates. These films were prepared in a manner identical to those on ITO. The thickness of the base layer was determined first, prior to gradient deposition. The gradient was subsequently formed over the base layer, aged, and film thickness remeasured. Thickness measurements were taken at 1mm intervals along and across each film, with measurements made at same points (to $\pm$ 0.5 mm) both before and after gradient deposition. The gradient thickness was taken as the difference between these two sets of measurements. All measurements were made under a dry (18 $\pm$ 2% RH) nitrogen environment. The gradient and base layer were modeled together as a single transparent layer on silicon. The Cauchy function was used to model film dispersion. Representative fits to the ellipsometric data (ψ and Δ curves) are shown in **Appendix Figure A1**. The goodness of fit was characterized by the mean-square error (MSE) and all fits employed had MSE < 2. Along with film thickness, these fits yield a refractive index of 1.57 $\pm$ 0.04 for TMOS-derived base layer and 1.62 $\pm$ 0.05 for the aminosilane-coated base layer at 633 nm. These are only modestly larger than the expected value of ~ 1.46.[165] The difference is likely due to a tilting of the sample on the ellipsometer stage, which would cause the incident angle to deviate from the expected value of 70˚. A sample tilt of only ~ 0.2˚ is sufficient to cause the observed deviation in refractive index.

Film Composition. The nitrogen content of the gradients was accessed by X-ray photoelectron spectroscopy (XPS). All XPS measurements were performed on a Thermo Fisher ESCAlab 250 imaging spectrometer. This instrument uses an Al Kα source (1486.68 eV). XPS data were acquired with a 200 μm spot size, 50 eV pass energy, and a 0.1 eV step size. Spectra were acquired at regular intervals along the gradient, starting ~ 1 mm from the high amine end. Effects due to charging of the sample surface were eliminated by measuring all peaks relative to the C(1s) peak at 284.6 eV. The area under the N(1s) peak was obtained by fitting and subtracting the neighboring background, followed by integration of the signal.

Optical Imaging. Detection of surface-adsorbed DNA molecules was accomplished by imaging through the optical transparent ITO substrate. For this purpose, the ITO substrate was used as the bottom surface of a small-volume electrochemical cell. A diagram of the cell is shown in **Figure 4.1**. It is comprised of a Teflon reservoir with a rectangular opening cut into the bottom. The gradient-modified ITO electrode was sealed against the bottom of the reservoir, covering the opening. Polydimethylsiloxane was employed as a "glue" to hold the electrode to the walls of the reservoir. The assembled cell was sandwiched between two metal plates used to hold it steady during optical imaging. For fluorescence detection of dye-labeled DNA, the cell was positioned over the objective lens of an inverted wide-field fluorescence microscope. This microscope has been described previously in detail.[166]

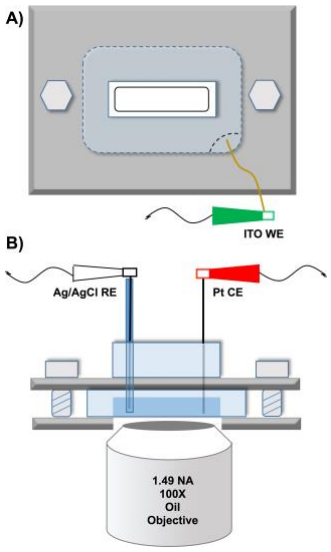

Figure 4.1 Small volume electrochemical cell used in single molecule detection. A) Top view of cell. B) Side view of cell positioned over the oil immersion objective used for sample illumination and collection of fluorescence from YOYO-1-labeled DNA. Connections to the ITO working electrode (WE), Ag/AgCl (satd KCl) reference electrode (RE) and the platinum counter electrode (CE) are also shown.

Excitation of the YOYO-1 dye was achieved by illuminating the ITO surface with 488 nm laser light. The through-objective total internal reflection fluorescence (TIRF) mode[167] was employed to minimize background from dye-labeled DNA molecules in bulk solution. For this purpose, the incident laser light was first reflected from an appropriate dichroic mirror and then focused, off-axis, into the back of a high numerical aperture (NA) oil immersion objective (Nikon APO-TIRF, 100X, 1.49 NA). The incident laser power, measured prior to entrance into the microscope, was maintained at 0.125 mW in all experiments, yielding a peak incident power density at the sample ~11 W/cm^2. Fluorescence from the YOYO-1 molecules was collected by the same objective, passed through the dichroic mirror and then through a bandpass filter (Chroma

HQ535/50M). Finally, the fluorescence was detected using a CCD camera (Andor iXon 897), using conventional gain. Fluorescence videos ~550 frames in length with a frame time of 0.55 s were recorded.

To explore DNA interactions with chemically modified ITO surface, fluorescence videos were recorded as the applied potential was stepped between -0.5 V and +1.4 V (see below), using a CH Instruments potentiostat. All potentials were measured versus an Ag/AgCl (satd KCl) reference electrode. Videos were recorded as a function of potential step size (i.e., voltage difference), electrolyte solution pH, and position along the gradients. In each case, the potential was stepped between high and low potentials a total of 30 times, at 10 s intervals. The precise timing of the potential steps and video framing was accomplished using a separate computer. The fluorescence videos obtained were analyzed using software written in house in the LabView programming environment.[138] The software was used to load the videos, subtract the background on a frame-by-frame basis and to detect, locate, and record the signal as a function of time for each position where an adsorbed DNA molecule was detected. The output was used to identify the time at which each molecule adsorbed to the surface, to observe YOYO-1 bleaching and DNA desorption behavior, and to determine the residence time on the surface for each molecule.

4.3 Results and Discussion

4.3.1 Gradient Preparation and Characterization

Gradient Deposition. Amine gradients were prepared by vapor phase deposition.[51, 127] Because APTMOS tends to form multilayer films, and because of variations in the steepness and position of the gradients caused by changes in laboratory temperature, ambient humidity and/or stray air currents, gradients preparation employed a modified version of earlier procedures.[51, 127] Specifically, the location of the region where the film thickness transitioned from approximately

one monolayer to submonolayer thickness was defined by placing a coverslip over the substrate, as shown in **Figure 3.4**. A thin PDMS gasket was used to position the coverslip a distance of 1 mm above the substrate during film deposition. The leading edge of the coverslip was mounted at 8.0 mm ($\pm$ 0.3mm) from the high amine end of the gradient in each deposition.

Water Contact Angle. Successful deposition of an amine gradient was initially verified by sessile drop water contact angle (WCA) measurements. **Figure 4.2A** plots the WCA data obtained from several replicate samples. These depict a gradual decrease in the contact angle from ~55˚ at the high amine end to ~5˚ at the low amine end. The values measured at the high amine end are similar to previously reported values for aminosilane modified surfaces.[168] The higher WCA at the high amine end demonstrates its greater hydrophobicity, relative to the unmodified silica base layer (low amine end). Note that WCA changes most dramatically between the 8 mm and 12 mm positions on the gradient. However, quantitative measurements of the WCA could not be obtained in this region because the droplets quickly and spontaneously spread or migrated to the more hydrophilic end of the gradient in every instance.[51] Based on the WCA data, it is concluded that the amine coverage transitions from approximately one monolayer (greatest hydrophobicity) around the 8 mm position to a small fraction of a monolayer (very hydrophilic) by the 12 mm position.

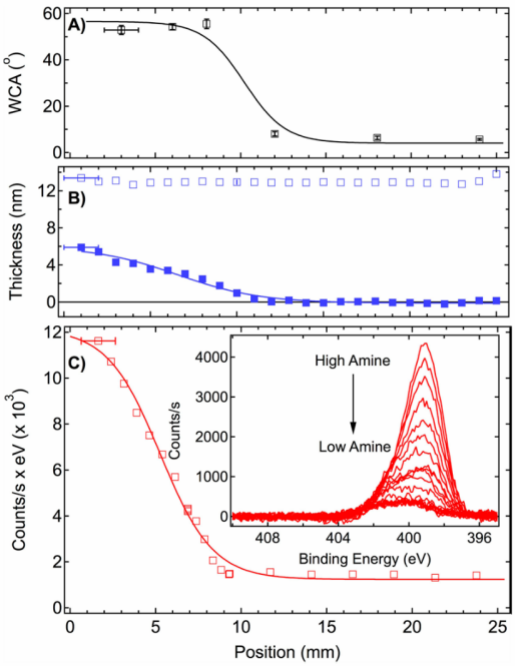

Figure 4.2 (A) Sessile drop water contact angle (WCA) data. (B) Ellipsometric data showing the base layer thickness (open squares) and the gradient film thickness (filled squares) after subtraction of the base layer. (C) XPS measurements of integrated N(1s) peak area from individual spectra acquired along the gradient (inset). The three data sets show the individual results obtained from three different gradients. Although all three are plotted on the same X-axis, the axes are not meant to indicate identical positions. The error in determining the exact position is estimated to be ±1 mm in each (see single X-axis error bars). The Y-axis error bars in panel A depict the standard deviation of three replicate measurements at each point. The ellipsometric data have been corrected for a 0.17 nm offset in thickness. The solid lines have been added to better depict the trends.

Gradient Thickness. Measurements of gradient film thickness provided confirmation of gradient formation and supporting evidence for the interpretations of the WCA data mentioned above. Because of the weak optical reflection from ITO coated substrates, all ellipsometry

measurements were performed on gradients prepared on silicon slides. The improved signal levels thus obtained afforded submonolayer sensitivity. The thickness of the base layer was measured first, with multiple measurements made at regularly spaced intervals along the gradient direction, prior to gradient deposition. These measurements revealed the presence of an uniformly coated base layer having a thickness of 13.2 $\pm$ 0.2 nm. Multiple replicate measurements performed on several different samples were used to verify the reproducibility of base layer formation.

The gradient was subsequently deposited over the base layer (see **Chapter 4.2** Experimental Considerations) and the full film thickness (gradient plus base layer) was then measured at the same series of positions (within $\pm$ 0.5 mm). Subtraction of the base layer thickness from the full film thickness gave the gradient thickness at each location. **Figure 4.2B** plots the gradient thickness for one representative sample. These data show a clear trend of decreasing thickness running from the high amine end (i.e., ~1 mm) to the low amine end (i.e., ~12-13 mm). The maximum film thickness of ~5.5 nm, at ~1 mm, is consistent with a relatively thick (i.e., ~ 8 layers) aminosilane polymer. In the region of greatest interest (8-12 mm), the film thickness drops from ~2 nm to near zero. A full monolayer of well-packed aminopropylsilane groups is expected to be ~0.7 nm thick.[169]

Gradient Composition. XPS data were also acquired as a function of position along the gradients. These data demonstrate that the increased hydrophobicity and film thickness observed toward the high amine end results from aminosilane deposition. **Figure 4.2C** depicts a series of spectra (inset) acquired in the N(1s) region at 0.75-2.5 mm intervals along a representative gradient. The integrated areas under these peaks are also plotted in **Figure 4.2C**. As has been observed previously, the N(1s) peak is comprised of two separate bands, one centered at 399.2 eV and the other at 401.6 eV.[123] The former is attributable to free amine, while the latter is assigned to

protonated or hydrogen bonded amine sites.[123] As these measurements were performed under high vacuum, little or no correlation between the level of protonation depicted and DNA adsorption under buffer (see below) is expected. Therefore, the full peak area was employed as a measure of total aminosilane coverage. The plot of peak area given in **Figure 4.2C** shows the expected trend, with the peak area decreasing along the gradient between the high and low amine ends. Importantly, at positions >9 mm, the nitrogen content of the film was found to be small and invariant with position, reflecting the presence of a small amount of adventitious nitrogen in/on the base layer. At positions <9 mm, the nitrogen content increased rapidly toward the high amine end, consistent with a growth in film thickness from submonolayer to monolayer and then multilayer levels. Taken together, the contact angle, ellipsometry and XPS data provide conclusive evidence for formation of an aminosilane gradient of gradually varying surface coverage.

Redox Stability of YOYO-1 and Useful Potential Window. One widely investigated method for controlling the adsorption and desorption of charged macromolecules at surfaces is through the application of an electrical potential.[144] The gradients investigated here were prepared on ITO-coated glass surfaces for the purpose of exploring these phenomena.

Cyclic voltammetry experiments were performed in order to determine the useable window in potential-dependent DNA adsorption experiments and to assess the redox stability of the YOYO-1 dye used to label the DNA. Representative voltammograms obtained in PBS buffer are shown in **Figure 4.3**. Those obtained in borate buffer (pH ~ 8) are similar (see **Appendix Figure A2**). The voltammograms obtained in PBS buffer alone (absent DNA and YOYO-1) depict an available potential window of ca. -0.5 V to +1.6V (vs Ag/AgCl), similar to what was employed in previous studies.[105, 159] All experiments were performed in this range.

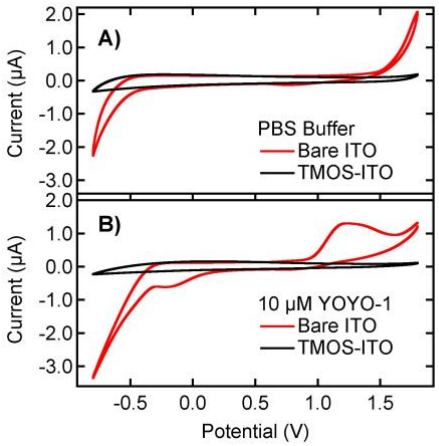

Figure 4.3 Cyclic voltammograms showing A) the background current under 0.01 mM PBS buffer at bare ITO and base-layer-coated ITO electrodes and B) the current in the presence of 10 µM YOYO-1 at bare ITO and base-layer-coated ITO in the same buffer solution. YOYO-1 dye exhibits an oxidation peak at ~ 1.2 V on bare ITO and a reduction peak at ~ -0.2 V (solid red curve). The electrode area was 0.07 cm2 in all cases, the pH was ~ 6, and the scan rate was 0.1 V/s. All potentials are measured vs. Ag/AgCl (satd KCl).

Voltammetric data were also obtained from 10 μM YOYO-1 solutions. These experiments show that YOYO-1 undergoes quasi-reversible oxidation and reduction reactions at 1.2 V and at -0.2 V (vs Ag/AgCl), respectively, on bare ITO. Voltammograms recorded on silica base-layer-coated ITO (both with and without the amine gradient) showed undetectable YOYO-1 redox current, demonstrating that the silica coating is insulating[164] and largely blocks the redox activity of the electrode. Unfortunately, it was not possible to explore the redox chemistry of YOYO-1 intercalated in the DNA, because sufficient concentrations of DNA could not be achieved. Based on the data obtained for coated ITO, it is concluded that the YOYO-1 redox reactions are unlikely to interfere with observations of potential-dependent DNA adsorption/desorption events. The

blocking of the YOYO-1 redox activity by the silica base layer implies that any redox activity of the DNA (i.e., guanine)[170] itself will also be suppressed.

4.3.2 Optical Imaging of DNA Adsorption

The primary goal of these studies was to obtain a better understanding of the potential-dependent adsorption of charged macromolecules along the gradient surface. Amine modified surfaces were selected because they afford a simple route to controlling native surface charge via alteration of the solution pH. DNA was selected as a prototypical polyelectrolyte because it carries significant charge and is readily labeled with fluorescent dyes like YOYO-1 for easy visualization. There is also significant interest in using electrical potentials to capture and release DNA and other biomolecules from surfaces in chemical sensing, sequencing, and transfection applications.[149-152]

Native DNA Interactions with Gradient Surfaces. Initial investigations of DNA interactions with the amine gradient were performed in the absence of an applied potential, with the film immersed in pH ~ 6 and pH ~ 8 buffers. The fluorescence images obtained ($32 \times 32\ \mu m^2$ regions) at 7-8 mm (near the high amine end) incorporated many bright fluorescent spots. The distinct spots are attributable to individual YOYO-1-labeled plasmid DNA molecules that are either adsorbed on or in close proximity to the gradient surface. As noted above, fluorescence images were acquired in the TIRF mode. Therefore, signal is only obtained from dye-labeled DNA molecules found within the ~150 nm (1/e) decay depth of the evanescent field. Adsorbed DNA molecules and those remaining in solution were easily distinguished from each other in the video data. Adsorbed molecules remained at the same location (to within ~100 nm) over long periods of time (i.e., tens to hundreds of video frames). Mobile molecules were found in one location for only a single video frame and moved several microns between frames.

Immersion of the gradient-coated ITO surface into a pH ~ 6 buffer resulted in strong adsorption of DNA at 7 mm, while little or no DNA adsorbed at 10 mm. A monotonic transition in coverage occurred between these points. Images obtained at pH ~ 8, were similar to those at pH ~ 6, with a high concentration of surface-adsorbed DNA again found near 7 mm, followed by a transition to little or no adsorbed DNA at 10 mm. No attempt was made to quantify the surface coverage of adsorbed DNA in the absence of an applied potential, because at positions < 8 mm, under both pH ~6 and pH ~ 8 buffers, the DNA continued to adsorb to the point at which individual DNA molecules could no longer be easily distinguished.

The results described above are consistent with those reported previously for patterned amine and acid terminated self-assembled monolayers on gold electrodes.[30, 33] These studies demonstrated that λ-DNA strongly adsorbs to amine-terminated surfaces at pH = 8.2. The authors attributed DNA adsorption to interactions of the unhybridized (single stranded) "sticky ends" of the λ-DNA with either hydrogen bonding sites or hydrophobic sites on the surface.[30, 33] The plasmid DNA employed here does not incorporate "sticky ends" but nevertheless exhibits strong adsorption near the 7 mm position (high amine end). This reflects the participation of relatively strong Coulombic and/or hydrophobic interactions between the DNA and the aminosilane film. The lack of favorable interactions between the DNA molecules and the silica surface near 10 mm (low amine end) precludes DNA adsorption in that region. Indeed, the interactions in this region are likely repulsive, as both the DNA and silica[171] carry negative charges at pH ~ 6 and pH ~ 8.

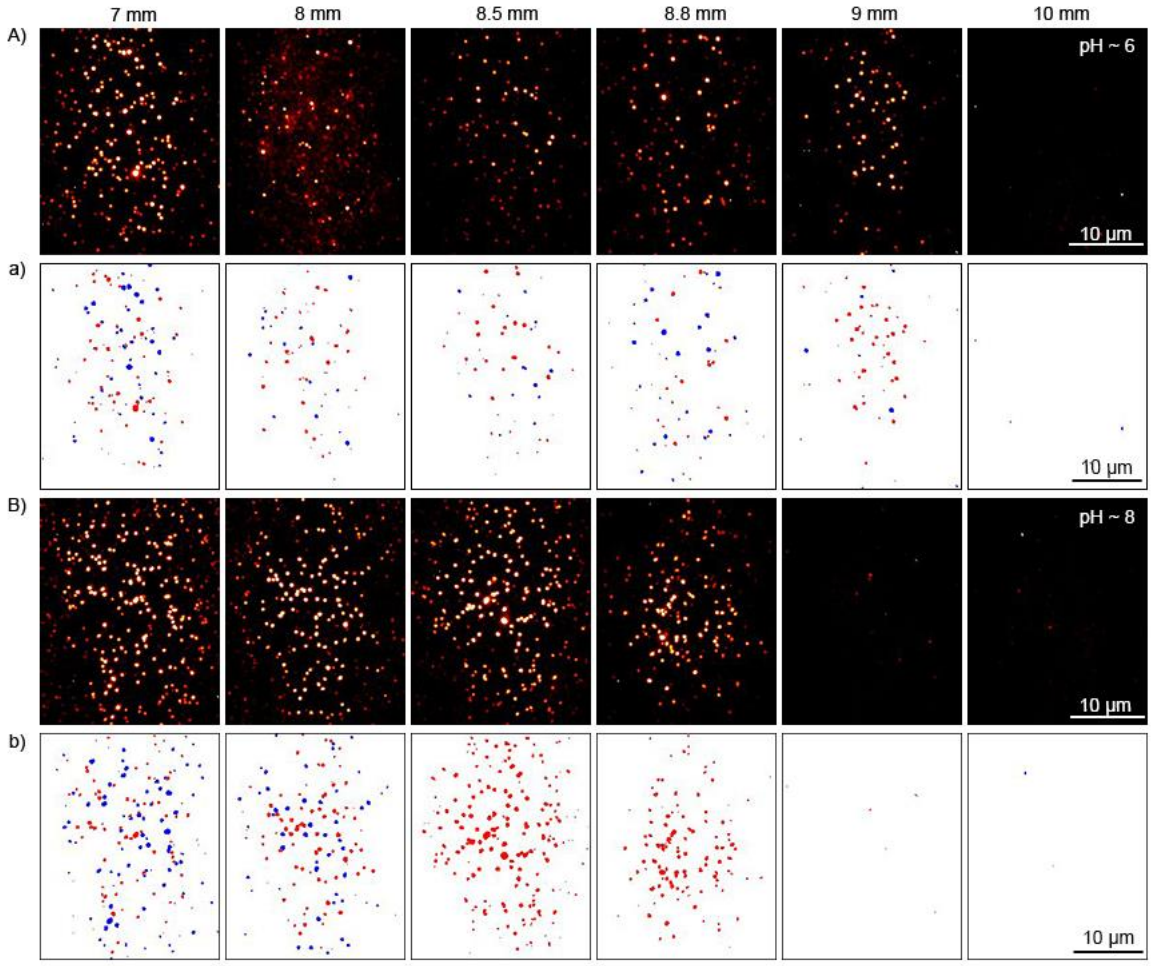

Figure 4.4 (A,B) Representative Z-project images along two different amine gradients acquired at pH ~ 6 and pH ~ 8, respectively. The fluorescence counts in each image are displayed using the same color scale, with the background-subtracted signals ranging from 0 to 1000 counts/pixel in each image. (a,b) Representative images showing which DNA molecules appeared at +1.4 V (red spots) and which at −0.5 V (blue spots), obtained as described in the main text. Scale bars are shown on the right (10 mm images) and are identical for all images.

Potential-Dependent DNA Adsorption and Desorption. Fluorescence videos depicting potential-dependent DNA adsorption and desorption along the gradients were acquired by imaging through the ITO electrode as its potential was stepped between positive and negative values. Prior to beginning each experiment, any YOYO-1 dye associated with surface adsorbed DNA was bleached by exposure to a high laser power density (180 W/cm^2) for 1-3 min. **Figure 4.4A,B** depicts representative fluorescence images acquired along the gradients in pH ~ 6 and pH ~ 8 buffer solutions of YOYO-1-labeled DNA. These images were constructed by plotting the maximum signal for each pixel observed across the entire length of the video analyzed. Such images are referred to as "Z-project images" and provide an integrated view of all DNA molecules that adsorbed to the surface during each video, regardless of the applied potential. The position labels above each image designate the location along the gradient (see **Figure 4.2**) at which each video was acquired.

The potentials employed (-0.5 V and +1.4V vs Ag/AgCl) were selected based on the potential window identified above. These afforded the greatest potential-dependent adsorption/desorption effects while avoiding solvent redox chemistry. Figure 4.4a,b depicts images constructed from two distinct Z-project images: one for negative potentials, the other for positive potentials, obtained by separately plotting the maximum signal at each pixel for each potential. The two Z-project images were then combined to identify molecules that appeared under negative potentials (blue spots) and those that appeared under positive potentials (red spots).

The images shown in **Figure 4.4** depict clear pH-, potential-, and position-dependent trends in DNA adsorption. DNA was found to adsorb to the gradient surface at ~7mm (high amine end) under both pH ~ 6 and ~ 8 buffers. The density of adsorbed DNA appeared to be largely independent of the applied potential in this region, with almost equal numbers of blue and red spots

shown in each image in Figure 4.4a,b. Counting of the spots in these images shows that ~55% of the DNA molecules adsorbed under positive potentials at 7 mm. In stark contrast, at 10 mm (low amine end), little or no DNA was found on the surface under any circumstances. The most interesting behavior was observed in regions near 8.5-9 mm, where the amine coverage changes rapidly from near monolayer to submonolayer values. Under pH ~ 6 buffer, the density of adsorbed DNA decreased gradually across the three associate images. Furthermore, DNA adsorption was only weakly dependent upon the applied potential (see **Figure 4.4a**) at pH ~ 6, as shown by the similar numbers of red and blue spots. In contrast, under pH ~ 8 buffer, the density of adsorbed DNA dropped abruptly in the 8.5-9 mm range. Adsorption of the DNA molecules in this region occurred almost exclusively at +1.4 V, as shown by the predominance of red spots in the associated images (**Figure 4.4b**).

The above observations indicate that both Coulombic attraction and hydrophobic interactions may play a role in strong DNA surface adsorption near 7 mm (high amine end). Indeed, near 7 mm, the gradient is expected to carry a positive charge at pH ~ 6, leading to strong Coulombic interactions with DNA. The pK_a for ammonium groups on similar aminosilane surfaces has been reported to be ~7 at intermediate levels of ionization, with ~70% of the amine groups protonated at pH ~ 6.[172] The level of amine protonation may be lower in the present films due to the presence of basic $Si\text{-}O^-$ groups on the surface. It may also be lower at the high amine end due to the expected decrease in ammonium group pK_a with increasing surface coverage.[173] Additional evidence for a positive surface charge is provided by streaming potential measurements on similar amine-modified silica surfaces.[50] These studies reported a Zeta potential of ca. +75 mV at pH = 6. Regions near 10 mm are expected to carry a negative charge and to repel the DNA. The pKas of surface silanol sites have been reported to fall in the 4.5-8.5 range,[171] the pI of silica is ~2.5, and streaming

potential measurements on similar surfaces yielded Zeta potential of ca. -75 mW at pH = 6.[50] In the 8.5-9 mm range, the near-monolayer amine coverage affords better potential dependent control over DNA adsorption, likely by balancing these attractive and repulsive interactions.

At pH ~ 8, only 30% of the surface amine groups are expected to be protonated at the high amine end,[172] and Zeta potential measurements on similar surfaces yielded values near zero.[50] In spite of the reduction in charge, strong adsorption of the DNA still appears to occur near the 7 mm position, suggestive of an important role for hydrophobic effects. In regions near 10 mm, the surface carries an even greater negative charge at pH ~ 8,[50] with strong repulsion of the DNA providing a clear explanation for the lack of detectable adsorption events. The best potential dependent control over DNA adsorption is observed in the 8.5-9 mm range, under pH ~ 8 buffer. This observation likely results from the tuning of the cationic surface site density into a range where it is optimally balanced with the density of deprotonated silanol groups.

Dynamics of DNA Adsorption and Desorption. Quantitative data on DNA adsorption and desorption events were obtained by identifying the adsorption location for each DNA molecule and recording the fluorescence across the video at each of these sites. Software developed in-house was employed for this purpose. The software first created a Z-project image from the video data. The individual spots in this image were then fit to two-dimensional (2D) Gaussian profiles to determine their precise locations. The list of spot locations was subsequently used to construct a fluorescence time transient for each location. This was accomplished by fitting a small (13 pixel × 13 pixel) region centered on each location in each video frame to a 2D Gaussian profile. In the absence of a fluorescent spot, this procedure returned a measure of the background-subtracted noise in the image. With a DNA molecule present, the fitted amplitude and X,Y-center of each fluorescent spot were obtained, giving the fluorescence signal level for the DNA molecule and its

precise location with subdiffraction-limited spatial resolution.[174] This procedure allowed for any DNA motions to be tracked and also for compensation of slight, random, X,Y drift during the ~ 5 min long videos. The time transients thus obtained show the approach, adsorption, and possible desorption of the individual DNA molecules. **Figure 4.5** depicts representative examples of these time transients.

The data shown in **Figure 4.5** provide valuable information on the DNA adsorption dynamics. In most cases, the DNA molecules abruptly appeared on the surface during a single video frame (~0.55 s exposure time). In a few cases, the molecules were visible for only 1-2 frames and then disappeared. It was concluded that these molecules did not adsorb to the surface and were therefore disregarded. Molecules that remained visible and in approximately the same location (see below) for 3 or more video frames were concluded to have adsorbed to the surface. Only these latter events are shown in **Figure 4.5** and only these are employed in the analyses described below. These data show that the DNA adsorption events were not correlated with a change in potential (i.e., with the individual potential steps). The DNA molecules adsorbed to the surface at a variety of times ranging from immediately after each potential step to immediately prior to the next potential step. This observation is consistent with adsorption of DNA molecules that have migrated from a range of different distances to the electrode surface.

The data shown in **Figure 4.5** allowed for the DNA adsorption rate constant to be determined. For this purpose, the number of detected adsorption events was simply counted and divided by the total observation time. Dividing by the area of the detection region yielded the average adsorption rate. The adsorption rate constant was then determined by manipulation of the following expression:

$$R_{ads} = k[\text{DNA}]$$

Here, R_{ads} is the measured adsorption rate, [DNA] is the concentration of DNA in solution, and k is the adsorption rate constant. The data obtained under pH ~ 6 buffer yielded an average R_{ads} of 4.7×10^4 molecules/(cm^2 s) and a k of 2.0×10^{-6} cm/s for positions between 7 mm and 9 mm. These decreased 10-fold at the 10 mm position to values of 3.6×10^3 molecules/(cm^2 s) and 1.5×10^{-7} cm/s, respectively. In pH ~ 8 buffer, values of 7.7×10^4 molecules/(cm^2 s) and 3.2×10^{-6} cm/s were obtained for positions between 7 mm and 8.8 mm, with their mean values again decreasing 10-fold at the 9 and 10 mm positions to 6.2×10^3 molecules/(cm^2 s) and 2.6×10^{-7} cm/s, respectively. Otherwise, neither data set exhibited a clear trend in the monolayer to multilayer region. The increase in adsorption rate constant observed with increasing buffer pH is most consistent with an important role played by hydrophobic interactions in governing DNA adsorption to the amine surface as the surface and DNA are expected to become less positively charged and more negatively charged, respectively, with increasing pH.

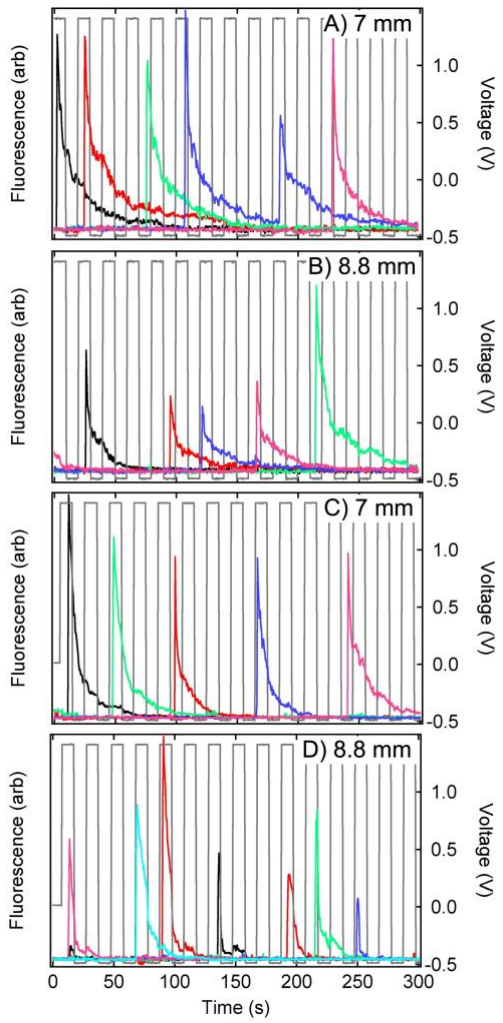

Figure 4.5 Representative time transients showing bursts of fluorescence caused by adsorption of single DNA molecules (in different colors) to the gradient surface. The applied potential waveforms are shown as gray lines. Data are shown for the 7 mm position (high amine end) and for a region with near-monolayer amine coverage (8.8 mm), respectively, under (A,B) pH ~ 6 buffer and for the same regions under (C,D) pH ~ 8 buffer. Two different molecules adsorbed at the same site in panel A, as shown by the blue transient.

In the vast majority of adsorption events, the DNA molecules adsorbed to the surface and remained at the same location (to within the spot localization precision) across many video frames. However, a small but easily detectable fraction was observed to remain mobile for a few frames after initially contacting the surface. These molecules later became immobile. Such events were most commonly observed in regions of near-monolayer amine coverage (8.5-9 mm) under both pH ~ 6 and pH ~ 8 buffers. **Figure 4.6** shows evidence of one such event, of several that were observed. These data show that the molecule approached the surface and then took three sequential ~100 nm steps before becoming immobile. Such behavior suggests that the films are somewhat heterogeneous and that the DNA molecules may search for favorable surface adsorption sites prior to becoming immobilized. The molecules that are immediately immobilized either adsorb directly at these sites or find them on a time scale that is too short to detect under the present conditions.

Figure 4.6 Consecutive video frames showing the initial adsorption and residual motion (left to right) of a single plasmid DNA molecule at +1.4 V in the near-monolayer region (8.8 mm) of the gradient, under pH ~ 8 buffer. A plot of the DNA position across several frames is shown at the far right. The DNA molecule fully adsorbs to the surface after the fourth frame.

Once adsorbed, the fluorescence from each DNA molecule immediately began to decay (**see Figure 4.5**) on two distinct time scales. The time scales for the YOYO-1 fluorescence decay were quantified by fitting the time transients to biexponential functions. The time constants obtained for the two decays differed by an order of magnitude on average, with the fast component occurring on a 1-3 s time scale and the slower decay on a 10-30 s time scale. The initial fast decay is

consistent with the few-frame adsorption-site search mentioned above, but it is unclear why such a search should lead to a decay in the fluorescence. Energy transfer quenching of YOYO-1 fluorescence to the electrode is not expected to play a role because of the relatively thick (~13 nm) silica base layer.[175] It is more likely that the fluorescence decays include contributions from photobleaching of the YOYO-1 dye. Indeed, photobleaching studies performed under an applied potential also produced biexponential fluorescence decays. These studies, and their results are described in more detail in the Appendix. (see **Appendix Figure A3**) Importantly, the fluorescence decay rates for both the fast and slow components increased with increasing laser power, but also included power independent components. These results demonstrate that both fluorescence decays are at least partially due to photobleaching of the dye.

The data shown in **Figure 4.5** provide clear visual evidence that the decays also arise from desorption of the DNA from the electrode surface, particularly at negative potentials, under pH ~ 8 buffer. Apparent deposition is manifested as a change in the appearance of the slow fluorescence decay and was most clearly observed in near-monolayer to submonolayer gradient regions (8.5-9 mm). This behavior is best evidenced by comparison of the transients shown in **Figure 4.5D** to those in **Figure 4.5A-C**. The transients in **Figure 4.5D** frequently exhibit an abrupt drop in the signal in conjunction with a potential step from +1.4 V to -0.5 V. Since the electrochemistry data described above indicates that YOYO-1 redox chemistry is blocked by the silica base layer, it is concluded these changes in fluorescence are most likely due to desorption of the DNA. As is well-known,[176] YOYO-1 can photocleave DNA, and this process could facilitate loss of the dye to the surrounding solution, with a corresponding decrease in the fluorescence. It is also possible that the power independent component of the fluorescence decay reflects simple escape of the dye from the surface-bound DNA, perhaps due to its displacement by interactions with the positively

charged surface ammonium ions. While it is not possible to exclude these alternative mechanisms at this point, the clear correlation between a change to negative potential and a drop in fluorescence in **Figure 4.5D** provides strong evidence that much of the drop is due to potential-dependent release of the DNA from the surface.

Interestingly, some of the apparent potential-dependent desorption events produced an incomplete drop in YOYO-1 fluorescence. In many of these cases, the very next step in potential from -0.5 V to +1.4 V led to an increase in YOYO-1 fluorescence. This behavior was sometimes repeated over several potential steps for the same DNA molecule. **Figure 4.7** provides a particularly dramatic example of this behavior. In this case, it is concluded the DNA molecule only partially desorbs from the electrode surface upon a step to -0.5 V. The associated change in proximity of the YOYO-1 dye molecules to the electrode leads to a reduction in their fluorescence as a result of the rapid distance dependent decay in the evanescent optical fields from the electrode surface. When the potential returns to +1.4 V, the DNA molecules is again brought into close proximity to the electrode and the fluorescence once again increases. This behavior may be viewed as a potential-dependent reorientation[175, 177] of the plasmid DNA in the electrochemical double layer.

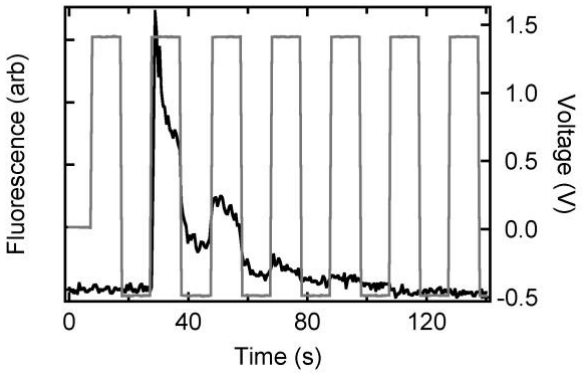

Figure 4.7 Representative time transient from YOYO-1 labeled DNA showing potential-dependent modulation of the fluorescence. The modulations observed are attributed to potential-dependent reorientation of a DNA molecule that is only partially bound to the gradient surface.

In order to better identify and quantify the potential-dependent release of DNA from the electrode surface, the apparent residence time was determined for each molecule as a function of its position along the gradient at each pH. In this analysis, the background level and DNA fluorescence signal were distinguished from each other through a statistical analysis of the time transient data. For a particular signal level to be counted as YOYO-1 fluorescence, the signal was required to be >10-fold larger than the standard deviation of the background level. The apparent residence time was then obtained as the total time the signal remained above background following each adsorption event.

Figure 4.8 depicts histograms showing the apparent residence times for the adsorbed DNA molecules as a function of position along each gradient. As expected, the longest residence times were found near 7 mm (high amine end) for both buffers. The residence times decreased with position along the gradients, with the shortest residence times observed at the 9 and 10 mm positions (low amine end). **Figure 4.8** (bottom) provides the best view of this trend by plotting the mean apparent residence time at each position. These same data show that the residence times were generally longer, on average, under pH ~ 6 buffer and relatively shorter at pH ~ 8. They provide supporting evidence for the conclusion that the DNA is more strongly bound to the surface at the high amine end of each gradient under lower pH buffer. Finally, these data also reveal that DNA adsorption is at least quasi-reversible at all positions beyond 7 mm (i.e., for the thinner aminosilane films) and that it becomes more reversible as the coverage approaches monolayer and

submonolayer levels. Again, DNA adsorption ceases to occur at the very lowest coverage where the silica surface is essentially unmodified.

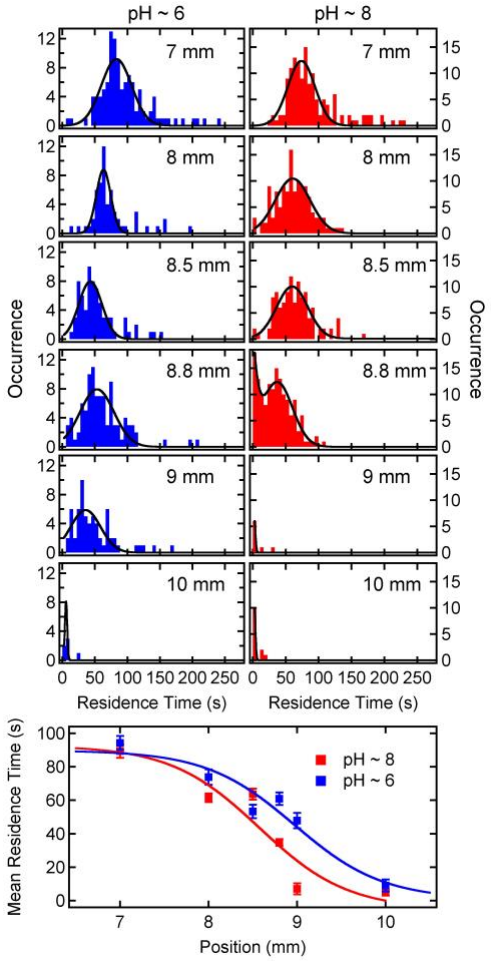

Figure 4.8 (Top) DNA single molecule residence time distributions on the gradient surface as a function of solution pH and position along the gradient. The residence time depends upon photobleaching of the YOYO-1 dye and desorption of DNA from the gradient surface. The solid lines show Gaussian fits to the distributions. (Bottom) Arithmetic mean residence times as a function of pH and position along the gradient. The results show that the residence time gets shorter as the amine coverage decreases at both pH ~ 6 and pH ~ 8. The solid lines show sigmoidal fits to the trends in the data.

The residence time results also provide support for the conclusion that DNA release can be triggered by application of a negative potential. The best evidence of potential-dependent DNA release was obtained from data acquired at the 8.8 mm position under pH ~ 8 buffer (see **Figure 4.5D**). While the residence time distributions appeared to be monomodal under other circumstances, at this position, a bimodal distribution was observed, with the shorter residence times yielding a distribution of values peaked near zero. The latter reflects molecules that only briefly interact with the gradient surface before being released back into solution. It is in this region of the gradient, under pH ~ 8 buffer, that the best potential-dependent control over DNA adsorption and desorption phenomena are achieved. At 9 mm and beyond (low amine end), release of the DNA from the surface is always very fast, and hence the DNA cannot be efficiently captured.

It should be noted that application of a dense silica coating to the ITO electrode could prevent potential dependent control over adsorption or desorption events. Indeed, the observation of potential dependent effects suggests the silica layer incorporates some pinholes and other defects that allow contact between the electrode surface and the solution. The cyclic voltammetry data provided in **Figure 4.3** lend supporting evidence for this conclusion, as the apparent electrode capacitance is similar for both the bare and silica-coated ITO surfaces.

Model for DNA Capture and Release. **Figure 4.9** shows a model for the DNA dynamics reflected in the fluorescence data. When the DNA molecules first adsorb to the surface, they initially remain mobile, seeking out sites where they can most strongly bind. This search takes a few seconds at most. In regions with a high density of amine sites to which the DNA can bind, especially at low pH, DNA adsorption is quasi-permanent. Moving down the gradient, the DNA-surface interactions become weaker and the DNA is held less tightly to the surface. In these regions, application of a negative potential can cause partially bound DNA to reorient in the applied field.

As the amine coverage decreases further, a step to negative potential can cause release of the DNA back into solution.

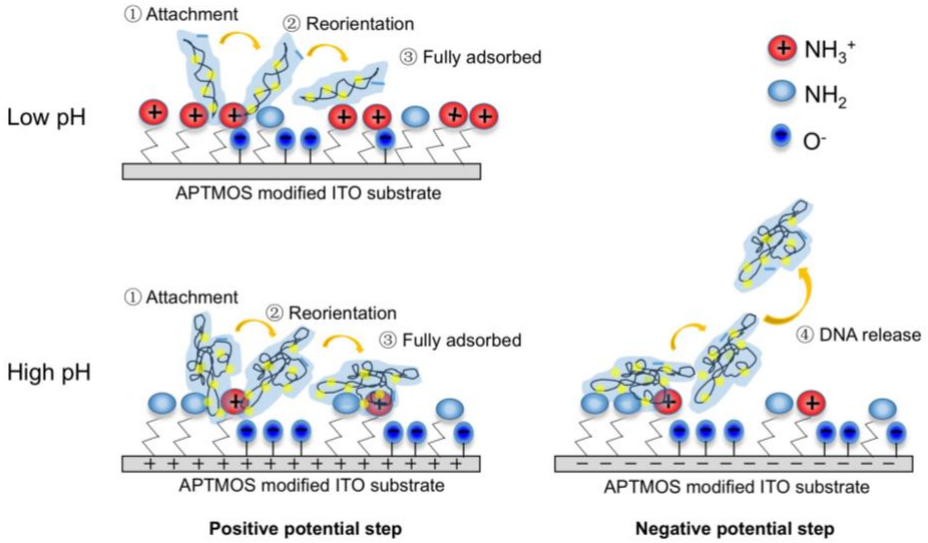

Figure 4.9 Model for DNA capture and release from the gradient aminosilane-modified ITO electrode surface. At the high amine end at pH ~ 6, the DNA molecules adsorb to the surface and may subsequently reorient or otherwise move to achieve a fully adsorbed state. The DNA molecules are most strongly adsorbed at pH ~ 6. At pH ~ 8 a similar adsorption process occurs but the decreased density of cationic ammonium ions and increase in deprotonated silanols leads to reduced binding strength. The DNA molecules may spontaneously desorb from the surface and can also be driven off the surface by a change to negative potential, particularly at low amine coverage.

4.4 Conclusion

In summary, the potential-dependent capture and release of YOYO-1-labeled plasmid DNA molecules along amine-gradient surfaces has been explored as a function of positon, solution pH and applied potential. The results reveal that DNA strongly and quasi-reversibly binds to

multilayer amine modified surfaces under pH ~ 6 buffer, when the majority of surface amine groups are protonated. As the amine coverage decreases to monolayer and submonolayer levels, DNA adsorption becomes more reversible and subsequently ceases to occur at the lowest amine coverage (i.e., on unmodified silica surfaces). DNA adsorption was shown to become more reversible under pH ~ 8 buffer, with clear evidence for potential-dependent release of adsorbed DNA appearing at monolayer to submonolayer aminosilane coverage. It is concluded that optimum conditions for potential-dependent capture and release of plasmid DNA are best achieved with near-monolayer aminosilane films under pH ~ 8 buffer. These results will have an impact on diverse fields ranging from the layer-by-layer assembly of polyelectrolyte-based thin films to the selective electronic sensing of charged biomolecules.

4.5 Contributions of Authors

Dr. Kayesh Ashraf helped make XPS measurements for the aminosilane gradient at VCU. Dr. Higgins and Collinson guided the research and provided tremendous help with the preparation of this work for publication.

Chapter 5 Probing the Local Dielectric Constant of Plasmid DNA in Solution and Adsorbed on Chemically Graded Aminosilane Surfaces

Originally published as Zi Li, Ruwandi Kumarasinghe, Maryanne M. Collinson and Daniel A. Higgins "Probing the Local Dielectric Constant of Plasmid DNA in Solution and Adsorbed on Chemically Graded Aminosilane Surfaces", *J. Phys. Chem. B,* **2018**, *22,* 2307-2313. This work is reprinted here with permission.

5.1 Introduction

The dielectric constant, ε, in different microenvironments within double stranded DNA (dsDNA) is an important parameter that affects its interactions with other polyelectrolytes (e.g., proteins), with small organic and inorganic molecules (e.g., drugs), and with surfaces. Its value has been widely explored in both the computational[178-180] and experimental literature.[181, 182] The values reported reflect a high degree of microheterogeneity. For example, the major groove of dsDNA is known to be very polar, giving $\varepsilon \sim 55$.[182] The major groove is where proteins usually bind. Its high dielectric constant derives in part from the presence of water in the groove. The minor groove is substantially less polar, yielding $\varepsilon \sim 20$.[181] Polar small molecules and some proteins bind along the minor groove. Its smaller dielectric constant reflects closer proximity to the sugars and nucleobases and reduced contributions from water. Regions comprising the stacked nucleobases within dsDNA are expected to be the least polar of all. Nonpolar small molecules intercalate into these regions, usually inserting between the nucleobases. Computational studies give values of $\varepsilon < 5$ for these microenvironments.[178-180] Unfortunately, it appears that no direct

measurements of the dielectric constant for the least polar environments in DNA have been reported to date. In depth knowledge of the dielectric properties of these environments is of importance to a full understanding of DNA polarity.

Along with its dependence on location and composition, ε is also expected to vary with DNA conformation. It is well known that the flexibility of DNA increases (i.e., its persistence length decreases) with an increase in solution ionic strength.[183, 184] Increased flexibility of DNA is attributable to reduced repulsion between the negatively charged phosphate groups along its backbone. Condensation of DNA at high ionic strengths[80, 178] is likely to produce a decrease in the local dielectric constant as the organic regions of the DNA become more compact and the associated dipoles become less mobile. Similar effects may also arise when DNA is dissolved in a poor solvent,[185-187] or upon binding to synthetic polycations[80, 188] or proteins, such as occurs in the cell nucleus. Few, if any, previous studies have looked at the impacts of these phenomena on the dielectric constant of the least polar microenvironments within DNA.

Probing the polarity of these microenvironments requires the use of a dye that intercalates into DNA. The dye must also be sufficiently solvatochromic to afford a good measure of the local dielectric constant. Nile Red (NR) is an ideal candidate for such studies because it is highly fluorescent, very sensitive to local polarity,[114, 189] and sufficiently hydrophobic to function as a DNA intercalator.[120] NR has been employed previously to examine the dielectric properties of liquids,[114] organic polymers,[115, 116] proteins,[189] zeolites,[117] nanotubes,[118] mesoporous silica,[119] and organically modified silica.[136] It is nonfluorescent in aqueous environments and highly fluorescent in nonpolar environments,[117] making it uniquely suited to studies of DNA polarity in aqueous solution.

For this report, the local dielectric constant within the least polar microenvironments in plasmid DNA were measured by fluorescence microspectroscopic methods. The dielectric constant of the plasmid was measured in both its supercoiled and relaxed forms in aqueous buffer solution, as a function of buffer concentration, and for DNA molecules adsorbed along aminosilane-derived chemical gradients. The latter serve as models for DNA bound to different proteins.[17] Chemically graded surfaces[48, 49, 126, 153] were employed because they allow for time-efficient investigations of how the density of amine groups impacts the dielectric properties of the DNA.

5.2 Experimental Considerations

5.2.1 Chemicals and Materials

Relaxed and supercoiled plasmid DNA (5386 base pairs) were purchased from New England Biolabs. These were obtained as 10 mM Tris-HCl solutions (pH 8.0 at 25 °C) with 1 mM EDTA. NR, phosphate buffered saline (PBS), tetramethylorthosilicate (TMOS, 98%) and (3-aminopropyl)trimethoxysilane (APTMOS, 97%) were all purchased from Sigma-Aldrich and all were used as received. NR was dissolved in HPLC-grade ethanol to form a 200 nM stock solution. All buffers and DNA solutions were prepared using pure water of 18 MΩ·cm resistivity. Glass coverslips were obtained from Fisher Scientific (FisherFinest Premium, 25 × 25 mm). Silicon wafers were obtained from University Wafer and were cut into 25 mm x 25 mm pieces prior to use. Both types of substrate were thoroughly cleaned prior to use, as defined below.

DNA solutions. DNA solutions were prepared in 0.01 mM, 0.1 mM, 1 mM, 2.5 mM, 5 mM, and 10 mM PBS. These solutions were obtained by diluting 1×PBS with deionized water. 1×PBS (Sigma-Aldrich) contains 10 mM phosphate, 138 mM NaCl, and 2.7 mM KCl. Stock DNA solution was prepared by diluting 3.5 μL of 1000 μg/mL relaxed or supercoiled plasmid DNA to

1 mL with 1×PBS. The concentration of the stock solution was 1 nM. The 40 pM relaxed and supercoiled plasmid DNA solutions used for optical measurements were prepared by mixing 40 μL of 1 nM stock of the selected plasmid and 72 μL of 200 nM stock NR solution with 890 μL of one of the PBS solutions. The NR-stained DNA solutions were stored in a refrigerator overnight prior to use. The final staining ratio was ~ 1 NR per 15 DNA base pairs.

TMOS sol. The coverslips employed as substrates were coated with a silica base layer prior to gradient deposition. The base layer served to enhance aminosilane adhesion. The silica base layers were derived from TMOS sols. Preparation of the TMOS sols involved mixing TMOS, ethanol (200 proof), and 0.1 M hydrochloric acid in a volume ratio of 1:99.6:5.4. The mixture was subsequently stirred for 1 h and then stored in a desiccator for 23 h prior to use.

Substrate pretreatment. Both glass coverslips and silicon wafers were employed as substrates and were cleaned by first rinsing with DI water and then drying under a stream of nitrogen gas. They were subsequently cleaned for 5 min in an air plasma. The TMOS base layer was deposited by spin coating (5000 rpm, 30 s) a 150 μL aliquot of the TMOS sol onto the substrate surface. The base-layer-coated substrates were stored in a desiccator overnight. They were subsequently treated in an air plasma for 2 min immediately prior to use. The latter step ensured that a sufficient density of silanol groups on the base-layer surface was obtained for gradient deposition.

Amine gradient deposition. Vapor phase deposition (VPD) was used for preparation of the aminosilane gradients.[51] While VPD methods are often employed directly to obtain gradients based on the natural vapor diffusion profile over a surface, a simple cell formed over the substrate was employed here instead.[39] This cell was used to ensure the gradient was formed at a reproducible, predefined position in replicate depositions. For this purpose, two 1 mm-thick PDMS spacers were attached parallel to each other and parallel to the edges of the substrate. A clean glass coverslip

was placed on top of the spacers to form a 1 mm gap between the substrate and coverslip. The coverslip only covered one half of the substrate surface, ending at a distance of 8 mm from its edge.

The VPD process was performed in a Plexiglas chamber to eliminate any air currents and to allow for control over the ambient humidity during gradient deposition. The deposition chamber was constructed in house and was shown in an earlier publication.[39] Just prior to initiating VPD, the precursor reservoir and TMOS-coated substrate were placed on a horizontal platform inside the deposition chamber. The separation between the reservoir and substrate edges was 4 mm. The precursor reservoir was filled with a mixture of 25 μL of APTMOS and 0.2 g paraffin oil. This mixture was added through an inlet in the top of Plexiglas chamber. Each substrate was exposed to aminosilane vapor for 8 min to form the APTMOS gradient.

5.2.2 Gradient Characterization

Water contact angle. Sessile drop water contact angle measurements were used to verify that APTMOS gradients had been obtained. These measurements were made using a home-built apparatus. It includes a CCD camera with an attached zoom lens (Navitar), sample stage, and a light source. Droplet images were acquired on the CCD camera and were analyzed using a plugin available for the freely available ImageJ software package.[128] For these measurements, 1 μL droplets of high purity (18 MΩ·cm) water were placed at ~ 3-6 mm intervals along the gradients using a microliter syringe. Three replicate measurements were made at ~ 3 mm spacings across each gradient. All measurements were made under ambient laboratory conditions.

Film thickness. Spectroscopic ellipsometry was used to measure the thicknesses of both the TMOS-derived base layers and the aminosilane gradients. A commercial instrument (α-SE, J. A. Woollam) was used for this purpose and all measurements were made under a dry (15 $\pm$ 1% RH) nitrogen atmosphere. To achieve enhanced sensitivity, all measurements were performed on base

layers and gradients deposited on silicon substrates. Prior to gradient deposition, the base-layer thickness was first measured at a series of points 1 mm apart along the substrate and at three positions across the substrate, at 3 mm spacings. After gradient deposition, the full film thickness (gradient plus base layer) was measured in the same manner. The gradient thickness was determined by subtracting the base-layer thickness from the total film thickness.

5.2.3 AFM Imaging of DNA

Atomic force microscopy (AFM) images of supercoiled and relaxed plasmid DNA were collected using a Digital Instruments Multimode AFM with Nanoscope IIIa electronics. Tapping mode was employed to avoid damaging the features of the surface-adsorbed DNA molecules. Conical AFM tips (nanoscience Instruments, Phoenix, AZ) were used for imaging in air. The scan rate was 0.5 Hz. To obtain better images, freshly cleaved mica was used and aminosilane was deposited on it in the same manner as on TMOS coated glass coverslips. DNA solutions were prepared in 1 mM Tris-HCl buffer (pH ~ 7.1). $MgCl_2$ was added to the DNA solution to give a final concentration of 1 mM. The concentration of DNA was 1 µg/mL for both supercoiled and relaxed plasmid. DNA solutions were shaken for 1 h using a vortex mixer (Fisher Scientific) prior to deposition. During DNA deposition, a 50 µL aliquot of DNA solution was placed onto the APTMOS gradient modified mica and incubated for 10 min. Afterwards, the samples were rinsed with DI water and blown dry with nitrogen.

5.2.4 Optical Imaging

All optical imaging experiments were performed on aminosilane gradients prepared on glass coverslips. Each was immersed in one of the DNA/PBS solutions described above during imaging. For this purpose, a cell was constructed to hold the DNA solution. This cell comprised a 2 cm x 1 cm x 0.5 cm polydimethylsiloxane (PDMS) monolith. The PDMS cell was attached to the glass

coverslip using uncured PDMS. Once cured, the latter helped avoid leakage of the solution from the cell.

All samples were imaged on a wide-field epi-fluorescence microscope. The microscope employed has been described previously, in detail.[138] In each experiment, the PDMS cell and substrate were first mounted atop the microscope. An ~ 350 μL volume of NR-doped DNA solution was then added to the cell. Imaging of the NR-doped DNA was accomplished by exciting NR fluorescence with 514 nm laser light. Prior to illumination of the sample, the excitation light was first passed through a spinning optical diffuser, reflected from a dichroic beam splitter (Chroma 555 DCLP), and then focused into the back aperture of an oil immersion objective (1.49 numerical aperture, Nikon APO TIRF, 100×). Fluorescence emitted by the dye was collected in reflection, using the same objective. It was subsequently directed back through the dichroic beam splitter and through a 570 nm colored glass long-pass filter (Schott Glass). The fluorescence was then directed into an image splitter (Cairn Research OptoSplit II) incorporating a second dichroic mirror (Chroma 605 DCLP) and two bandpass filters. The image splitter divided the fluorescence into two image channels centered at ~ 580 and ~ 625 nm, respectively, each having a ~ 40 nm passband. Fluorescence in these image channels was detected simultaneously using an electron-multiplying CCD camera (Andor iXon DU-897). Fluorescence videos depicting DNA motion in solution and molecules adsorbed to the gradient surface were acquired as movies 100−500 frames in length.

5.3 Result and Discussion

5.3.1 Gradient Preparation and Characterization

Amine gradients were prepared on silica base-layer-coated coverslips by a vapor diffusion method that has been described previously.[39, 51] Gradient formation was verified by sessile drop

water contact angle (WCA) measurements. **Figure 5.1A** shows representative results. An abrupt transition from high WCAs at the high amine end to low values at the low amine (high silica) end is observed at ~ 10 mm. While WCAs could be measured at both ends of the gradient, it was not possible to obtain values in the steepest part of the gradient. In this region, water droplets placed on the surface moved spontaneously towards the low amine end.[51] The WCAs measured at the high and low amine ends are consistent with fully amine-modified and unmodified silica surfaces, respectively.[96, 190]

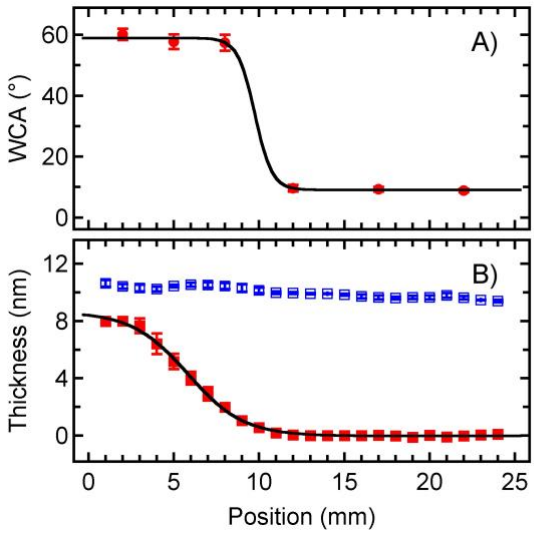

Figure 5.1 A) Sessile drop water contact angle along the amine gradient surface. No contact angle data could be obtained from the steepest region because the water droplets spontaneously moved towards the low amine end of the gradient. B) Spectroscopic ellipsometry data showing the thickness of the TMOS-derived base layer (blue symbols) and the aminosilane gradient (red symbols). Gradient thickness was obtained by subtracting the base layer thickness from the full film thickness. The positions along the X-axis in the two panels are not identical but indicate similar positions to ~ ± 1 mm. The solid lines are fits to sigmoidal functions and have been added only to better show the trends in the data.

The thicknesses of the silica base-layer coating and the amine gradient were determined by spectroscopic ellipsometry. The results are shown in **Figure 5.1B**. The base layer was nominally 10 nm thick. The gradient thickness was ~ 8 nm at the high amine end, indicating a multilayer aminosilane film had been formed.[190] The amine layer thickness quickly dropped to values near zero by the 11 mm position. The experiments described below focus on positions between 6 and 12 mm along the gradients.

5.3.2 AFM Imaging of Surface-Adsorbed Plasmid DNA

AFM was employed to verify the conformational differences between the relaxed and supercoiled forms of plasmid DNA adsorbed to the amine surface. For this purpose, DNA was adsorbed on aminosilane coated mica substrates by incubating them for a period of 10 min in 1 mM pH ~ 7.1 Tris-HCl buffer containing 1 mM $MgCl_2$ and 1 µg/mL (286 pM) plasmid DNA. The substrates were subsequently rinsed with DI water and blown dry with nitrogen.

Figure 5.2 shows representative tapping mode AFM images of surface-adsorbed supercoiled and relaxed plasmid DNA. The topographic heights of the DNA molecules were measured to be ~ 1 nm or less, consistent with previous observations of dsDNA.[94] The primary differences between the two forms of the plasmid are in their conformations, with the supercoiled DNA exhibiting significant superhelical twisting. The use of supercoiled and relaxed plasmid allowed for conclusions to be drawn on the relationship between DNA conformation, as observed by AFM, and the local dielectric constant in the least polar DNA microenvironments (see below).

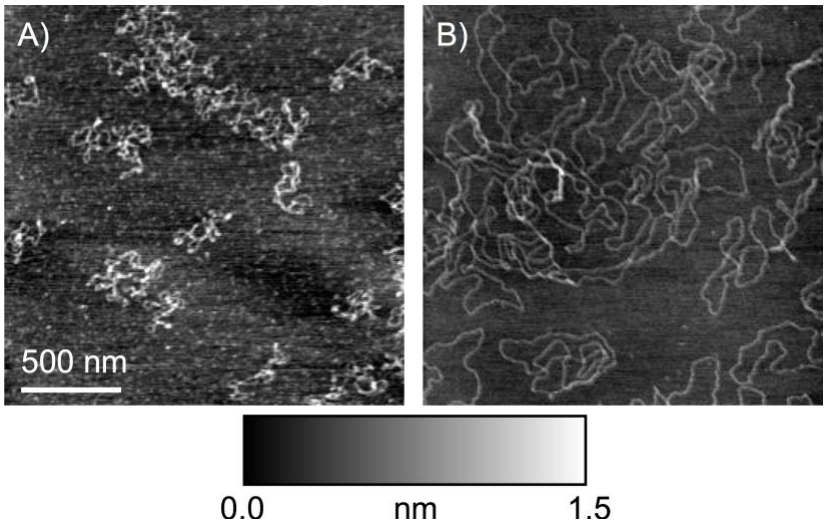

Figure 5.2 AFM images of A) supercoiled and B) relaxed plasmid DNA on APTMOS-coated mica. Plasmid DNA was deposited from 1 mM Tris-HCl solutions also containing 1 mM $MgCl_2$.

5.3.3 Dielectric Constant Measurements for Plasmid DNA in Solution

The dielectric constant within the least polar microenvironments of both solution-phase and surface-bound plasmid DNA was determined by using NR as a spectroscopic probe. It is well known that the fluorescence emission of NR shifts to the red with increasing ε.[114, 189] When its emission is recorded simultaneously in two spectral bands (i.e., 580 ± 20 nm and 625 ± 20 nm), the environment-dependent spectral shift of NR emission can be used to quantitatively determine ε.[116, 119, 138] Here, the emission ratio, E, defined as $E = (I_{625} - I_{580})/(I_{625} + I_{580})$ was employed, where I_{580} and I_{625} represent the measured fluorescence signal in each of the two spectral bands. As has been shown previously,[119, 138] E scales approximately linearly with the Clausius-Mossotti (CM) factor (see **Appendix Figure A4**, this work was completed by Ruwandi Kumarasinghe) of the local environment, where $CM = (\varepsilon - 1)/(2\varepsilon + 1)$. The CM factor comprises the dominant contribution[116] to the orientation polarizability by the dipoles surrounding NR within the DNA.

The results of the solution-phase fluorescence experiments will be described first. Phosphate buffered saline (PBS) solutions (0.01, 0.1, 1.0, 2.5, 5, and 10 mM phosphate concentrations, pH ~ 7.2 at all but 0.01 mM) containing 40 pM plasmid DNA and 14.4 nM NR were employed. Under these conditions, the level of dye loading in the DNA was ~ 1 NR for every 15 base pairs. The relatively dilute loading of the DNA by the uncharged NR dye is not expected to cause changes in its conformation.[120] Changes to the DNA structure induced by a higher staining ratio could alter the local dielectric properties. A higher staining ratio could also lead to increased intercalation of NR into more polar (less favorable) microenvironments. The small NR concentration precludes such effects and also helps avoid the formation of dye aggregates. Furthermore, NR aggregates have been reported to be non-fluorescent,[121] and should make no contribution to the measured signal.

All fluorescence imaging experiments were performed on an inverted wide-field microscope operated in the total internal reflection fluorescence (TIRF) mode. A solution filled cell fabricated from PDMS was employed and was positioned atop the microscope. A plasma-cleaned cover glass having no base layer or gradient coating was used to form the optical window of the cell in solution-phase experiments. The microscope was set to focus on DNA molecules diffusing in solution.[105] Representative two-color fluorescence videos show bright fluorescent spots that move rapidly from frame to frame within the area imaged. NR is known to be non-fluorescent in aqueous solution,[117] and control experiments performed in the absence of DNA were consistent with this expectation. Therefore, the bright spots observed in the videos are attributable to detection of individual NR-doped plasmid DNA molecules. Each molecule appears twice in the individual frames, once in each of the two channels (580 nm and 625 nm).

Solution-phase *E* values and the corresponding *CM* factors were obtained by measuring the background-subtracted signal level for each fluorescent spot. The results from a series of samples prepared at different buffer concentrations are plotted in **Figure 5.3** for both supercoiled and relaxed forms of the plasmid DNA. The *CM* factors all fall between 0.397 and 0.286, consistent with ε values ranging from 6.75 to 3.00, respectively. Taken together with theoretical predications of ε in the least polar regions of DNA,[178-180] these results provide conclusive evidence that NR behaves as an intercalator. The values obtained also provide experimental confirmation of the low ε values predicted for regions internal to the dsDNA double helix.[178-180]

The data shown in **Figure 5.3** depict a clear relationship between the *CM* factor and buffer concentration (proportional to ionic strength at constant pH in PBS buffer, see Experimental Considerations). The *CM* factor gradually increases as the buffer concentration decreases from 10 mM. It becomes relatively invariant at concentrations < 1 mM, although measurement error becomes significant at such low concentrations. The large error bars at 0.01 mM are attributable to the increased variability in ionic strength caused by reduced buffer capacity and increased variability in pH. The level of error also reflects the relatively weaker fluorescence observed from NR intercalated into DNA at lower buffer concentrations. Weaker NR fluorescence under these conditions is consistent with the observed increase in ε. NR is known to be less fluorescent in more polar environments.[117]

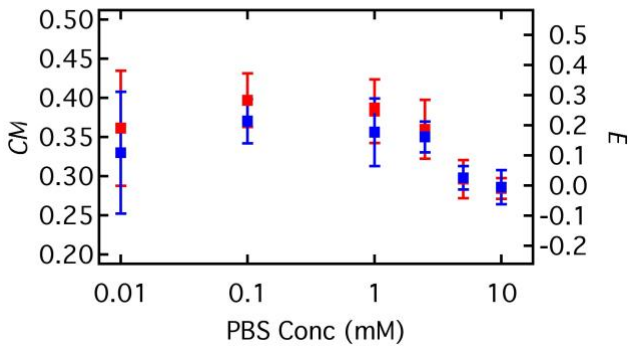

Figure 5.3 Solution phase E values (right axis) and CM factors (left axis) obtained from Nile Red in supercoiled (red symbols) and relaxed (blue symbols) plasmid DNA. The error bars depict the 95% confidence intervals for each value.

The decrease in ε with increasing buffer concentration correlates well with the known dependence of DNA persistence length on solution ionic strength.[183, 184] Extensive data reported in the literature show that the DNA persistence length is ~ 100 nm for ionic strengths of ~ 1 mM.[184] As the ionic strength increases, the persistence length decreases to ~ 50 nm.[184] This correlation suggests there might be a direct link between DNA conformation and local polarity.

While it is tempting to conclude that increased bending of the DNA at higher ionic strengths leads to a decrease in ε, the computational literature demonstrates that the dielectric constant depends most strongly on the composition and molecular structure within ~ 0.5 nm of the microenvironment being probed.[179] Changes in DNA conformation associated with changes in persistence length are manifested on longer (i.e., tens of nanometers) length scales. Furthermore, comparison of the data from relaxed and supercoiled plasmid reveals no measurable difference in ε despite their significant differences in conformation. It is concluded that the observed conformational differences are not the cause of changes in the local polarity. Rather, it is believed that the same factors that lead to increased flexibility of the DNA at higher ionic strengths also lead to changes in the DNA structure on much shorter length scales. These, in turn, cause a decrease in ε. Based on these observations, the lower dielectric constant sensed by NR at higher buffer concentrations is attributed to condensation of the DNA due to decreased repulsion between the negatively charged phosphate groups.[80] A contraction of the DNA structure occurs upon

condensation, driving water molecules from the structure and also leading to reduced mobility of the dipoles comprising the DNA microenvironment.

5.3.4 Dielectric Constant Measurements for Surface-Adsorbed Plasmid DNA

The binding of DNA to surfaces can also cause a contraction of its structure[191] and may lead to a similar decrease in the local dielectric constant. To explore such effects, measurements of ε were undertaken for DNA bound to aminosilane gradients exhibiting a spatially varying density of amine groups. As with the solution-phase experiments, these studies were performed under 0.01 mM to 10 mM pH ~ 7.2 PBS buffers incorporating 40 pM plasmid DNA and 14.4 nM NR. These solutions were left in contact with the amine gradients for a minimum of 5 min prior to imaging and remained in contact with the gradients for the duration of each experiment. The pK_a of surface-bound ammonium groups has been reported to be ~ 7,[172] and our earlier studies show that the high amine end of similar gradients carries a positive charge under the present conditions.[50] Binding of DNA to the high amine end is therefore expected to involve a combination of coulombic and hydrophobic interactions. Similarly, the negative charge carried by the low amine (high silica) end of the gradient under the same conditions[50] likely prevents binding of DNA at low ionic strengths.

Figure 5.4 shows representative two-color fluorescence images of surface-adsorbed, NR-doped DNA molecules. Surface-adsorbed DNA molecules appeared as bright, immobile fluorescent spots that remained at the same location over several video frames. The individual fluorescent spots are attributed to adsorption of single DNA molecules. While DNA can form aggregates in the presence of polyamines,[192, 193] their formation is usually observed at much higher DNA concentrations. Neither the video data obtained here nor in our previous studies[39] provide clear evidence of aggregate formation on the amine gradient surface. The vast majority of DNA molecules were observed to adsorb onto the surface in a single event. The fluorescence from each

molecule remained approximately constant or slowly decreased after adsorption. Little if any evidence for stepwise increases in fluorescence from these same spots was observed, as might be expected if aggregation of the DNA occurred on the gradient surface. Control experiments performed in the absence of DNA yielded fluorescent spots that were ~ 20-50-fold weaker, consistent with the assignment of the bright spots to NR-doped DNA. The *E* value for each spot was again obtained from the background-subtracted fluorescence signals in each of the two imaging channels.

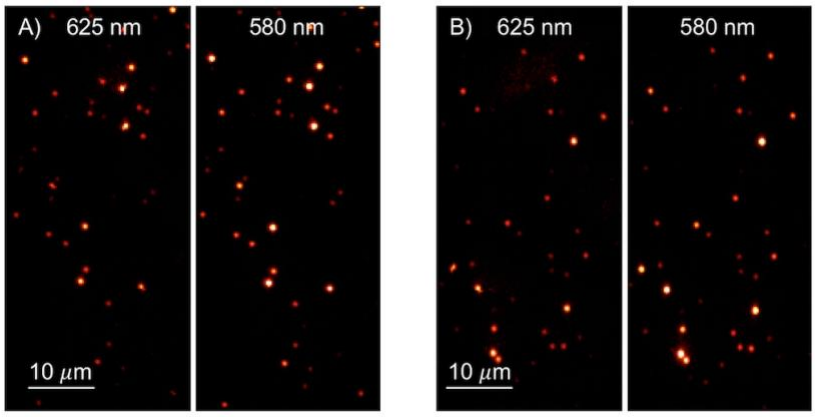

Figure 5.4 Two-color fluorescence images of NR-doped A) supercoiled and B) relaxed plasmid DNA adsorbed at the high amine end (6 mm position) of an APTMOS-derived gradient. These images were acquired under 2.5 mM pH ~ 7.2 PBS buffer. The color scale for both images is the same and depicts photon counts up to 1000 counts/pixel.

Figure 5.5 plots the average *CM* factors and dielectric constants (ε) for surface-adsorbed DNA molecules as a function of gradient position and buffer concentration. The reproducibility of the data was verified by repeating the experiments on several different gradients prepared on different days. Data from the lowest buffer concentrations (0.01 mM and 0.1 mM) were discarded because they produced very few detectable DNA adsorption events. The *CM* factors and ε for the

supercoiled and relaxed forms of the DNA were again found to be statistically indistinguishable from each other, confirming that conformational changes associated with superhelical twisting have little impact on ε for the least polar environments.

The polarity of the microenvironments was once again observed to vary as a function of buffer concentration, and also as a function of position along each gradient. At low PBS concentration, ε was measured to be ~ 1.90 and ~ 2.84 in DNA adsorbed at the high and low amine ends of the gradient, respectively. Similar to the solution-phase experiments, the ε value at the low amine (high silica) end also decreased as the PBS concentration increased. At the high amine end, ε remained approximately constant across the buffer concentrations employed. It is concluded that binding of the DNA to the amine groups at the high amine end of the gradient causes a condensation of the DNA structure and a corresponding decrease in ε as the microenvironments take on greater organic character and the associated dipoles become less mobile. Condensation of the DNA is again attributed to screening of the negatively charged phosphate groups by the ions on the surface and in solution. Increased ionic strength may also lead to closer approach of the DNA to the silica surface. However, the latter would likely cause an increase in ε at the low amine end with increasing ionic strength, and is discounted as a possible explanation.

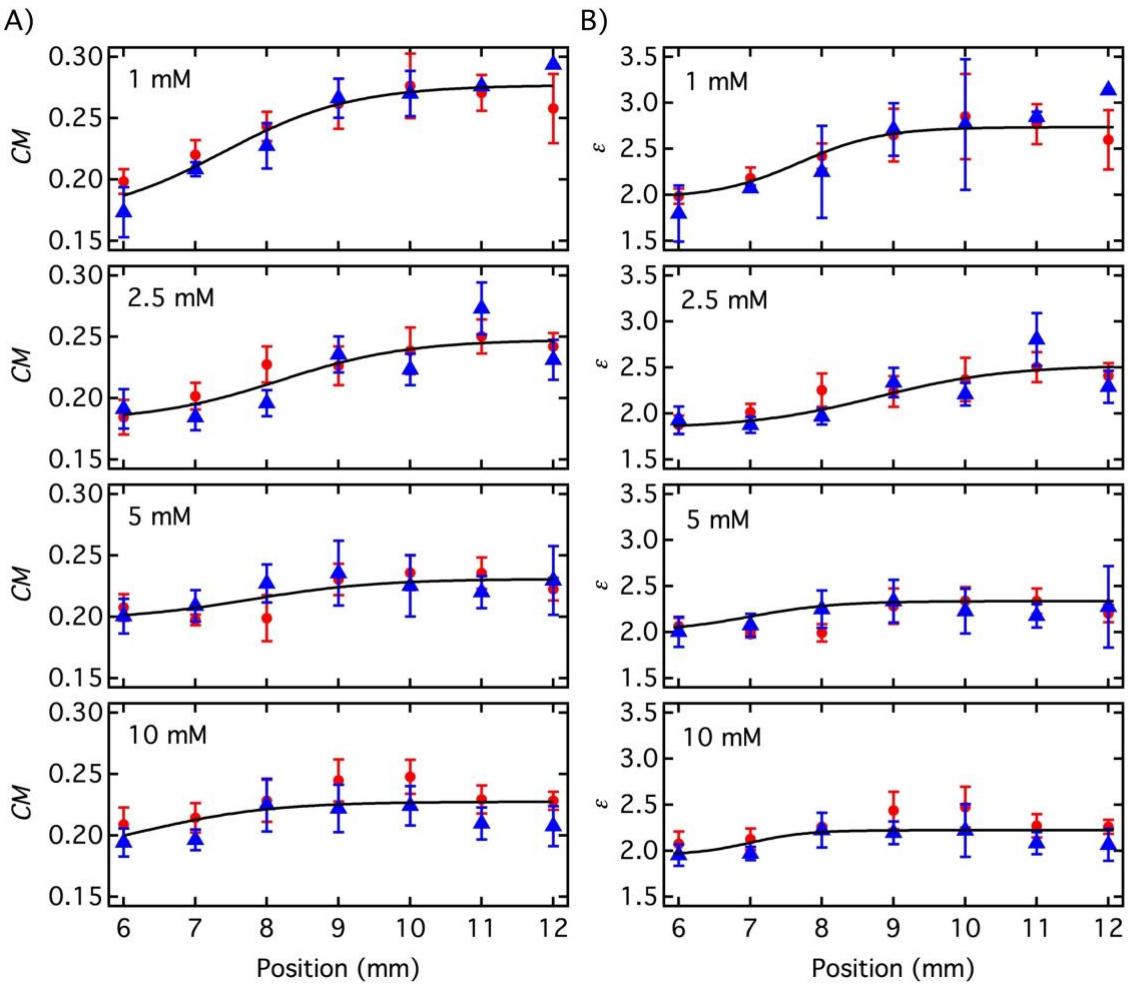

Figure 5.5 A) CM factor and B)dielectric constant for Nile Red doped supercoiled (red points) and relaxed (blue triangles) plasmid DNA as a function of position along APTMOS-derived gradients, and as a function of buffer concentration. All DNA molecules analyzed were adsorbed on the gradient surface. The 6 mm position represents the high amine end, with decreasing amine coverage towards the 12 mm position. The error bars show the 95% confidence intervals for each value.

5.4 Conclusion

In summary, the present studies provide experimental confirmation that NR behaves as an intercalator when binding to DNA, and that the dielectric constant of the microenvironments in

which it binds is small and similar to that predicted in computational studies. More importantly, the results obtained provide new knowledge on how the local dielectric constant within dsDNA is impacted by changes in the solution ionic strength and binding to amine-modified surfaces. The results showed that there is no measureable difference in ε for the least polar microenvironments in relaxed and supercoiled forms of plasmid DNA. In contrast, a clear decrease in ε was observed with increasing ionic strength and for higher amine density along chemically graded surfaces. These results provide an enhanced understanding of the least polar microenvironments in DNA and the factors that determine their dielectric constants.

5.5 Contributions of Authors

I was responsible for the DNA solution and chemical gradient preparations, AFM imaging of the DNA and optical experiments. Ruwandi Kumarasinghe helped calibrate of the nile red response as shown in Appendix. Also, she helped with the alignment of wide-field microscope and provided her valuable experience in spectroscopic imaging. Both of Ruwandi Kumarasinghe and I worked on the data analysis and summarization. Dr. Higgins guided the research patiently. He and Dr. Collinson provided indispensable help for the publication preparation.

Chapter 6 Studies of DNA Interactions with C8-silane/APTMOS Two-Component Opposed Chemical Gradients Under Potential Control

6.1 Introduction

Electrostatic and hydrophobic interactions between biomolecules (i.e. proteins and nucleic acids) and different chemically modified surfaces play a vital role in governing the performance of biological and biomedical devices.[25, 105, 194] For instance, a full understanding of the dynamics and variations of DNA adsorption/desorption on charged surfaces or hydrophobic surfaces is significantly important to the development and advancement of DNA microarrays,[21] DNA-based biosensors, [6, 105, 195] chromatographic techniques for DNA purification,[24-26] and for fundamental studies of protein-DNA interactions.[196, 197] A large number of research studies have been performed to investigate the mechanisms of DNA adsorption/desorption at a wide range of different surfaces such as glass,[198] silicon,[25] porous silica, nanoparticles,[40, 107, 199] gold[30] and so forth. The main driving force of DNA adsorption that has been most widely investigated are the electrostatic interactions of negatively charged DNA with positively charged surfaces. In this case, surfaces carrying positive charges, often derived from amine-terminated surface modifiers, are very common. Owning to the pK_a (~ 2) of the phosphate groups on DNA backbone,[66] DNA carries a significant negative charge at common pH values.

However, in addition to the charge-charge interactions mentioned above, DNA also incorporates nonpolar moieties (i.e., its aromatic nitrogenous bases) that can also interact with surfaces through hydrophobic effects. Single-stranded DNA shows larger hydrophobicity than double-stranded DNA because of its exposure of the bases.[44, 83] Despite their importance, studies

of the hydrophobic interactions of DNA with surfaces are less common. It is important to understand DNA adsorption/desorption on hydrophobic surfaces for other applications such as purification of plasmid DNA using hydrophobic interaction chromatography (HIC).[44, 46] Particularly important are studies that explore the strength and stability of DNA adsorption on hydrophobic surfaces. Comparisons of the results to those obtained in situations where electrostatic interactions dominate are important to understanding DNA adsorption/desorption under more general circumstances.

DNA adsorption/desorption behaviors have been studied using various techniques such as atomic force microscopy,[29, 97, 100] absorbance[200] and fluorescence spectroscopy,[25, 194, 199] x-ray reflectivity,[201] radiological methods[202] and single molecule fluorescence detection methods.[31, 32, 39, 105, 106] Among these techniques, single molecule fluorescence microscopy is capable to detecting DNA adsorption/desorption behaviors at various solid/liquid interfaces in real-time. Additionally, the dynamics and kinetics of DNA adsorption/desorption can be explored using single molecule fluorescence microscopy. The most important advantage of single molecule fluorescence detection over other methods for studying DNA-surface interactions is that it excludes from averaging data but allows for examining every single molecule data.[203] The data from each molecule can be used to construct an actual distribution in terms of a certain parameter of interest.

Single molecule studies of DNA adsorption have been reported in the literature since the initial work of Yeung's group.[30-33] Their studies[31] showed that DNA conformations and adsorption behaviors depend on both solution pH and buffer composition. According to the results, they also stated that hydrophobic interactions rather than electrostatic interactions are the major driving force of DNA adsorption. Later, they studied DNA adsorption at compositionally patterned self-assembled monolayers as models of various chromatographic packings using single molecule

fluorescence microscopy.[30] The results showed that the affinity strength of DNA with amine-terminated self-assembled layers is larger than alcohol- and acid-terminated surfaces at relatively basic pH (pH ~ 8). They also found that the boundary between two adlayers is favorable for DNA adsorption. This result indicates that DNA adsorption can be affected by the defects and surface topography of adlayers.

Although studies of spontaneous adsorption of DNA to surfaces are important to understanding the fundamental driving forces for DNA adsorption, new device technologies often require the ability to modulate and control DNA adsorption. That is, devices that allow DNA capture and release on demand would be particularly valuable in DNA sensing. One means for achieving controlled capture and release of DNA is through the application of an electrical potential to the capturing surface.[39, 105]

A wide array of metal electrodes could be used for DNA capture and release. While these may be ideal for application of an electrical potential, they are not well suited to optical detection of DNA. Optically transparent indium tin oxide (ITO) electrodes are one of the most promising candidates for use in devices capable of achieving controllable DNA capture and release,[39, 105] while also allowing fluorescence detection of the capture events. ITO electrodes are sufficiently conductive so that an electrical potential can still be applied to achieve DNA capture and release on the silica-coated ITO substrates. Our previous study showed that DNA can be captured and released at partially modified aminosilane surfaces on ITO substrates at pH ~ 8 under potential control.[39]

This chapter focuses on the investigation of the stability of DNA adsorption on an opposed two-component hydrophobic C8-silane and positively charged aminosilane gradient as a function

of solution pH and silane surface coverage. Preliminary results regarding DNA adsorption and the mobility of surface-adsorbed DNA molecules are given and discussed.

6.2 Experimental Considerations

6.2.1 Chemicals and Materials

The supercoiled plasmid DNA (5386 base pairs) and YOYO-1 fluorescent dye employed in this chapter are the same as those used in **Chapter 4**. Phosphate buffered saline (PBS) powder was purchased from Sigma-Aldrich. Potassium phosphate, sodium hydroxide and sodium acetate were obtained from Fisher Scientific. The ITO coated cover slips (22 × 26 mm, 0.13-0.17 mm thick, 8-12 Ω/cm^2) employed are also the same as those used in **Chapter 4**. Tetramethylorthosilicate (TMOS, 98%), (3-Aminopropyl)trimethoxysilane (APTMOS, 97%) and Trichloro(octyl)silane (C8-silane) were purchased from Sigma-Aldrich. All chemicals were used as received. All buffers and solutions were prepared using pure water with 18 MΩ·cm resistivity.

***DNA solutions*.** DNA buffer solutions were prepared from three different weak acid/base conjugate pairs to obtain solutions buffered to different pH values. The three types of buffers employed in this chapter were 0.2 mM acetate, 0.01 mM PBS, and 0.1 mM phosphate solutions having pH values of ~ 3.6, ~ 5.5, and ~ 7.3, respectively. The ionic strengths of these three buffers were similar, each being approximately 0.2 mM. The DNA stock solution was 1 nM, prepared by diluting 3.5 µL of the 1000 µg/mL plasmid DNA with one of the three buffers to a final volume of 1 mL. A 1 µM YOYO-1 stock solution was prepared by diluting the 1µL of the original YOYO-1 dye (1 mM) in DMSO to 1 mL final volume, using 1X PBS buffer. The YOYO-1 doped plasmid DNA solution had a DNA concentration of 40 pM and was prepared by mixing 80 µL of 1 nM plasmid DNA and 29 µL of 1 µM YOYO-1 dye solution with 0.2 mM acetate buffer, 0.01 mM PBS or 0.1 mM phosphate solution to yield a total solution volume of 2 mL. The YOYO-1 labeled

DNA solutions were stored in a refrigerator overnight prior to use. Overnight storage allowed the YOYO-1 dye to fully intercalate into the DNA. The final staining ratio of plasmid DNA by YOYO-1 dye was 1 dye molecule per 15 base pairs.

TMOS sol and ITO substrate pretreatment. The TMOS sol used for the substrate base-layer coating was prepared in the same manner as described in **Chapter 4.2.1**. Briefly, it was prepared by mixing TMOS, 200 proof ethanol, 0.1 M HCl in a volume ratio of 1:99.6:5.4. The mixture was stirred for 1 h and then stored in a desiccator for 23 h prior to use. For the pretreatment of ITO substrates, a 150 µL aliquot of the TMOS sol was deposited on the plasma cleaned ITO surface and subsequently spin coated (5000 rpm, 30s) to form a thin silica base layer. As noted above, the silane base layer afforded better modification of the substrate by the organosilanes used in gradient formation. The silica base layer-coated ITO substrates were stored in a desiccator for overnight prior to use.

Two-component organosilane gradient deposition. Aminosilane and C8-silane precursors were deposited from opposite ends of a TMOS base-layer-coated ITO substrate using the vapor phase deposition method described in **Chapter 3**. The deposition setup is shown in **Figure 3.4**. In the two-component gradient preparation, APTMOS was first deposited from one end of the base-layer-coated ITO substrate and the C8-silane was subsequently deposited from the other end of the same substrate. The front edge of a clean glass coverslip was placed at 12 mm position from one short edge of the ITO substrate and was separated from the substrate by two, 2 mm thick PDMS spacers (14 mm × 2 mm × 2 mm) placed along the long edges of the ITO substrate. The glass coverslip placed atop of the ITO substrate was used to better control gradient deposition and to ensure that reproducible opposed two-component gradients could be obtained. The two slides and PDMS spacers formed a vapor deposition cell that defined the precise location at which the vapor

diffusion profile forms. Specifically, the mixture of the two silanes are supposed to be in the middle of the ITO substrate (position 13 mm and 14 mm).

Prior to gradient deposition, the silica base layer was activated in an air plasma for 2 min to generate sufficient hydroxyl groups for silane deposition. Each substrate was first exposed to APTMOS vapor and then C8-silane vapor. In each case, the exposure time was 15 min. The APTMOS and C8-silane opposed two-component gradient-modified ITO substrate was then used to form the bottom of an electrochemical cell and was subsequently immersed in the DNA buffer solution. The electrochemical cell employed here is shown in **Figure 4.1**.

6.2.2 Gradient Characterization

Water contact angle and ellipsometric film thickness measurements were also conducted to verify two-component gradient formation and to characterize their profiles and overall quality. The detailed procedures of these two measurements can be found in **Chapter 3.3** and **Chapter 4.2.2**.

6.2.3 AFM imaging

Plasmid DNA solution of 1 μg/mL was prepared by mixing 899 μL of 0.2 mM acetate buffer (pH ~ 3.6), 100 μL of 10 mM $MgCl_2$, and 1 μL of DNA stock solution (1000 μg/mL, in 10 mM Tris-HCl and 1 mM EDTA, pH ~ 8.0 at 25˚C) to a total volume of 1 mL. The final concentration of $MgCl_2$ is 1mM in the DNA solution. The DNA solution was then shaken for 1 h. Subsequently, 100 μL of the DNA solution was placed on the gradient modified mica surfaces and incubated for 15 min. Finally, the sample were rinsed with DI water and blown dry with nitrogen. They were subsequently transferred to the AFM for imaging.

AFM images were taken for the surface-adsorbed DNA molecules on the opposed two-component C8-silane/aminosilane gradient. Freshly cleaved mica substrates were employed here because they are atomically flat and therefore, facilitate observation of the adsorbed DNA

molecules. In this case, C8-silane and aminosilane were directly deposited onto the freshly cleaved mica. No silica base layer was applied, because these films often have sufficient roughness that observation of the adsorbed DNA becomes difficult. Before silane deposition, each mica substrate was plasma cleaned for 2 min. The same gradient preparation procedure employed in **Chapter 6.2.1** was again used here to obtain the gradients. Because the gradients were too long to fit in the AFM instrument, they were cut into two pieces at 13 mm position prior to imaging. Each piece was attached to one AFM sample stage (1 cm in diameter). AFM images were acquired using a Digital Instruments Multimode AFM with Nanoscope III electronics. The images acquired were 2 $\mu m \times 2\ \mu m$ in size. As usual, tapping mode was employed to avoid damaging the features of the surface-adsorbed DNA molecules. The scan rate was 0.5 Hz.

6.2.4 Single Molecule Detection of DNA-Surface Interactions

TIRF mode fluorescence microscopy was also employed to study DNA interactions with APTMOS and C8-silane opposed gradients on ITO substrates under potential control. The wide-field microscope setup is shown in **Figure 3.8**. The detailed optical imaging procedures are described in **Chapter 3.4.2.1**. and **Chapter 4.4.2**. In this case, fluorescence videos of 460 frames in length (0.55 s frame time) were recorded along the opposed two-component gradients (from the 6 mm position at the high C8-silane end to the 20 mm position at the high amine end). The square wave potentials (-0.5 V to +1.4 V vs Ag/AgCl) were again applied to the ITO substrates using a CH instruments potentiostat during fluorescence measurements. A total of 25 steps were employed starting with a positive potential +1.4V vs an Ag/AgCl reference electrode. This applied potential range was determined in **Chapter 4**. To investigate and compare the stability of DNA adsorption on APTMOS and C8-silane gradient surfaces, the surface-adsorbed DNA molecules were tracked

using single molecule tracking software written in-house in the LabView programming environment.

6.3 Preliminary Results and Discussion

6.3.1 Characterization of Opposed Two-Component Gradients

The C8-silane and aminosilane opposed two-component gradients were characterized by sessile drop water contact angle and ellipsometric thickness measurements. **Figure 6.1** shows the representative results. The WCAs are ~ 100˚ at the high C8-silane end, confirming the successful deposition of C8-silane onto the TMOS coated ITO substrate. The WCA decreases along the C8-silane gradient from 1 mm to 15 mm (from the left to the middle shown in **Figure 6.1A**). Meanwhile, the WCAs are ~ 60˚ at the high amine end and decrease along the aminosilane gradient from 26 mm to 15 mm (from the right to the middle shown in **Figure 6.1A**) The lowest WCA angle is observed at ~ 15 mm, approximately where the mixture of the C8-silane and the aminosilane are deposited. The larger error bar at 15 mm depicts the inhomogeneous deposition of the C8-silane and aminosilane mixture, whereas the relatively large error bar at 25 mm represents the larger roughness of the high aminosilane end.

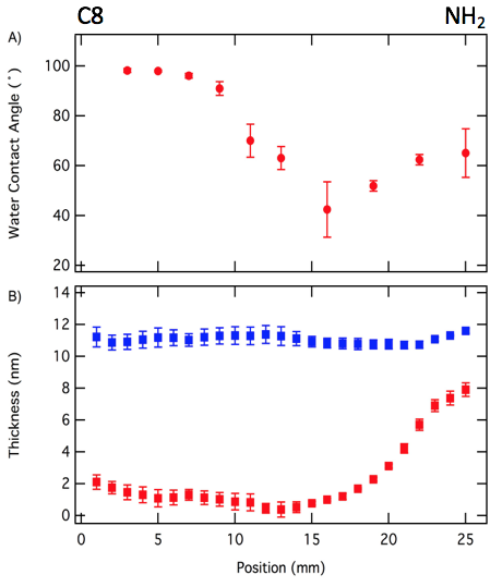

Figure 6.1 A) Sessile drop water contact angles from an opposed C8-silane/APTMOS two-component gradient. B) Thickness of TMOS silica base layer (blue square) and C8-silane/APTMOS opposed two-component gradient (red square). The error bars depict the standard deviation of three replicate measurements at each position.

The thickness of the opposed two-component C_8 – NH_2 gradient was measured using spectroscopic ellipsometry. In this case, the C_8 – NH_2 gradients were prepared on a TMOS coated silicon wafer. For this purpose, a silicon wafer was cut into small pieces having the same size as the ITO substrates (22 mm × 26 mm). The silica base layer was spin coated onto the silicon substrates in the same manner as described previously. Prior to gradient deposition, the thickness of the TMOS silica base layer was first measured at a series of points with 1 mm apart along the substrate and at three positions at 3 mm spacings across the substrate. All measurements were made under a dry nitrogen environment. The C_8 – NH_2 gradient was subsequently deposited onto the base-layer-coated silicon substrate. Finally, the full film thickness of the C_8 – NH_2 gradient plus the base layer was measured at the same series of positions along and across the substrate as described above. The thickness of C_8 – NH_2 gradient was obtained by subtraction of the full film thickness from the TMOS base layer thickness.

Figure 6.1B shows representative film thickness results for a C_8 – NH_2 gradient on a base-layer-coated silicon substrate. The thickness of the C8-silane gradient was approximately equivalent to that of a monolayer (~ 1.1 nm) at the 6 mm position. The film thickness decreased slowly along the C8-silane gradient. At the high amine end (i.e., near the 20 mm position), the thickness was measured to be ~ 3 nm. The thickness of the aminosilane film dropped to mono- and submonolayer thickness near the 15 mm position. At the intersection of the C8-silane and

aminosilane (near the 13 mm and 14 mm position), the substrate was only partially modified, yielding a film thickness of ~ 0.4 nm- ~ 0.5 nm.

6.3.2 AFM Imaging of DNA on $C_8 – NH_2$ Gradient Surfaces

Representative AFM images of surface-adsorbed DNA are shown in **Figure 6.2**. The top row shows the AFM images acquired at the C8-silane end from 8 mm to 11 mm, while the bottom row images were taken at the aminosilane end from 18 mm to 15mm. Interestingly, DNA attachment was only observed at the C8-silane end, not at the aminosilane end. This can be explained by the differences in the thickness and roughness of the C8-silane and aminosilane films. As shown in **Figure 6.1B**, the C8-silane gradient thin film is approximately one monolayer thick from 8 mm to 11 mm. Also, the roughness of the C8-silane gradient thin film is small. Previous publications have shown that the roughness of C8-silane-based self-assembled monolayer is less than 0.3 nm.[204] Adsorbed DNA molecules might be attached to the C8-silane through hydrophobic interactions or to the bare mica surface with the help of Mg^{2+} as a bridge between both negatively charged DNA and mica surfaces. In contrast, at the high aminosilane end, the thin film gradient is a multilayer, about 2-3 nm thick (the thickness of a monolayer aminosilane thin film is about 0.7 nm) and it is relatively rough. According to previous studies, the roughness of a multiplayer aminosilane thin film is on the nanometer scale.[205, 206] The roughness of these physical properties of the aminosilane gradient thin film might prevent the attached DNA molecules from being observed in the AFM images because the roughness of the film could overshadow the features of the DNA molecules. As it has been reported, the topographic height of dsDNA is ~ 1 nm. Therefore, AFM imaging cannot detect the surface-adsorbed DNA at the aminosilane end, where the average surface roughness is probably more than 1 nm.

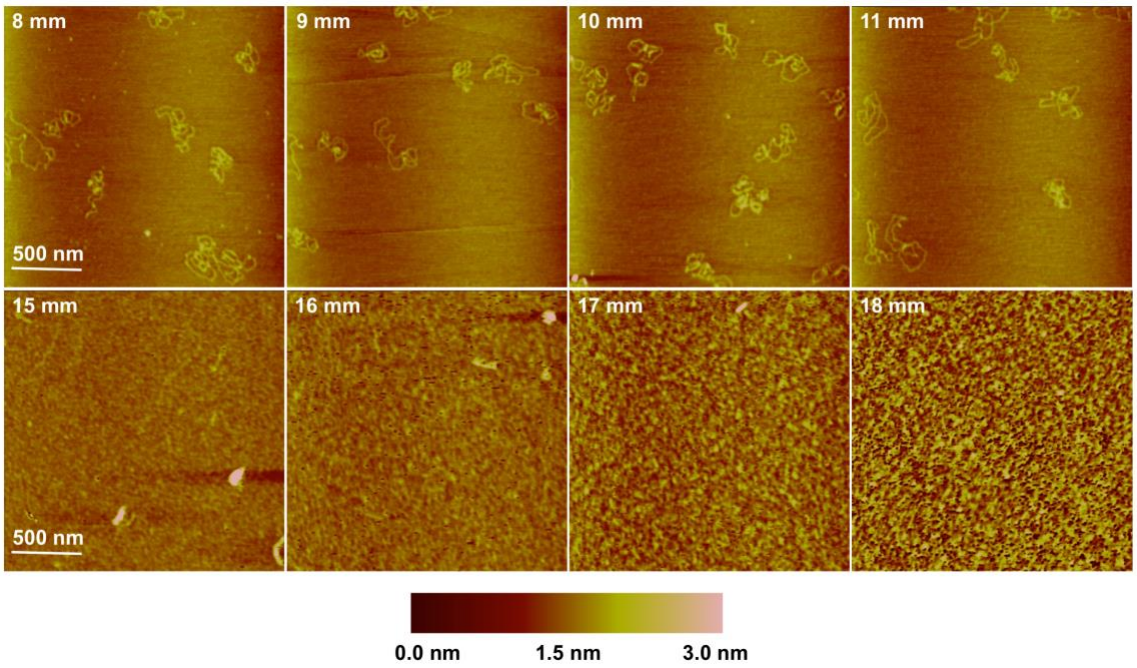

Figure 6.2 AFM images of surface-adsorbed supercoiled plasmid DNA at the C8-silane end (8 mm – 11 mm) and at the aminosilane end (18 mm – 15 mm) of the gradient. Scale bars are 500 nm in length and apply to all the images.

6.3.3 Single Molecule Studies of Surface-adsorbed Plasmid DNA

Single molecule detection of plasmid DNA adsorption onto opposed C8-silane and aminosilane two-component gradients was performed using a wide-field fluorescence microscope under potential control. In these experiments, the electrical potential applied was repeatedly stepped between + 1.4 V and -0.5 V vs a Ag/AgCl reference electrode. The useful potential window was determined and discussed in **Chapter 4.3.1**. In this session, the adsorption behavior of the plasmid DNA and its mobility along the opposed C8-silane and aminosilane two-component gradients were examined and discussed.

Adsorption Behavior of Plasmid DNA on C_8 – NH_2 Gradient

To study the adsorption behavior of plasmid DNA on the opposed two-component $C_8 - NH_2$ gradient, 40 pM YOYO-1 labeled plasmid DNA solutions were prepared in 0.02 mM acetate buffer (pH 3.6), 0.01 mM PBS buffer (pH 5.5) and 0.1 mM phosphate buffer (pH 7.3). The ionic strengths of these three buffers were similar, all having values of ~ 0.2 mM. Since the pK_a of the amine group on the surface has been reported to be ~ 7,[172] most of the amine groups on the surface should be protonated under all three pH conditions. Therefore, the aminosilane-modified surfaces are positively charged. The amount of positive charge decreases from the high amine end to the low amine end. No positive charge is present at the C8-silane end. The driving force of DNA adsorption onto the C8-silane film is expected to arise from hydrophobic interactions between the nonpolar stacked bases of the DNA and the nonpolar C8-silane surfaces, while the mechanism of DNA adsorption onto the aminosilane surfaces is a combination of electrostatic and hydrophobic interactions.

The density of surface-adsorbed DNA molecules was obtained by counting each molecule observed in the images recorded at positions from 6 mm (high C8-silane end) to 20 mm (high aminosilane end) along the opposed C_8-NH_2 gradients. These experiments were performed under solutions of various pH values. As shown in the histograms of **Figure 6.3**, maximum DNA adsorption to the C8-silane surfaces was achieved at pH ~ 3.6. This might be due to the greater neutralization of the negative charges on the DNA backbone at the lower pH. The neutralization of DNA charge causes a decrease in electrostatic repulsion between the nucleotides. The DNA appears less polar at low pH and hence the hydrophobic interactions of DNA with the C8-silane surfaces are enhanced.[31] Thus, among all the three pH environments, DNA adsorption at the C8-silane end is highest at pH ~ 3.6. However, there are other possible explanations. According to the thickness results presented in **Figure 6.2B**, the C8-silane film is roughly a monolayer at the high

C8-silane end of the gradient. Even at this coverage, defects are expected to be present in the film.[207] Any defects present in the C8-silane thin film are expected to expose silanol groups on the silica base layer. As the pI of silica is known to be ~ 2.5, these sites are expected to carry appreciable negative charges. As the isoelectric point of DNA is ~ 5,[208] the DNA is expected to carry a positive charge below pH 5. Therefore, the positively charged DNA could adsorb to negatively charged silanol groups on the surface at the C8-silane end.

At the high amine end, DNA adsorption is mostly driven by electrostatic interactions between the DNA molecules and the protonated amine groups on the surface under all the three pH conditions because the pK_a for the amine groups on the similar aminosilane surfaces has been reported to be ~ 7.[172] As has been reported earlier, the degree of ionization of surface amine groups decreases as the solution pH increases,[172] and hence, the positive charges on the high amine end would decrease at higher pH values. Consequently, adsorption events of DNA on the high amine end are expected to decrease in frequency with an increase in the solution pH. However, a large increase in the population of surface-adsorbed DNA was observed at pH ~ 7.3, as shown in **Figure 6.3C**. This observation is consistent with the results we have reported earlier.[39] The cause of the increase in the DNA adsorption at the high amine surface under higher pH is not clear at present. A possible explanation might be that there is an enhanced contribution of hydrophobic effects to DNA adsorption under such conditions. However, one might say that almost no DNA adsorption was observed to adsorb at the nonpolar high C8-silane end under these same circumstances, contradicting this hypothesis. This might be explained by the fact the hydrophobicity of DNA is enhanced via charge neutralization of the DNA molecules. The positive charges in the protonated amine groups on the surface could neutralize the negative charges on the DNA phosphate backbone. Meanwhile, many research studies have shown that the charge neutralization of DNA

by the positive charges on the surface can lead to the conformational changes in DNA.[29] In this case, the surface charge induced conformational changes in DNA might be the reason for the increase in DNA adsorption at the high amine end under pH ~ 7.3.

Comparing DNA adsorption at the high C8-silane end and that at the high amine end under the three pH environments, DNA adsorption at the high C8-silane end is more dependent on the solution pH. In contrast, DNA adsorption to the aminosilane modified surfaces are mostly independent of solution pH when the solution pH falls between 3.6 and 7.3. Based on these phenomena, we can generally conclude that electrostatic interactions of DNA with the amine surface are relatively more important at pH ~ 5.5 and pH ~ 7.3 than hydrophobic interactions of DNA with the C8-silane surface.

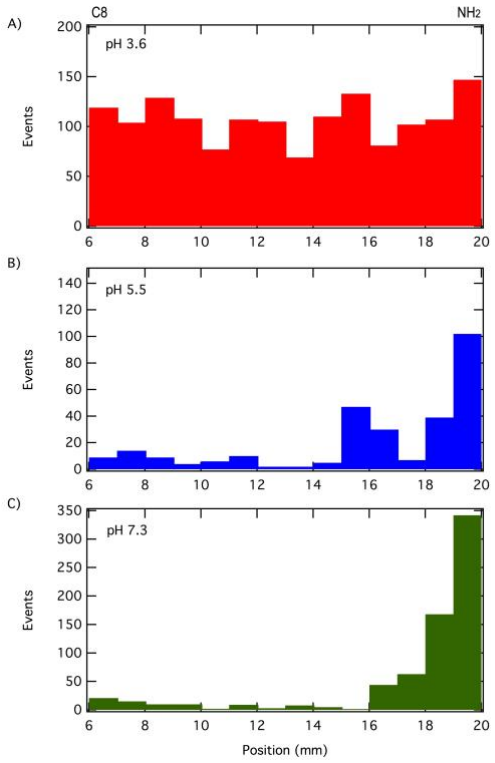

Figure 6.3 Histograms showing the number of DNA adsorption events distribution as a function of position along the opposed C8-silane and aminosilane gradients and as a function of pH for A) ~ 3.6; B) ~ 5.5; C) ~ 7.3.

The Mobility of Surface-Adsorbed Plasmid DNA on $C_8 - NH_2$ Gradients

To investigate the stability of DNA adsorption, the mobility of surface-adsorbed DNA was obtained using single molecule tracking methods. In this case, the mobility was assessed via the evolution of the radius of gyration (R_g evolution) exhibited by each molecule as it moved around the surface. The radius of gyration explicitly describes the size of the region that a single DNA molecule explores in its trajectory. The R_g analysis was first employed in single molecule studies by Lindsay C. C. Elliott, et.al.[203] The radius of gyration, R_g, of a single molecule trajectory depicts the spatial exploration of that molecule during its movement. It is calculated as the root mean square distance from the single molecule trajectory's initial center of mass in Equation 4.1.

$$R_g = \sqrt{{R_1}^2 + {R_2}^2} \qquad \textbf{(Equation 4.1)}$$

Where R_1 and R_2 represent the major and minor eigenvalues of the radius of gyration tensor, $\boldsymbol{T}$, repectively. The tensor $\boldsymbol{T}$, shown in Equation 4.2, is calculated from the x and y positions of a single molecule in the trajectory.

$$\hat{T} = \begin{pmatrix} \frac{1}{N}\sum_{j=1}^{N}\left(x_j - \langle x\rangle\right)^2 & \frac{1}{N}\sum_{j=1}^{N}\left(x_j - \langle x\rangle\right)\left(y_j - \langle y\rangle\right) \\ \frac{1}{N}\sum_{j=1}^{N}\left(x_j - \langle x\rangle\right)\left(y_j - \langle y\rangle\right) & \frac{1}{N}\sum_{j=1}^{N}\left(y_j - \langle y\rangle\right)^2 \end{pmatrix} \qquad \textbf{(Equation 4.2)}$$

In Equation 4.2, N represents the total number of frames in the trajectory. The variables x and y represent the position of a single DNA molecule in the fluorescence video. While a single value for R_g can be determined from the entire trajectory, the evolution of R_g is acquired by determining its value after each frame in the trajectory to illustrate how it evolves over time. The main advantage of using R_g as a means to quantify the mobility of surface-adsorbed DNA molecules is that it provides information on even brief mobile periods of the DNA molecules in what are otherwise relatively immobile trajectories.

The R_g values of DNA molecules were obtained by tracking and analyzing the trajectory of each of every surface-adsorbed plasmid DNA at each position from the 6 mm (high C8-silane end) to the 20 mm position (high amine end) along the opposed two-component gradients under solutions of different pH. **Figure 6.4** shows the average R_g values for surface-adsorbed DNA molecules along the gradients at pH ~ 3.6, ~ 5.5 and ~ 7.3. As shown in **Figure 6.4A**, the R_g values obtained at the high C8-silane end are similar as those obtained at the high amine end at pH ~ 3.6. The increase in R_g values between the 13 mm and 14 mm positions might be due to a decrease in available binding sites of C8-silane and aminosilane on the surface. DNA adsorption is less stable with fewer binding spots. **Figure 6.4B** shows a dramatic increase in the R_g values of surface-adsorbed DNA molecules on the high C8-silane end at pH ~ 5.5, but not on the high aminosilane end. As the DNA might show less hydrophobic effect at pH ~ 5.5 than that at pH ~ 3.6, less DNA adsorption events are observed. Meanwhile, the binding strength of the DNA with the C8-silane surface is diminished. The result is an increase in the mobility of surface-adsorbed DNA at the high C8-silane end. This is described by the increase of the R_g values shown in **Figure 6.4B**. However, the R_g values of surface-adsorbed DNA at the high C8-silane end at pH ~ 7.3 are not as large as expected. Instead, the average R_g values are only a little larger than those at pH ~ 3.6. The reason for the decrease in R_g values from pH ~ 5.5 to pH ~ 7.3 at the high C8-silane end is not clear. It might be caused by the intrinsic inhomogeneity of the C8-silane gradient deposited by vapor diffusion methods. At the aminosilane end, the average R_g values increase with an increase in pH. The increment of R_g values from pH ~ 3.6 to pH ~ 5.5 is small. At pH ~ 7.3, the average R_g values at the aminosilane end are relatively larger compared with those at the other two pH conditions but they are more randomly dispersed with large standard deviations. The large variability in the R_g values might be caused by a lack of DNA adsorption events at the low amine

end. Furthermore, a decrease in the density of the protonated amine groups on the surface would be expected to weaken the binding strengths between the DNA molecules and amine surfaces. Therefore, the R_g values increase and the surface-adsorbed DNA molecules are less stable.

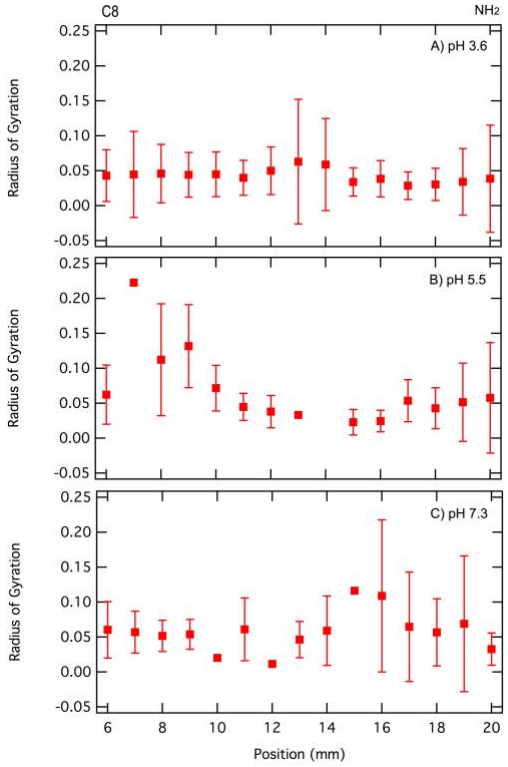

Figure 6.4 Evolution of the Radius of gyration for surface-adsorbed DNA molecules along the opposed C8-silane/aminosilane two-component gradients at A) pH ~ 3.6; B) pH ~ 5.5; and C) pH ~ 7.3. The error bars show the standard deviation for each value.

6.4 Conclusion

In this chapter, DNA adsorption along opposed C8-silane and aminosilane two-component gradients prepared on transparent ITO substrates was studied using TIRF microscopy and single molecule tracking methods. The maximum density of DNA adsorption on the C8-silane end was found to occur at pH ~ 3.6. The adsorbed density decreased dramatically as the solution pH was increased to ~ 5.5 and 7.3. In contrast, the density of adsorbed DNA was always very high at these

three pH values at the high amine end of the gradient. The latter was attributed to electrostatic interactions between the DNA and the positively charged surfaces and possibly hydrophobic effects. Interestingly, some of the adsorbed DNA molecules were found to be mobile over short periods of time (i.e. several video frames, 0.55 s/frame) during the adsorption event. This phenomenon was explored in some detail to investigate the possible position or pH dependence of the behavior. It was found that the mobility of the surface-adsorbed DNA molecules increased as the solution pH was increased at both ends. However, the exact origins of this phenomenon remain unclear. Although the original purpose for investigating DNA adsorption along the opposed C8-silane and aminosilane gradients was to uncover cooperative effects particularly in the mixed regions of the gradients, no such effects were detected in the data.

Chapter 7 General Conclusions and Future Directions

7.1 General Conclusions

In this dissertation, DNA adsorption/desorption and DNA dielectric properties were investigated across different chemically graded surfaces using single molecule fluorescence imaging approaches. TIRF microscopy, spectroscopic imaging and single molecule tracking allow for the dynamics and variations of DNA-surface interactions to be monitored and the results obtained reveal the mechanisms of DNA-surface interactions and the influencing factors that affect their interaction strength. The single molecule detection methods have important advantages over other traditional techniques because they take every single molecule into consideration rather than acquire averaged information from numerous events. TIRF microscopy could be used to observe DNA interactions at the interfaces of liquid solutions and solid substrates. TIRF method eliminates the background from bulk solutions and enhances the signal to noise ratio. Spectroscopic imaging provided data from a solvatochromic environment-sensitive probe sensing the local dielectric properties within DNA molecules. Last but not least, single molecule tracking, along with TIRF microscopy enabled studies of the mobility of surface-adsorbed DNA molecules.

In **Chapter 4**, DNA interactions with aminosilane gradient surfaces on TMOS-coated ITO substrates were investigated as a function of solution pH, surface aminosilane coverage and applied potential by employing TIRF microscopy. The results showed that potential-dependent DNA capture and release could be achieved under slightly basic solution (i.e. pH ~ 8) in regions where a monolayer or submonolayer aminosilane film was present. On the other hand, DNA molecules were quasi-reversibly adsorbed at the high aminosilane end under slightly acidic solution (i.e. pH ~ 6) due to strong electrostatic interactions between the negatively charged DNA molecules and protonated ammonium groups on the surface. According to the single molecule

detection data, DNA molecules were observed to search for favorable binding sites before they were fully adsorbed onto the aminosilane surfaces, especially under pH ~ 8 solution.

In **Chapter 5**, the local dielectric constant of the least polar environments in plasmid DNA was measured in solution and along aminosilane gradient surfaces using TIRF-based spectroscopic imaging with a solvatochromic dye, nile red. The results revealed that the nile red dye employed intercalates into the DNA, likely inserting between the stacked base pairs. The local dielectric constant inside the DNA decreased with increasing solution ionic strength. The ionic-strength-dependent reduction in polarity was attributed to the condensation of DNA, which was induced by the charge naturalization of the anions along the DNA phosphate backbone by the cations in solution. In addition, the dielectric constant within the surface-adsorbed DNA was also obtained. Its value was found to be generally smaller than the value obtained in solution, indicating that the protonated amine groups on the surface had a larger effect on the condensation of DNA and largely affected the local dielectric properties of DNA. However, at the low amine end, the dielectric constant of surface-adsorbed DNA decreased again with an increase in buffer concentration. This result demonstrated that the solution ionic strength also affected the local dielectric constant of surface-adsorbed DNA molecules.

In **Chapter 6**, two-component opposed chemical gradients of C8-silane and aminosilane were successfully prepared and characterized. DNA interactions with the $C_8 - NH_2$ gradient surfaces were again explored by TIRF microscopy and single molecule tracking approaches under applied potential and at a series of pH conditions. The preliminary results showed that more DNA molecules were adsorbed onto the aminosilane surfaces than onto the C8-silane surfaces at pH ~ 5.5 and ~ 7.3. These results were attributed to differences in the strengths of electrostatic and hydrophobic interactions of DNA with the gradient surfaces, with the electrostatic interactions of

DNA with charged surfaces being stronger than the hydrophobic interactions of DNA with the hydrophobic C8-silane surfaces. Radius of gyration data obtained from single molecule tracking results for surface-adsorbed DNA molecules revealed that molecules adsorbed to the C8-silane end exhibited higher mobilities than those absorbed to the aminosilane end at pH ~ 5.5. However, the mobility of surface-adsorbed DNA was found to increase at pH ~ 7.3 at the high amine end. This phenomenon is likely due to the decrease in protonated amine groups leading to weaker interactions between DNA and aminosilane surfaces.

In summary, this dissertation clearly demonstrated the advantages of employing chemical gradients in studies of DNA-surface interactions. Both electrostatic and hydrophobic interactions of the DNA with different organosilane gradient surfaces were investigated. Various factors of influencing DNA-surface interactions such as solution pH, surface charges, and solution ionic strength were also explored. These fundamental studies provide a better understanding of DNA interactions with surfaces and knowledge useful for the advancement of DNA-based biological and biomedical devices. In addition, the local dielectric constants of DNA obtained in solution and on chemical surfaces will aid in the development of DNA-related small drugs. Moreover, the knowledge of the local dielectric properties of DNA might be beneficial for studying protein-DNA interactions.

7.2 Future Directions

Overall, this dissertation has illustrated DNA adsorption/desorption behavior and the partitioning of nile red within DNA molecules on organosilane gradient surfaces. The results obtained afford a better understanding of the mechanisms of DNA-surface interactions and local DNA dielectric properties. The dependence of DNA adsorption/desorption and condensation on the solution pH, electric potentials, surface organosilane coverages and DNA conformations have

been investigated and discussed. However, while these studies answered some questions, they raised many more that need to be addressed in the future to fully understand DNA-surface interactions and the local dielectric properties of DNA.

In the first study of this dissertation, plasmid DNA with 5386 base pairs was investigated. Extensions of these studies could involve investigating the effects of DNA size and hybridization state (single-stranded or double-stranded) in affecting its surface adsorption/desorption on aminosilane gradient surfaces. As the size of the DNA fragments become smaller, DNA would more weakly interact with the surface and should therefore desorb more easily. On the contrary, if the size of DNA fragments becomes larger (i.e. lambda DNA, 48502 base pairs), the interactions between the DNA and the charged surfaces would be stronger and hence more difficult to desorb from charged surfaces. In turn, the surface aminosilane coverages needed to induce DNA capture and release under applied potential might vary according to the size of DNA. As for single-stranded DNA, it shows more hydrophobic properties than double-stranded DNA due to the exposure of its nitrogenous bases. By using a short single-stranded DNA, DNA-surface interactions would be governed by both electrostatic and hydrophobic interactions. Besides, owning to the decrease in the negative charges in single-stranded DNA, solution ionic strength effects on ssDNA-surface interactions would be different from those on dsDNA-surface interactions. These studies are again important for the development of DNA-based biosensors and microarrays.

Future investigations of DNA dielectric properties might include 1) systematically changing the doping ratio of NR in DNA, 2) investigating the effect of pH on local dielectric properties probed by NR in solution and on surfaces, and 3) exploring how divalent and trivalent cations affect DNA dielectric constants using NR and spectroscopic imaging. Increasing the doping ratio of the NR to DNA base pairs might cause NR to insert into different environments within the DNA,

such as in regions along the minor grooves of DNA. The ultimate local dielectric constant of DNA might be different from the value obtained in this dissertation. As for the pH effect on the local dielectric constant of DNA, it might stem from the variations in the protonation and deprotonation states of the nitrogenous bases in DNA at various pH conditions. However, it is hard to predict how the local dielectric constant of DNA would change. Nevertheless, since multivalent cations can easily induce DNA condensation, the local dielectric constant of DNA is expected to decrease with an increase in the number of multivalent cations in solution. These experiments would provide a better understanding of local dielectric properties of DNA under different conditions, which would be useful for studying DNA interactions with other molecules.

As for the studies of DNA mobility along two-component gradients, the origin of the observed mobility of surface-adsorbed DNA needs to be further investigated. These studies were challenging because of the inhomogeneity of the chemical gradients employed so far. One way to solve this problem might be to instead study the mobility of surface-adsorbed DNA on a homogenous C8-silane or aminosilane thin films. However, such studies would be time-consuming and tedious because they would require preparing many thin films of various surface orgnosilane surface coverages. Additionally, it would be interesting to see how DNA interacts with the C8-silane and aminosilane two-component aligned gradient surfaces. The cooperative effects on DNA interactions with the aligned two-component thin film might be explored.

References

1. Watson, J. D.; Crick, F. H. C., Molecular Structure of Nucleic Acids - A Structure for Deoxyribose Nucleic Acid. *Nature* **1953,** *171* (4356), 737-738.

2. Levy-Sakin, M.; Ebenstein, Y., Beyond sequencing: optical mapping of DNA in the age of nanotechnology and nanoscopy. *Current Opinion in Biotechnology* **2013,** *24* (4), 690-698.

3. Aston, C.; Mishra, B.; Schwartz, D. C., Optical mapping and its potential for large-scale sequencing projects. *Trends in Biotechnology* **1999,** *17* (7), 297-302.

4. Yokota, H.; Johnson, F.; Lu, H. B.; Robinson, R. M.; Belu, A. M.; Garrison, M. D.; Ratner, B. D.; Trask, B. J.; Miller, D. L., A new method for straightening DNA molecules for optical restriction mapping. *Nucleic Acids Research* **1997,** *25* (5), 1064-1070.

5. Lu, H. J.; Wang, J. K.; Wang, T.; Zhong, J.; Bao, Y.; Hao, H. X., Recent Progress on Nanostructures for Drug Delivery Applications. *Journal of Nanomaterials* **2016**.

6. Josephs, E. A.; Ye, T., Electric-Field Dependent Conformations of Single DNA Molecules on a Model Biosensor Surface. *Nano Letters* **2012,** *12* (10), 5255-5261.

7. Liu, J. W., Adsorption of DNA onto gold nanoparticles and graphene oxide: surface science and applications. *Physical Chemistry Chemical Physics* **2012,** *14* (30), 10485-10496.

8. Gao, Z. Q.; Tansil, N. C., An ultrasensitive photoelectrochemical nucleic acid biosensor. *Nucleic Acids Research* **2005,** *33* (13).

9. Nakamura, F.; Ito, E.; Hayashi, T.; Hara, M., Fabrication of COOH-terminated self-assembled monolayers for DNA sensors. *Colloids and Surfaces a-Physicochemical and Engineering Aspects* **2006,** *284*, 495-498.

10. Schreiner, S. M.; Hatch, A. L.; Shudy, D. F.; Howard, D. R.; Howell, C.; Zhao, J. L.; Koelsch, P.; Zharnikov, M.; Petrovykh, D. Y.; Opdahl, A., Impact of DNA-Surface Interactions on the Stability of DNA Hybrids. *Analytical Chemistry* **2011,** *83* (11), 4288-4295.

11. Caruso, F.; Rodda, E.; Furlong, D. F.; Niikura, K.; Okahata, Y., Quartz crystal microbalance study of DNA immobilization and hybridization for nucleic acid sensor development. *Analytical Chemistry* **1997,** *69* (11), 2043-2049.

12. Nelson, B. P.; Grimsrud, T. E.; Liles, M. R.; Goodman, R. M.; Corn, R. M., Surface plasmon resonance imaging measurements of DNA and RNA hybridization adsorption onto DNA microarrays. *Analytical Chemistry* **2001,** *73* (1), 1-7.

13. Brockman, J. M.; Frutos, A. G.; Corn, R. M., A multistep chemical modification procedure to create DNA arrays on gold surfaces for the study of protein-DNA interactions with surface plasmon resonance imaging. *Journal of the American Chemical Society* **1999,** *121* (35), 8044-8051.

14. Rao, A. N.; Grainger, D. W., Biophysical properties of nucleic acids at surfaces relevant to microarray performance. *Biomaterials Science* **2014,** *2* (4), 436-471.

15. Chu, S. K.; Hsu, M.; Ku, W. C.; Tu, C. Y.; Tseng, Y. T.; Lau, W. K.; Yan, R. Y.; Ma, J. T.; Tzeng, C. M., Synergistic effects of epoxy- and amine-silanes on microarray DNA immobilization and hybridization. *Biochemical Journal* **2003,** *374*, 625-632.

16. Luscombe, N. M.; Laskowski, R. A.; Thornton, J. M., Amino acid-base interactions: a three-dimensional analysis of protein-DNA interactions at an atomic level. *Nucleic Acids Research* **2001,** *29* (13), 2860-2874.

17. Podesta, A.; Indrieri, M.; Brogioli, D.; Manning, G. S.; Milani, P.; Guerra, R.; Finzi, L.; Dunlap, D., Positively charged surfaces increase the flexibility of DNA. *Biophysical Journal* **2005,** *89* (4), 2558-2563.

18. Gong, P.; Levicky, R., DNA surface hybridization regimes. *Proceedings of the National Academy of Sciences of the United States of America* **2008,** *105* (14), 5301-5306.

19. Tymoczko, J.; Schuhmann, W.; Gebala, M., Electrical Potential-Assisted DNA Hybridization. How to Mitigate Electrostatics for Surface DNA Hybridization. *Acs Applied Materials & Interfaces* **2014,** *6* (24), 21851-21858.

20. Thiel, A. J.; Frutos, A. G.; Jordan, C. E.; Corn, R. M.; Smith, L. M., In situ surface plasmon resonance imaging detection of DNA hybridization to oligonucleotide arrays on gold surfaces. *Analytical Chemistry* **1997,** *69* (24), 4948-4956.

21. Elder, R. M.; Pfaendtner, J.; Jayaraman, A., Effect of Hydrophobic and Hydrophilic Surfaces on the Stability of Double-Stranded DNA. *Biomacromolecules* **2015,** *16* (6), 1862-1869.

22. Shi, B.; Shin, Y. K.; Hassanali, A. A.; Singer, S. J., DNA Binding to the Silica Surface. *Journal of Physical Chemistry B* **2015,** *119* (34), 11030-11040.

23. Wen, J.; Legendre, L. A.; Bienvenue, J. M.; Landers, J. P., Purification of nucleic acids in microfluidic devices. *Analytical Chemistry* **2008,** *80* (17), 6472-6479.

24. Price, C. W.; Leslie, D. C.; Landers, J. P., Nucleic acid extraction techniques and application to the microchip. *Lab on a Chip* **2009,** *9* (17), 2484-2494.

25. Nakagawa, T.; Tanaka, T.; Niwa, D.; Osaka, T.; Takeyama, H.; Matsunaga, T., Fabrication of amino silane-coated microchip for DNA extraction from whole blood. *Journal of Biotechnology* **2005,** *116* (2), 105-111.

26. Pasquardini, L.; Lunelli, L.; Potrich, C.; Marocchi, L.; Fiorilli, S.; Vozzi, D.; Vanzetti, L.; Gasparini, P.; Anderle, M.; Pederzolli, C., Organo-silane coated substrates for DNA purification. *Applied Surface Science* **2011,** *257* (24), 10821-10827.

27. Lyubchenko, Y. L.; Shlyakhtenko, L. S., Visualization of supercoiled DNA with atomic force microscopy in situ. *Proceedings of the National Academy of Sciences of the United States of America* **1997,** *94* (2), 496-501.

28. Hu, J.; Wang, M.; Weier, H. U. G.; Frantz, P.; Kolbe, W.; Ogletree, D. F.; Salmeron, M., Imaging of single extended DNA molecules on flat (aminopropyl)triethoxysilane-mica by atomic force microscopy. *Langmuir* **1996,** *12* (7), 1697-1700.

29. Schmatko, T.; Muller, P.; Maaloum, M., Surface charge effects on the 2D conformation of supercoiled DNA. *Soft Matter* **2014,** *10* (15), 2520-2529.

30. Park, H. Y.; Li, H. W.; Yeung, E. S.; Porter, M. D., Single molecule adsorption at compositionally patterned self-assembled monolayers on gold: Role of domain boundaries. *Langmuir* **2006,** *22* (9), 4244-4249.

31. Kang, S. H.; Shortreed, M. R.; Yeung, E. S., Real-time dynamics of single-DNA molecules undergoing adsorption and desorption at liquid-solid interfaces. *Analytical Chemistry* **2001,** *73* (6), 1091-1099.

32. He, Y.; Li, H. W.; Yeung, E. S., Motion of single DNA molecules at a liquid-solid interface as revealed by variable-angle evanescent-field microscopy. *Journal of Physical Chemistry B* **2005,** *109* (18), 8820-8832.

33. Li, H. W.; Park, H. Y.; Porter, M. D.; Yeung, E. S., Single DNA molecules as probes of chromatographic surfaces. *Analytical Chemistry* **2005,** *77* (10), 3256-3260.

34. Nguyen, T. H.; Elimelech, M., Plasmid DNA adsorption on silica: Kinetics and conformational changes in monovalent and divalent salts. *Biomacromolecules* **2007,** *8* (1), 24-32.

35. Vanzetti, L.; Pasquardini, L.; Potrich, C.; Vaghi, V.; Battista, E.; Causa, F.; Pederzolli, C., XPS analysis of genomic DNA adsorbed on PEI-modified surfaces. *Surface and Interface Analysis* **2016,** *48* (7), 611-615.

36. Nabok, A.; Tsargorodskaya, A.; Davis, F.; Higson, S. P. J., The study of genomic DNA adsorption and subsequent interactions using total internal reflection ellipsometry. *Biosensors & Bioelectronics* **2007,** *23* (3), 377-383.

37. Peterson, E. M.; Manhart, M. W.; Harris, J. M., Single-Molecule Fluorescence Imaging of Interfacial DNA Hybridization Kinetics at Selective Capture Surfaces. *Analytical Chemistry* **2016,** *88* (2), 1345-1354.

38. Peterson, E. M.; Manhart, M. W.; Harris, J. M., Competitive Assays of Label-Free DNA Hybridization with Single-Molecule Fluorescence Imaging Detection. *Analytical Chemistry* **2016,** *88* (12), 6410-6417.

39. Li, Z.; Ashraf, K. M.; Collinson, M. M.; Higgins, D. A., Single Molecule Catch and Release: Potential-Dependent Plasmid DNA Adsorption along Chemically Graded Electrode Surfaces. *Langmuir* **2017,** *33* (35), 8651-8662.

40. Tanaka, T.; Sakai, R.; Kobayashi, R.; Hatakeyama, K.; Matsunaga, T., Contributions of Phosphate to DNA Adsorption/Desorption Behaviors on Aminosilane-Modified Magnetic Nanoparticles. *Langmuir* **2009,** *25* (5), 2956-2961.

41. Li, H.; Zhang, J.; Zhou, X. Z.; Lu, G.; Yin, Z. Y.; Li, G. P.; Wu, T.; Boey, F.; Venkatraman, S. S.; Zhang, H., Aminosilane Micropatterns on Hydroxyl-Terminated Substrates: Fabrication and Applications. *Langmuir* **2010,** *26* (8), 5603-5609.

42. Metwalli, E.; Haines, D.; Becker, O.; Conzone, S.; Pantano, C. G., Surface characterizations of mono-, di-, and tri-aminosilane treated glass substrates. *Journal of Colloid and Interface Science* **2006,** *298* (2), 825-831.

43. Honarvarfard, E.; Gamella, M.; Guz, N.; Katz, E., Electrochemically-controlled DNA Release under Physiological Conditions from a Monolayer-modified Electrode. *Electroanalysis* **2017,** *29* (2), 324-329.

44. Moreira, K. A.; Diogo, M.; Prazeres, D. M.; de Lima, J. L.; Porto, A. L. F., Purification of plasmid (pVaxLacZ) by hydrophobic interaction chromatography. *Brazilian Archives of Biology and Technology* **2005,** *48*, 113-117.

45. Kastantin, M.; Schwartz, D. K., DNA Hairpin Stabilization on a Hydrophobic Surface. *Small* **2013,** *9* (6), 933-941.

46. Diogo, M. M.; Queiroz, J. A.; Monteiro, G. A.; Martins, S. A. M.; Ferreira, G. N. M.; Prazeres, D. M. F., Purification of a cystic fibrosis plasmid vector for gene therapy using hydrophobic interaction chromatography. *Biotechnology and Bioengineering* **2000,** *68* (5), 576-583.

47. Giri, D.; Li, Z.; Ashraf, K. M.; Collinson, M. M.; Higgins, D. A., Molecular Combing of lambda-DNA using Self-Propelled Water Droplets on Wettability Gradient Surfaces. *Acs Applied Materials & Interfaces* **2016,** *8* (36), 24265-24272.

48. Genzer, J.; Bhat, R. R., Surface-bound soft matter gradients. *Langmuir* **2008,** *24* (6), 2294-2317.

49. Genzer, J., Surface-Bound Gradients for Studies of Soft Materials Behavior. *Annual Review of Materials Research, Vol 42* **2012,** *42*, 435-468.

50. Ashraf, K. M.; Giri, D.; Wynne, K. J.; Higgins, D. A.; Collinson, M. M., Cooperative Effects in Aligned and Opposed Multicomponent Charge Gradients Containing Strongly Acidic, Weakly Acidic, and Basic Functional Groups. *Langmuir* **2016,** *32* (16), 3836-3847.

51. Chaudhury, M. K.; Whitesides, G. M., How To Make Water Run Uphill. *Science* **1992,** *256* (5063), 1539-1541.

52. van Dover, R. B.; Schneemeyer, L. D.; Fleming, R. M., Discovery of a useful thin-film dielectric using a composition-spread approach. *Nature* **1998,** *392* (6672), 162-164.

53. Lee, J. H.; Jeong, B. J.; Lee, H. B., Plasma protein adsorption and platelet adhesion onto comb-like PEO gradient surfaces. *Journal of Biomedical Materials Research* **1997,** *34* (1), 105-114.

54. Chargaff, E.; Lipshitz, R.; Green, C.; Hodes, M. E., The Composition of the Deoxyribonucleic Acid of Salmon Sperm. *Journal of Biological Chemistry* **1951,** *192* (1), 223-230.

55. Lodish Harvey, B. A., Zipursky S. L, Matsudaira Paul, Baltimore David, Darnell James E., *Molecular Cell Biology*. 4th Edition ed.; W. H. Freeman: New York, 2000.

56. Travers, A.; Muskhelishvili, G., DNA structure and function. *Febs Journal* **2015,** *282* (12), 2279-2295.

57. Mills, J. B.; Hagerman, P. J., Origin of the intrinsic rigidity of DNA. *Nucleic Acids Research* **2004,** *32* (13), 4055-4059.

58. Collins, M.; Thrasher, A., Gene therapy: progress and predictions. *Proceedings of the Royal Society B-Biological Sciences* **2015,** *282* (1821).

59. Dias, R. S.; Lindman, B.; Miguel, M. G., Compaction and decompaction of DNA in the presence of catanionic amphiphile mixtures. *Journal of Physical Chemistry B* **2002,** *106* (48), 12608-12612.

60. Hays, M. E.; Jewell, C. M.; Lynn, D. M.; Abbott, N. L., Reversible condensation of DNA using a redox-active surfactant. *Langmuir* **2007,** *23* (10), 5609-5614.

61. Bloomfield, V. A., DNA condensation by multivalent cations. *Biopolymers* **1997,** *44* (3), 269-282.

62. Ageno, M.; Dore, E.; Frontali, C., Alkaline Denaturation of DNA. *Biophysical Journal* **1969,** *9* (11), 1281-&.

63. Albert L. Lehninger, D. L. N., Michael M. Cox, *Principles of Biochemistry 2nd Ed*. 2nd Edition ed.; Worth Publishers, Inc.: New York, 1992.

64. Khandelwal, G.; Bhyravabhotla, J., A Phenomenological Model for Predicting Melting Temperatures of DNA Sequences. *Plos One* **2010,** *5* (8).

65. Lee, C. H.; Mizusawa, H.; Kakefuda, T., Unwinding of Double-Stranded DNA Helix by Dehydration. *Proceedings of the National Academy of Sciences of the United States of America-Biological Sciences* **1981,** *78* (5), 2838-2842.

66. Moran Laurence, H. R., Scrimgeour Gray, Perry Marc, Principles of Biochemistry 5th Edition. Pearson Education, Inc.: 2011.

67. Monserud, J. H.; Schwartz, D. K., Mechanisms of Surface-Mediated DNA Hybridization. *Acs Nano* **2014,** *8* (5), 4488-4499.

68. Strekowski, L.; Wilson, B., Noncovalent interactions with DNA: An overview. *Mutation Research-Fundamental and Molecular Mechanisms of Mutagenesis* **2007,** *623* (1-2), 3-13.

69. Privalov, P. L.; Dragan, A. I.; Crane-Robinson, C.; Breslauer, K. J.; Remeta, D. P.; Minetti, C., What drives proteins into the major or minor grooves of DNA? *Journal of Molecular Biology* **2007,** *365* (1), 1-9.

70. Sathyapriya, R.; Vijayabaskar, M. S.; Vishveshwara, S., Insights into Protein-DNA Interactions through Structure Network Analysis. *Plos Computational Biology* **2008,** *4* (9).

71. Strauss, J. K.; Maher, L. J., DNA Bending by Asymmetric Phosphate Neutralization. *Science* **1994,** *266* (5192), 1829-1834.

72. Savelyev, A.; Materese, C. K.; Papoian, G. A., Is DNA's Rigidity Dominated by Electrostatic or Nonelectrostatic Interactions? *Journal of the American Chemical Society* **2011,** *133* (48), 19290-19293.

73. Schlick, T.; Li, B.; Olson, W. K., The Influence of Salt on the Structure and Energetics of Supercoiled DNA. *Biophysical Journal* **1994,** *67* (6), 2146-2166.

74. Bezanilla, M.; Manne, S.; Laney, D. E.; Lyubchenko, Y. L.; Hansma, H. G., Adsorption of DNA to Mica, Silylated Mice, and Minerals - Characterization by Atomic-Force Microscopy. *Langmuir* **1995,** *11* (2), 655-659.

75. Brett, A. M. O.; Chiorcea, A. M., Effect of pH and applied potential on the adsorption of DNA on highly oriented pyrolytic graphite electrodes. Atomic force microscopy surface characterisation. *Electrochemistry Communications* **2003,** *5* (2), 178-183.

76. Carre, A.; Lacarrriere, V.; Birch, W., Molecular interactions between DNA and an aminated glass substrate. *Journal of Colloid and Interface Science* **2003,** *260* (1), 49-55.

77. Yoda, S.; Han, S. P.; Kudo, H.; Kwak, K. J.; Fujihira, M., Deoxyribonucleic acid interaction with silanized surfaces. *Japanese Journal of Applied Physics Part 1-Regular Papers Short Notes & Review Papers* **2004,** *43* (9A), 6297-6302.

78. Kim, H. J.; Bae, I. S.; Cho, S. J.; Boo, J. H.; Lee, B. C.; Heo, J.; Chung, I.; Hong, B., Synthesis and characteristics of NH2-functionalized polymer films to align and immobilize DNA molecules. *Nanoscale Research Letters* **2012,** *7*, 1-7.

79. Benke, A.; Mertig, M.; Pompe, A., PH- and salt-dependent molecular combing of DNA: experiments and phenomenological model. *Nanotechnology* **2011,** *22* (3).

80. Bloomfield, V. A., DNA condensation. *Current Opinion in Structural Biology* **1996,** *6* (3), 334-341.

81. Matulis, D.; Rouzina, I.; Bloomfield, V. A., Thermodynamics of cationic lipid binding to DNA and DNA condensation: Roles of electrostatics and hydrophobicity. *Journal of the American Chemical Society* **2002,** *124* (25), 7331-7342.

82. Bhattacharya, S.; Mandal, S. S., Interaction of surfactants with DNA. Role of hydrophobicity and surface charge on intercalation and DNA melting. *Biochimica Et Biophysica Acta-Biomembranes* **1997,** *1323* (1), 29-44.

83. Huang, P. J. J.; Liu, J. W., Separation of Short Single- and Double-Stranded DNA Based on Their Adsorption Kinetics Difference on Graphene Oxide. *Nanomaterials* **2013,** *3* (2), 221-228.

84. Uzek, R.; Ozkara, S.; Gungunes, H.; Uzun, L.; Senel, S., Magnetic Nanoparticles for Plasmid DNA Purification through Hydrophobic Interaction Chromatography. *Separation Science and Technology* **2014,** *49* (14), 2193-2203.

85. Xia, F.; Nagrath, D.; Cramer, S. M., Effect of pH changes on water release values in hydrophobic interaction chromatographic systems. *Journal of Chromatography A* **2005,** *1079* (1-2), 229-235.

86. Kim, S.; Park, C.; Gang, J., Effect of pH and Salt on Adsorption of Double-Stranded DNA on Graphene Oxide. *Journal of Nanoscience and Nanotechnology* **2015,** *15* (10), 7913-7917.

87. Lei, H. Z.; Mi, L. J.; Zhou, X. J.; Chen, J. J.; Hu, J.; Guo, S. W.; Zhang, Y., Adsorption of double-stranded DNA to graphene oxide preventing enzymatic digestion. *Nanoscale* **2011,** *3* (9), 3888-3892.

88. Yakovchuk, P.; Protozanova, E.; Frank-Kamenetskii, M. D., Base-stacking and base-pairing contributions into thermal stability of the DNA double helix. *Nucleic Acids Research* **2006,** *34* (2), 564-574.

89. Cieplak, P.; Kollman, P. A., Calculation of the Free-Energy of Association of Nucleic-Acid Bases in Vacuo and Water Solution. *Journal of the American Chemical Society* **1988,** *110* (12), 3734-3739.

90. Dang, L. X.; Kollman, P. A., Molecular-Dynamics Simulations Study of the Free-Energy of Association of 9-Methyladenine and 1-Methylthymine Bases in Water. *Journal of the American Chemical Society* **1990,** *112* (2), 503-507.

91. Petersheim, M.; Turner, D. H., Base-Stacking and Base-Pairing Contributions to Helix Stability - Thermodynamics of Double-Helix Formation With CCGG, CCGGP, CCGGAP, ACCGGP, CCGGUP, and ACCGGUP. *Biochemistry* **1983,** *22* (2), 256-263.

92. T. B. O., *Nucleic Acids Book.* ATDBio: Online, 2005.

93. Brett, A. M. O.; Chiorcea, A. M., Effect of pH and applied potential on the adsorption of DNA on highly oriented pyrolytic graphite electrodes. Atomic force microscopy surface characterization. *Electrochemistry Communications* **2003,** *5* (2), 178-183.

94. Hansma, H. G.; Sinsheimer, R. L.; Li, M. Q.; Hansma, P. K., Atomic Force Microscopy of Single-Stranded and Double-Stranded DNA. *Nucleic Acids Research* **1992,** *20* (14), 3585-3590.

95. Bezanilla, M.; Manne, S.; Laney, D. E.; Lyubchenko, Y. L.; Hansma, H. G., Adsorption of DNA to Mica, Silylated Mica, and Minerals - Characterization by Atomic-Force Microscopy. *Langmuir* **1995,** *11* (2), 655-659.

96. Fiorilli, S.; Rivolo, P.; Descrovi, E.; Ricciardi, C.; Pasquardini, L.; Lunelli, L.; Vanzetti, L.; Pederzolli, C.; Onida, B.; Garrone, E., Vapor-phase self-assembled monolayers of aminosilane on plasma-activated silicon substrates. *Journal of Colloid and Interface Science* **2008,** *321* (1), 235-241.

97. Pastre, D.; Hamon, L.; Landousy, F.; Sorel, I.; David, M. O.; Zozime, A.; Le Cam, E.; Pietrement, O., Anionic polyelectrolyte adsorption on mica mediated by multivalent cations: A solution to DNA imaging by atomic force microscopy under high ionic strengths. *Langmuir* **2006,** *22* (15), 6651-6660.

98. Tongu, C.; Kenmotsu, T.; Yoshikawa, Y.; Zinchenko, A.; Chen, N.; Yoshikawa, K., Divalent cation shrinks DNA but inhibits its compaction with trivalent cation. *Journal of Chemical Physics* **2016,** *144* (20).

99. Sasou, M.; Sugiyama, S.; Yoshino, T.; Ohtani, T., Molecular flat mica surface silanized with methyltrimethoxysilane for fixing and straightening DNA. *Langmuir* **2003,** *19* (23), 9845-9849.

100. Liu, L. F.; Li, Y. L.; Wang, Y.; Zheng, J. W.; Mao, C. D., Regulating DNA Self-assembly by DNA-Surface Interactions. *Chembiochem* **2017,** *18* (24), 2404-2407.

101. Seeman, N., *Structural DNA Nanotechnology*. Cambridge University Press: Cambridge, 2016.

102. Zhang, G. M.; Surwade, S. P.; Zhou, F.; Liu, H. T., DNA nanostructure meets nanofabrication. *Chemical Society Reviews* **2013,** *42* (7), 2488-2496.

103. Surwade, S. P.; Zhao, S. C.; Liu, H. T., Molecular Lithography through DNA-Mediated Etching and Masking of SiO2. *Journal of the American Chemical Society* **2011,** *133* (31), 11868-11871.

104. Peterson, E. M.; Harris, J. M., Quantitative Detection of Single Molecules in Fluorescence Microscopy Images. *Analytical Chemistry* **2010,** *82* (1), 189-196.

105. Peterson, E. M.; Harris, J. M., Single-Molecule Fluorescence Imaging of DNA at a Potential-Controlled Interface. *Langmuir* **2013,** *29* (26), 8292-8301.

106. Isailovic, S.; Li, H. W.; Yeung, E. S., Adsorption of single DNA molecules at the water/fused-silica interface. *Journal of Chromatography A* **2007,** *1150* (1-2), 259-266.

107. Liu, B. W.; Liu, J. W., DNA Adsorption by Indium Tin Oxide Nanoparticles. *Langmuir* **2015,** *31* (1), 371-377.

108. Wang, Y.; Schellenberg, H.; Walhorn, V.; Toensing, K.; Anselmetti, D., Binding mechanism of PicoGreen to DNA characterized by magnetic tweezers and fluorescence spectroscopy. *European Biophysics Journal with Biophysics Letters* **2017,** *46* (6), 561-566.

109. Wang, J. C., Degree of Unwinding of DNA Helix by Ethidium .1. Titration of Twisted PM2 DNA-Molecules in Alkaline Cesium-Chloride Density Gradients. *Journal of Molecular Biology* **1974,** *89* (4), 783-801.

110. Rye, H. S.; Yue, S.; Wemmer, D. E.; Quesada, M. A.; Haugland, R. P.; Mathies, R. A.; Glazer, A. N., Stable Fluorescent Complexes of Double-Stranded DNA with Bis-Intercalating Asymmetric Cyanine Dyes - Properties and Applications. *Nucleic Acids Research* **1992,** *20* (11), 2803-2812.

111. Kundukad, B.; Yan, J.; Doyle, P. S., Effect of YOYO-1 on the mechanical properties of DNA. *Soft Matter* **2014,** *10* (48), 9721-9728.

112. Larsson, A.; Carlsson, C.; Jonsson, M.; Albinsson, B., Characterization of the Binding of the Fluorescent Dyes YO and YOYO to DNA by Polarized-Light Spectroscopy. *Journal of the American Chemical Society* **1994,** *116* (19), 8459-8465.

113. Paik, D. H.; Perkins, T. T., Dynamics and Multiple Stable Binding Modes of DNA Intercalators Revealed by Single-Molecule Force Spectroscopy. *Angewandte Chemie-International Edition* **2012,** *51* (8), 1811-1815.

114. Deye, J. F.; Berger, T. A.; Anderson, A. G., Nile Red as a Solvatochromic Dye for Measuring Strength in Normal Liquids and Mixtures of Normal Liquids with Supercritical and Near Critical Fluids. *Analytical Chemistry* **1990,** *62* (6), 615-622.

115. Hou, Y. W.; Bardo, A. M.; Martinez, C.; Higgins, D. A., Characterization of molecular scale environments in polymer films by single molecule spectroscopy. *Journal of Physical Chemistry B* **2000,** *104* (2), 212-219.

116. Hess, C. M.; Riley, E. A.; Palos-Chavez, J.; Reid, P. J., Measuring the Spatial Distribution of Dielectric Constants in Polymers through Quasi-Single Molecule Microscopy. *Journal of Physical Chemistry B* **2013,** *117* (23), 7106-7112.

117. Sarkar, N.; Das, K.; Nath, D. N.; Bhattacharyya, K., Twisted Charge-Transfer Process of Nile Red in Homogeneous Solution and in Faujasite Zeolite. *Langmuir* **1994,** *10* (1), 326-329.

118. Xu, H.; Nagasaka, S.; Kameta, N.; Masuda, M.; Ito, T.; Higgins, D. A., Spectroscopic imaging studies of nanoscale polarity and mass transport phenomena in self-assembled organic nanotubes. *Physical Chemistry Chemical Physics* **2017,** *19* (30), 20040-20048.

119. Kumarasinghe, R.; Higgins, E. D.; Ito, T.; Higgins, D. A., Spectroscopic and Polarization-Dependent Single-Molecule Tracking Reveal the One-Dimensional Diffusion Pathways in

Surfactant-Templated Mesoporous Silica. *Journal of Physical Chemistry C* **2016,** *120* (1), 715-723.

120. Gattuso, H.; Besancenot, V.; Grandemange, S.; Marazzi, M.; Monari, A., From non-covalent binding to irreversible DNA lesions: nile blue and nile red as photosensitizing agents. *Scientific Reports* **2016,** *6*.

121. Kurniasih, I. N.; Liang, H.; Mohr, P. C.; Khot, G.; Rabe, J. P.; Mohr, A., Nile Red Dye in Aqueous Surfactant and Micellar Solution. *Langmuir* **2015,** *31* (9), 2639-2648.

122. Dutta, A. K.; Kamada, K.; Ohta, K., Spectroscopic studies of nile red in organic solvents and polymers. *Journal of Photochemistry and Photobiology a-Chemistry* **1996,** *93* (1), 57-64.

123. Kannan, B.; Dong, D.; Higgins, D. A.; Collinson, M. M., Profile Control in Surface Amine Gradients Prepared by Controlled-Rate Infusion. *Langmuir* **2011,** *27* (5), 1867-1873.

124. Cui, C. C.; Kirkeminde, A.; Kannan, B.; Collinson, M. M.; Higgins, D. A., Spatiotemporal Evolution of Fixed and Mobile Dopant Populations in Silica Thin-Film Gradients as Revealed by Single Molecule Tracking. *Journal of Physical Chemistry C* **2011,** *115* (3), 728-735.

125. Angst, D. L.; Simmons, G. W., Moisture Absorpton Characteristics of Organosiloxane Self-Assembled Monolayers. *Langmuir* **1991,** *7* (10), 2236-2242.

126. Collinson, M. M.; Higgins, D. A., Organosilane Chemical Gradients: Progress, Properties, and Promise. *Langmuir* **2017,** *33* (48), 13719-13732.

127. Giri, D.; Ashraf, K. M.; Collinson, M. M.; Higgins, D. A., Single-Molecule Perspective on Mass Transport in Condensed Water Layers over Gradient Self-Assembled Monolayers. *Journal of Physical Chemistry C* **2015,** *119* (17), 9418-9428.

128. Stalder, A. F.; Melchior, T.; Muller, M.; Sage, D.; Blu, T.; Unser, M., Low-bond axisymmetric drop shape analysis for surface tension and contact angle measurements of sessile drops. *Colloids and Surfaces a-Physicochemical and Engineering Aspects* **2010,** *364* (1-3), 72-81.

129. Bhat, R. R.; Fischer, D. A.; Genzer, J., Fabricating planar nanoparticle assemblies with number density gradients. *Langmuir* **2002,** *18* (15), 5640-5643.

130. Kumar, S.; Kaur, I.; Kumari, N.; Jain, S.; Dharamveer, K.; Jindal, V. K.; Verma, N. K.; Bharadwaj, L. M., Atomic force microscope manipulation of multiwalled and single walled carbon nanotubes with reflux and ultrasonic treatments. *Applied Nanoscience* **2014,** *4* (1), 19-26.

131. Postma, H. W. C.; Sellmeijer, A.; Dekker, C., Manipulation and imaging of individual single-walled carbon nanotubes with an atomic force microscope. *Advanced Materials* **2000,** *12* (17), 1299-+.

132. Percec, V.; Rudick, J. G.; Wagner, M.; Obata, M.; Mitchell, C. M.; Cho, W. D.; Magonov, S. N., AFM visualization of individual and periodic assemblies of a helical dendronized polyphenylacetylene on graphite. *Macromolecules* **2006,** *39* (21), 7342-7351.

133. Magonov, S. N.; Reneker, D. H., Characterization of polymer surfaces with atomic force microscopy. *Annual Review of Materials Science* **1997,** *27*, 175-222.

134. Axelrod, D., Total internal reflection fluorescence microscopy in cell biology. *Traffic* **2001,** *2* (11), 764-774.

135. Thorn, K., A quick guide to light microscopy in cell biology. *Molecular Biology of the Cell* **2016,** *27* (2), 219-222.

136. Bardo, A. M.; Collinson, M. M.; Higgins, D. A., Nanoscale properties and matrix-dopant interactions in dye-doped organically modified silicate thin films. *Chemistry of Materials* **2001,** *13* (8), 2713-2721.

137. Richardson, S. C. W.; Wallom, K. L.; Ferguson, E. L.; Deacon, S. P. E.; Davies, M. W.; Powell, A. J.; Piper, R. C.; Duncan, R., The use of fluorescence microscopy to define polymer localisation to the late endocytic compartments in cells that are targets for drug delivery. *Journal of Controlled Release* **2008,** *127* (1), 1-11.

138. Giri, D.; Hanks, C. N.; Collinson, M. M.; Higgins, D. A., Single-Molecule Spectroscopic Imaging Studies of Polarity Gradients Prepared by Infusion-Withdrawal Dip-Coating. *Journal of Physical Chemistry C* **2014,** *118* (12), 6423-6432.

139. Decher, G., Fuzzy nanoassemblies: Toward layered polymeric multicomposites. *Science* **1997,** *277* (5330), 1232-1237.

140. Wang, Y.; Angelatos, A. S.; Caruso, F., Template synthesis of nanostructured materials via layer-by-layer assembly. *Chemistry of Materials* **2008,** *20* (3), 848-858.

141. Borges, J.; Mano, J. F., Molecular Interactions Driving the Layer-by-Layer Assembly of Multilayers. *Chemical Reviews* **2014,** *114* (18), 8883-8942.

142. Rusling, J. F.; Hvastkovs, E. G.; Hull, D. O.; Schenkman, J. B., Biochemical applications of ultrathin films of enzymes, polyions and DNA. *Chemical Communications* **2008,** (2), 141-154.

143. Rusling, J. F.; Wasalathanthri, D. P.; Schenkman, J. B., Thin multicomponent films for functional enzyme devices and bioreactor particles. *Soft Matter* **2014,** *10* (41), 8145-8156.

144. Van Tassel, P. R., Polyelectrolyte adsorption and layer-by-layer assembly: Electrochemical control. *Current Opinion in Colloid & Interface Science* **2012,** *17* (2), 106-113.

145. Hikosaka, R.; Nagata, F.; Tomita, M.; Kato, K., Adsorption and desorption characteristics of DNA onto the surface of amino functional mesoporous silica with various particle morphologies. *Colloids and Surfaces B-Biointerfaces* **2016,** *140*, 262-268.

146. Lynn, D. M., Peeling back the layers: Controlled erosion and triggered disassembly of multilayered polyelectrolyte thin films. *Advanced Materials* **2007,** *19* (23), 4118-4130.

147. Sousa, A.; Sousa, F.; Queiroz, J. A., Advances in chromatographic supports for pharmaceutical-grade plasmid DNA purification. *Journal of Separation Science* **2012,** *35* (22), 3046-3058.

148. Cao, W. D.; Easley, C. J.; Ferrance, J. P.; Landers, J. P., Chitosan as a polymer for pH-induced DNA capture in a totally aqueous system. *Analytical Chemistry* **2006,** *78* (20), 7222-7228.

149. Sosnowski, R. G.; Tu, E.; Butler, W. F.; Oconnell, J. P.; Heller, M. J., Rapid determination of single base mismatch mutations in DNA hybrids by direct electric field control. *Proceedings of the National Academy of Sciences of the United States of America* **1997,** *94* (4), 1119-1123.

150. Heaton, R. J.; Peterson, A. W.; Georgiadis, R. M., Electrostatic surface plasmon resonance: Direct electric field-induced hybridization and denaturation in monolayer nucleic acid films and label-free discrimination of base mismatches. *Proceedings of the National Academy of Sciences of the United States of America* **2001,** *98* (7), 3701-3704.

151. Yamauchi, F.; Kato, K.; Iwata, H., Layer-by-layer assembly of poly(ethyleneimine) and plasmid DNA onto transparent indium-tin oxide electrodes for temporally and spatially specific gene transfer. *Langmuir* **2005,** *21* (18), 8360-8367.

152. Hook, A. L.; Thissen, H.; Hayes, J. P.; Voelcker, N. H., Spatially controlled electro-stimulated DNA adsorption and desorption for biochip applications. *Biosensors & Bioelectronics* **2006,** *21* (11), 2137-2145.

153. Morgenthaler, S.; Zink, C.; Spencer, N. D., Surface-chemical and -morphological gradients. *Soft Matter* **2008,** *4* (3), 419-434.

154. Fasolka, M. J.; Stafford, C. M.; Beers, K. L., Gradient and Microfluidic Library Approaches to Polymer Interfaces. *Polymer Libraries* **2010,** *225*, 63-105.

155. Fujiwara, M.; Yamamoto, F.; Okamoto, K.; Shiokawa, K.; Nomura, R., Adsorption of duplex DNA on mesoporous silicas: Possibility of inclusion of DNA into their mesopores. *Analytical Chemistry* **2005,** *77* (24), 8138-8145.

156. Vandeventer, P. E.; Lin, J. S.; Zwang, T. J.; Nadim, A.; Johal, M. S.; Niemz, A., Multiphasic DNA Adsorption to Silica Surfaces under Varying Buffer, pH, and Ionic Strength Conditions. *Journal of Physical Chemistry B* **2012,** *116* (19), 5661-5670.

157. Mercier, P.; Savoie, R., Interaction of DNA with silica particles: A vibrational spectroscopic study. *Biospectroscopy* **1997,** *3* (4), 299-306.

158. Ando, T.; Uchihashi, T.; Kodera, N., High-Speed AFM and Applications to Biomolecular Systems. *Annual Review of Biophysics, Vol 42* **2013,** *42*, 393-414.

159. Li, L.; Tian, X. Z.; Zou, G. Z.; Shi, Z. K.; Zhang, X. L.; Jin, W. R., quantitative counting of single fluorescent molecules by combined electrochemical adsorption accumulation and total internal reflection fluorescence microscopy. *Analytical Chemistry* **2008,** *80* (11), 3999-4006.

160. Malone, S. M.; Schwartz, D. K., Macroscopic Liquid Crystal Response to Isolated DNA Helices. *Langmuir* **2011,** *27* (19), 11767-11772.

161. Rill, R. L.; Locke, B. R.; Liu, Y. J.; Van Winkle, D. H., Electrophoresis in lyotropic polymer liquid crystals. *Proceedings of the National Academy of Sciences of the United States of America* **1998,** *95* (4), 1534-1539.

162. Svingen, R.; Alexandridis, P.; Akerman, B., On the mechanism of electrophoretic migration of DNA in pluronic gels. *Langmuir* **2002,** *18* (22), 8616-8619.

163. Xu, H.; Minter, C. J.; Nagasaka, S.; Ito, T.; Higgins, D. A., Elongation, Alignment, and Guided Electrophoretic Migration of ds-DNA in Flow-Aligned Hexagonal F127 Gels. *Journal of Physical Chemistry B* **2014,** *118* (15), 4151-4159.

164. Robertson, J. W.; Cai, M.; Pemberton, J. E., Insulating ultrathin silica films formed by a room-temperature sol-gel process. *Advanced Materials* **2001,** *13* (9), 662-667.

165. Legrange, J. D.; Markham, J. L.; Kurkjian, C. R., Effects of Surface Hydration on the Deposition of Silane Monolayers on Silica. *Langmuir* **1993,** *9* (7), 1749-1753.

166. Khanh, H. T. B.; Everett, T. A.; Ito, T.; Higgins, D. A., Trajectory angle determination in one dimensional single molecule tracking data by orthogonal regression analysis. *Physical Chemistry Chemical Physics* **2011,** *13* (5), 1827-1835.

167. Moerner, W. E.; Fromm, D. P., Methods of single-molecule fluorescence spectroscopy and microscopy. *Review of Scientific Instruments* **2003,** *74* (8), 3597-3619.

168. Zeng, X. X.; Xu, G. H.; Gao, Y. A.; An, Y., Surface Wettability of (3-Aminopropyl)triethoxysilane Self-Assembled Monolayers. *Journal of Physical Chemistry B* **2011,** *115* (3), 450-454.

169. Vandenberg, E. T.; Bertilsson, L.; Liedberg, B.; Uvdal, K.; Erlandsson, R.; Elwing, H.; Lundstrom, I., Structure of 3-Aminopropyl Triethoxy Silane on Silicon-Oxide. *Journal of Colloid and Interface Science* **1991,** *147* (1), 103-118.

170. Armistead, P. M.; Thorp, H. H., Oxidation kinetics of guanine in DNA molecules adsorbed onto indium tin oxide electrodes. *Analytical Chemistry* **2001,** *73* (3), 558-564.

171. Ong, S. W.; Zhao, X. L.; Eisenthal, K. B., Polarization of Water-Molecules at a Charged Interface - 2^{ND} Harmonic Studies of the Silica Water Interfaces. *Chemical Physics Letters* **1992,** *191* (3-4), 327-335.

172. vanderVegte, E. W.; Hadziioannou, G., Acid-base properties and the chemical imaging of surface-bound functional groups studied with scanning force microscopy. *Journal of Physical Chemistry B* **1997,** *101* (46), 9563-9569.

173. Kannan, B.; Higgins, D. A.; Collinson, M. M., Aminoalkoxysilane Reactivity in Surface Amine Gradients Prepared by Controlled-Rate Infusion. *Langmuir* **2012,** *28* (46), 16091-16098.

174. Thompson, R. E.; Larson, D. R.; Webb, W. W., Precise nanometer localization analysis for individual fluorescent probes. *Biophysical Journal* **2002,** *82* (5), 2775-2783.

175. Li, Q.; Cui, C. C.; Higgins, D. A.; Li, J., Fluorescence Quenching Studies of Potential-Dependent DNA Reorientation Dynamics at Glassy Carbon Electrode Surfaces. *Journal of the American Chemical Society* **2012,** *134* (35), 14467-14475.

176. Akerman, B.; Tuite, E., Single- and double-strand photocleavage of DNA by YO, YOYO and TOTO. *Nucleic Acids Research* **1996,** *24* (6), 1080-1090.

177. Jennings, T. L.; Singh, M. P.; Strouse, G. F., Fluorescent lifetime quenching near d=1.5 nm gold nanoparticles: Probing NSET validity. *Journal of the American Chemical Society* **2006,** *128* (16), 5462-5467.

178. Lamm, G.; Pack, G. R., Calculation of dielectric constants near polyelectrolytes in solution. *Journal of Physical Chemistry B* **1997,** *101* (6), 959-965.

179. Young, M. A.; Jayaram, B.; Beveridge, D. L., Local dielectric environment of B-DNA in solution: Results from a 14 ns molecular dynamics trajectory. *Journal of Physical Chemistry B* **1998,** *102* (39), 7666-7669.

180. Yang, L. Q.; Weerasinghe, S.; Smith, P. E.; Pettitt, B. M., Dielectric Response of Triplex DNA in Ionic Solution From Simulations. *Biophysical Journal* **1995,** *69* (4), 1519-1527.

181. Jin, R.; Breslauer, K. J., Characterization of the Minor Groove Environment in a Drug DNA Complex - Bisbenzimide Bound to the Poly D(AT). Poly D(AT) Duplex. *Proceedings of the National Academy of Sciences of the United States of America* **1988,** *85* (23), 8939-8942.

182. Barawkar, D. A.; Ganesh, K. N., Fluorescent D(CGCGAATTCGCG) - Characterization of Major Groove Polarity and Study of Minor-Groove Interactions Through a Major Groove Semantophore Conjugate. *Nucleic Acids Research* **1995,** *23* (1), 159-164.

183. Savelyev, A., Do monovalent mobile ions affect DNA's flexibility at high salt content? *Physical Chemistry Chemical Physics* **2012,** *14* (7), 2250-2254.

184. Baumann, C. G.; Smith, S. B.; Bloomfield, V. A.; Bustamante, C., Ionic effects on the elasticity of single DNA molecules. *Proceedings of the National Academy of Sciences of the United States of America* **1997,** *94* (12), 6185-6190.

185. Arscott, P. G.; Ma, C. L.; Wenner, J. R.; Bloomfield, V. A., DNA Condensation by Cobalt Hexammine(III) in Alcohol-Water Mixtures - Dielectric-Constant and Other Solvent Effects. *Biopolymers* **1995,** *36* (3), 345-364.

186. Mel'nikov, S. M.; Khan, M. O.; Lindman, B.; Jonsson, B., Phase behavior of single DNA in mixed solvents. *Journal of the American Chemical Society* **1999,** *121* (6), 1130-1136.

187. Wang, Y. W.; Ran, S. Y.; Man, B. Y.; Yang, G. C., Ethanol induces condensation of single DNA molecules. *Soft Matter* **2011,** *7* (9), 4425-4434.

188. Ainalem, M. L.; Carnerup, A. M.; Janiak, J.; Alfredsson, V.; Nylander, T.; Schillen, K., Condensing DNA with poly(amido amine) dendrimers of different generations: means of controlling aggregate morphology. *Soft Matter* **2009,** *5* (11), 2310-2320.

189. Sackett, D. L.; Wolff, J., Nile Red As a Polarity-Sensitive Fluorescent-Probe of Hydrophobic Protein Surfaces. *Analytical Biochemistry* **1987,** *167* (2), 228-234.

190. Yadav, A. R.; Sriram, R.; Carter, J. A.; Miller, B. L., Comparative study of solution-phase and vapor-phase deposition of aminosilanes on silicon dioxide surfaces. *Materials Science & Engineering C-Materials for Biological Applications* **2014,** *35*, 283-290.

191. Faas, F. G. A.; Rieger, B.; van Vliet, L. J.; Cherny, D. I., DNA Deformations near Charged Surfaces: Electron and Atomic Force Microscopy Views. *Biophysical Journal* **2009,** *97* (4), 1148-1157.

192. Osland, A.; Kleppe, K., Polyamine Induced Aggregation of DNA. *Nucleic Acids Research* **1977,** *4* (3), 685-695.

193. Raspaud, E.; de la Cruz, M. O.; Sikorav, J. L.; Livolant, F., Precipitation of DNA by polyamines: A polyelectrolyte behavior. *Biophysical Journal* **1998,** *74* (1), 381-393.

194. Hook, A. L.; Thissen, H.; Quinton, J.; Voelcker, N. H., Comparison of the binding mode of plasmid DNA to allylamine plasma polymer and poly(ethylene glycol) surfaces. *Surface Science* **2008,** *602* (10), 1883-1891.

195. Monserud, J. H.; Schwartz, D. K., Effects of Molecular Size and Surface Hydrophobicity on Oligonucleotide Interfacial Dynamics. *Biomacromolecules* **2012,** *13* (12), 4002-4011.

196. Misra, V. K.; Hecht, J. L.; Yang, A. S.; Honig, B., Electrostatic contributions to the binding free energy of the lambda cl repressor to DNA. *Biophysical Journal* **1998,** *75* (5), 2262-2273.

197. Norberg, J., Association of protein-DNA recognition complexes: electrostatic and nonelectrostatic effects. *Archives of Biochemistry and Biophysics* **2003,** *410* (1), 48-68.

198. Chan, V.; Graves, D. J.; Fortina, P.; McKenzie, S. E., Adsorption and surface diffusion of DNA oligonucleotides at liquid/solid interfaces. *Langmuir* **1997,** *13* (2), 320-329.

199. Elaissari, A.; Pichot, C.; Delair, T.; Cros, P.; Kurfurst, R., Adsorption and Desorption Studies of Polyadenylic-Acid Onto Positively Charged Latex-Particles. *Langmuir* **1995,** *11* (4), 1261-1267.

200. Melzak, K. A.; Sherwood, C. S.; Turner, R. F. B.; Haynes, C. A., Driving forces for DNA adsorption to silica in perchlorate solutions. *Journal of Colloid and Interface Science* **1996,** *181* (2), 635-644.

201. Douarche, C.; Cortes, R.; de Villeneuve, C. H.; Roser, S. J.; Braslau, A., DNA adsorption at functionalized Si/buffer interfaces studied by x-ray reflectivity. *Journal of Chemical Physics* **2008,** *128* (22).

202. Romanowski, G.; Lorenz, M. G.; Wackernagel, W., Adsorption of Plasmid DNA to Mineral Surfaces and Protection Against DNASE-I. *Applied and Environmental Microbiology* **1991,** *57* (4), 1057-1061.

203. Elliott, L. C. C.; Barhoum, M.; Harris, J. M.; Bohn, P. W., Trajectory analysis of single molecules exhibiting non-Brownian motion. *Physical Chemistry Chemical Physics* **2011,** *13* (10), 4326-4334.

204. Escorihuela, J.; Pujari, S. P.; Zuilhof, H., Organic Monolayers by B(C6F5)(3)-Catalyzed Siloxanation of Oxidized Silicon Surfaces. *Langmuir* **2017,** *33* (9), 2185-2193.

205. Amemiya, Y.; Hatakeyama, A.; Shimamoto, N., Aminosilane Multilayer Formed on a Single-Crystalline Diamond Surface with Controlled Nanoscopic Hardness and Bioactivity by a Wet Process. *Langmuir* **2009,** *25* (1), 203-209.

206. Jain, R. Formation of Aminosilane and Thiol Monolayers on Semiconductor Surfaces and Bulk Wet Etching of III--V Semiconductors The Univeristy of Arizona, 2012.

207. Jalali, H.; Gates, B. D., Monitoring and Mapping Imperfections in Silane-Based Self-Assembled Monolayers by Chemical Amplification. *Langmuir* **2009,** *25* (16), 9078-9084.

208. Stotzky, G., Persistence and biological activity in soil of insecticidal proteins from Bacillus thuringiensis and of bacterial DNA bound on clays and humic acids. *Journal of Environmental Quality* **2000,** *29* (3), 691-705.

Appendix A

1. Representative spectroscopic ellipsometry data model fitting

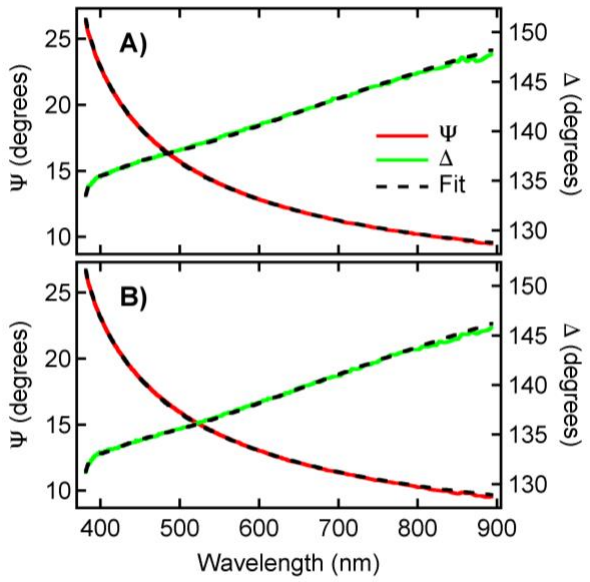

Figure A1. Spectroscopic ellipsometry data for A) a thin TMOS-derived base layer on silicon and B) a TMOS base layer coated with a self-assembled aminosilane layer. The raw data are plotted as colored lines. The fits of these data to a model for a single transparent film on silicon are shown as the dashed lines. The Cauchy relationship was employed to model film dispersion. The parameters obtained from global fits to the above data are: A = 1.528 ± 0.0062, B = 0.00442 ± 0.002024 μm^2, C = -0.00077946 ± 0.00022376 μm^4 and n = 1.53428 for panel (a) and A = 1.590 ± 0.0079, B = 0.00323 ± 0.002731 μm^2, C = -0.00119 ± 0.00029608 μm^4 and n = 1.59099 for panel (b). The mean square error in the two cases was 1.156 and 1.358, respectively.

2. Redox Stability of YOYO-1 and Useful Potential Window in Borate Buffer

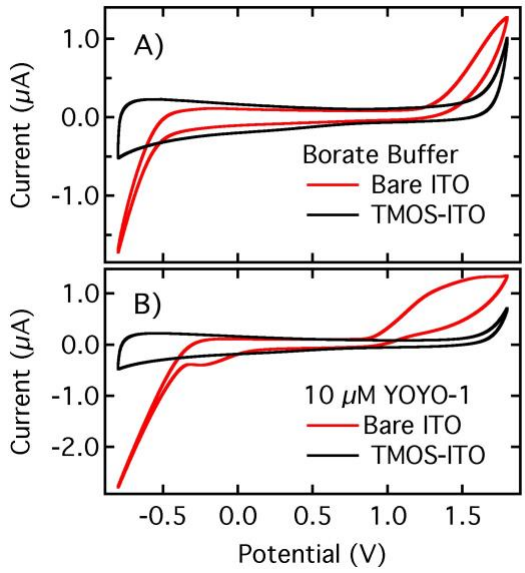

Figure A2. Cyclic voltammograms showing A) the background current in 0.10 mM borate buffer at bare ITO and base-layer-coated ITO electrodes and B) the current in the presence of 10 μM YOYO-1 at bare ITO and base-layer-coated ITO in the same buffer solution. YOYO-1 dye exhibits an oxidation peak at ~ 1.5 V on bare ITO and a reduction peak at ~ -0.2 V (solid red curve). The electrode area was 0.07 cm^2 in all cases, the pH was ~ 8, and the scan rate was 0.1 V/s. All potentials are measured vs. Ag/AgCl (satd KCl).

3. YOYO-1 bleaching studies

YOYO-1 dye bleaching experiments were performed at various laser powers (0.125, 0.25, 0.5 and 1.0 mW) in the presence of applied potentials (-0.5V and 1.4V vs Ag/AgCl). While all other factors remained the same as described in the main text, bleaching experiments were only performed under pH ~ 6 buffer. Fluorescence videos were obtained at 4 distinct spots across the gradient at the 7 mm position (high amine end). Before each bleaching experiment, the selected spot was first bleached with relatively high laser power (2 mW) for 1-3 min. Only DNA molecules that first appeared in the videos after this initial bleaching step were further analyzed. A total of

20 DNA molecules from each video were analyzed using the same procedure described in the main text. The time transients acquired were again fitted to a biexponential function to obtain the decay times. Plots of the two time constants for the YOYO-1 fluorescence decay observed following each adsorption event are shown in **Figure A3.** The time constants are fit to a model that includes both power dependent and power independent components, so that each decay constant, k, is represented as $k = AP + B$, where P is the laser power and A and B are fitting constants. The fitted data (using $\tau = 1/k$) yield power independent time constants, B, of ~ 5 s and ~ 10^2 s, for the fast and slow components, respectively, with relatively large error bars. The latter value is deemed consistent with the residence time data shown in **Figure 4.8** (main dissertation) at the 7 mm position.

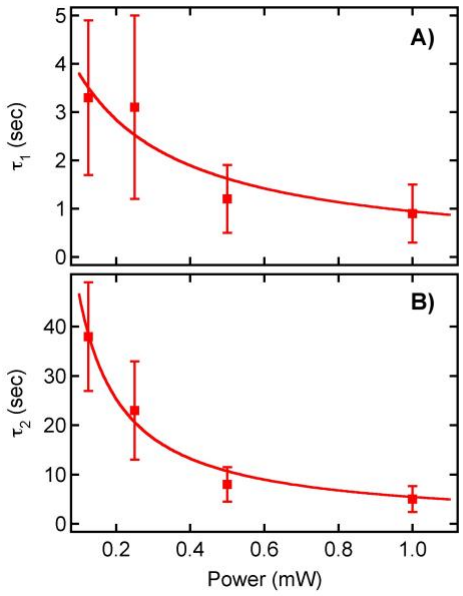

Figure A3. Time constants for YOYO-1 fluorescence decay after a DNA adsorption event, as a function of laser power, in the absence of an applied potential. The fluorescence decays were fit to biexponential functions. Plotted are the decay constants for the fast component (A) and the slow component (B). The data are consistent with each component incorporating both power dependent and power independent mechanisms for the fluorescence decay. The solid lines show fits to such a model. The solid lines show fits to such a model. The peak power

densities for the four measurements made in these experiments were ~ 11 W/cm^2, 22 W/cm^2 , 44 W/cm^2 and 88 W/cm^2, respectively.

4. Calibration of Nile Red Response

Measurement of ε for microenvironments within DNA requires the careful calibration of the NR response. Calibration of the response was accomplished by dissolving NR in a series of bulk ethanol/hexane mixtures. These solutions were used to fill a specially designed cell that was mounted atop the microscope. The background-subtracted average signals in the 580 and 625 nm image channels were determined from the collected fluorescence videos of each solution. The emission ratio, *E*, for each solution was then calculated, as defined in Equation A1. **Figure A4** plots the *E* values obtained from the solution mixtures as a function of their *CM* factors.

$$E = \frac{I_{625} - I_{580}}{I_{625} + I_{580}} \qquad \textbf{(Equation A1)}$$

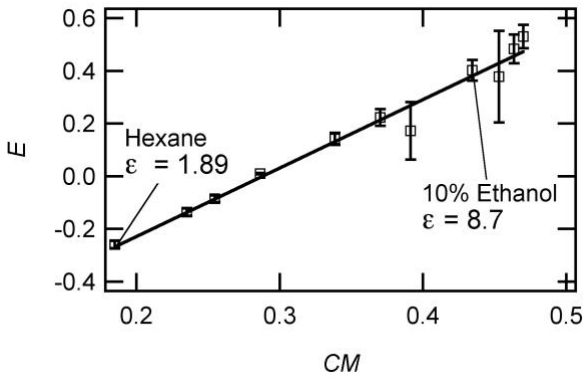

Figure A4. Calibration of the NR spectroscopic response to environments having different dielectric constants. The plot shows the NR emission ratio E in bulk solution for a series of hexane-ethanol mixtures. The polarity of each solution is defined by its Clausius-Mossotti (*CM*) factor (ε-1)/(2ε+1). From the left, the solution compositions are 0, 2, 3, 5, 10, 15, 20, 40,

60, 80 and 100% ethanol. The NR concentration was 2 μM in each case. The solid line shows a linear fit to the data; the slope and intercept were used to interpret the imaging results obtained from NR doped single plasmid DNA molecules.